UNIVERSITY OF SOUTHAMPTON

Faculty of Engineering and the Environment

Energy Technology Research Group

DISSOLUTION DYNAMICS OF LIQUID/LIQUID BINARY MIXTURES IN POROUS MEDIA

by

Mihaela S. P. Stevar

Thesis submitted for the degree of Doctor of Philosophy

February 2013

UNIVERSITY OF SOUTHAMPTON

ABSTRACT

FACULTY OF ENGINEERING AND THE ENVIRONMENT

Doctor of Philosophy

DISSOLUTION DYNAMICS OF LIQUID/LIQUID BINARY MIXTURES IN POROUS MEDIA

by Mihaela S. P. Stevar

In this project has been undertaken an experimental study aimed at understanding the dissolution dynamics of binary mixtures within porous media. The porous medium can be roughly represented as a network of capillary tubes. This allowed for the initial research to be focused on understanding the dissolution dynamics of binary mixtures (i.e. glycerol/water, soybean oil/hexane, and isobutyric acid/water) within single capillary tubes. Further, the dissolution process was investigated within a $2D$ micromodel built as a network of capillary tubes.

In the experiments with the capillary tubes, the dissolution (i.e. the interfacial mass transfer) could be isolated from the hydrodynamic motion while using glycerol/water and soybean oil/hexane binary mixtures. Despite the fact that these are fully miscible liquids, the interface could be observed for rather long time periods. In particular, two phase boundaries were observed moving from the ends into the middle section of the capillary tube with the speeds $v \sim D^{1/3}t^{-2/3}d^2$ (D, t and d are the coefficient of diffusion, time and diameter of the capillary tube, respectively). The boundaries slowly smeared but their smearing occurred very slow in comparison to their motion. The motion of the phase boundaries cannot be explained by the dependency of the diffusion coefficient on concentration, and could possibly be explained by the effect of barodiffusion. In addition, these solute/solvent boundaries were endowed with non-zero interfacial tension.

This experimental study also revealed that the solvent penetration into the micromodel is diffusion-dominated for completely miscible binary mixtures. This is however non-Fickian diffusion with the dissolution rate $dV/dt \sim D^{1/3}t^{-0.4}$ for almost the entire duration of the experiment (V is the volume occupied by the solvent, D is the diffusion coefficient and t is time). For the IBA/water mixture the experiments performed at undercritical temperatures revealed that the diffusive mass transport was negligible despite the mixture being out of its thermodynamic equilibrium.

Despite a seeming simplicity of the experiments, to the author's best knowledge, there is no theory that could correctly describe the observed diffusional penetration of a solvent into a solute-filled capillary tube and hence, into a more complex porous volume.

Contents

List of Figures

List of Tables

Declaration of Authorship

I, Mihaela S. P. Stevar, declare that the thesis entitled DISSOLUTION DYNAMICS OF LIQUID/LIQUID BINARY MIXTURES IN POROUS MEDIA and the work presented in the thesis are both my own, and have been generated by me as the result of my own original research. I confirm that:

- this work was done wholly or mainly while in candidature for a research degree at this University;
- where any part of this thesis has previously been submitted for a degree or any other qualification at this University or any other institution, this has been clearly stated;
- where I have consulted the published work of others, this is always clearly attributed;
- where I have quoted from the work of others, the source is always given. With the exception of such quotations, this thesis is entirely my own work;
- I have acknowledged all main sources of help;
- where the thesis is based on work done by myself jointly with others, I have made clear exactly what was done by others and what I have contributed myself;
- parts of this work have been published as:

  1. M. S. P. Stevar and A. Vorobev, Dissolution behaviour of a binary mixture in a capillary tube, 16^{th} European Symposium on Improved Oil Recovery, Cambridge, UK, 12–14 April 2011.

  2. Mihaela S. P. Stevar and Anatoliy Vorobev, Dissolution behaviour of binary mixtures in capillary tubes. Experimental study, 8^{th} Liquid Matter Conference, Wien, Austria, 6–10 September 2011.

  3. M. S. P. Stevar and A. Vorobev, Shapes and dynamics of miscible liquid/liquid interfaces in horizontal capillary tubes. Journal of Colloid and Interface Science, 383:184–197, 2012.

  4. Mihaela S. P. Stevar and Anatoliy Vorobev, Dissolution dynamics of miscible liquid/liquid interfaces, 8^{th} International Conference on Diffusion in Solids and Liquids, Istanbul, Turkey, 25–29 June 2012.

  5. M. S. P. Stevar and A. Vorobev, Dissolution of liquid/liquid binary mixtures in micromodels, in preparation for re-submission to International Journal of Multiphase Flow.

Signed:.....

Date:.....

Acknowledgements

First and foremost, I would like to express my deepest gratitude towards my supervisor Dr. Anatoliy Vorobev for giving me the opportunity to carry out this research project and for his constant guidance and support. Without his knowledge, patience and encouragement this work would have not been possible and this thesis would have not attain its current form. Other academics to whom I must thank for examining me throughout my PhD and for providing valuable insight on aspects of my work are Dr. John Shrimpton, Dr. Xunli Zhang and Prof. V. Starov. In addition, I must thank for the financial support from the Engineering and Physical Sciences Research Council (EPSRC).

I would particularly like to thank Simon Klitz for his invaluable help with manufacturing different parts of the experimental setup. Without his manufacturing skills my experimental work would have been much harder. I must also thank Dolomite Centre Ltd. for their technical support and for manufacturing the micromodels utilized in this work. The technicians from the Glassblowing facility and EDMC (University of Southampton) are also thanked for manufacturing various other bits and pieces.

Some very special thanks are addressed to my lab colleague and friend, Dr. Dehao (Andy) Ju for his invaluable help in the lab.

I am also deeply grateful to all my present and former colleagues for sharing with me their knowledge, for creating a nice and warm working environment, for their friendly attitude and for all the good discussions we have had work-related or not. They are: Abdul, Alex, Andrea, Badr, Badril, Chao, Derek, Irene, Iole, Maria, Mohamed, Natalya, Oliver, Par, Rachel, Ravi, Recep, Ruben, Steven, Tony, Uchi and Vanesa. Additional thanks to Natalya for our weekly Diegos tradition.

I would also like to address my sincere thanks to my best friends from Romania for always being there for me even from far away. They are: Florentina, Laura, Madalina, Nicoleta, Oana and Roxana. Thanks girls for everything.

Last but not least, I sincerely thank my family: my parents, by brothers and their families and my sister. I am glad having all of you in my life to remind me the reasons and the happiness of my existence. I would also like to thank to a very special person in my heart, Jurgen, who endured, understood and loved me during all these years. Many thanks for existing in my life.

Abbreviations

CCD	Charged coupled device
DNAPL	Dense non-aqueous phase liquids
EAR	Enhanced aquifer remediation
EIT	Effective interfacial tension
EOR	Enhanced oil recovery
GDL	Gas diffusion layer
IBA	Isobutyric acid
L-CO_2	Liquid carbon dioxide
LCST	Lower critical solution temperature
LNAPL	Light non-aqueous phase liquids
NAPL	Non-aqueous phase liquids
NMR	Nuclear Magnetic Resonance
PEM	Polymer electrolyte membrane
REV	Representative Elementary Volume
SC-CO_2	Supercritical carbon dioxide
UCST	Upper critical solution temperature
UK	United Kingdom
US	United States

Nomenclature

Symbols	Definition	Unit
A	Surface area	m^2
A_r, B_r	(Dissolution rate) Coefficients	$m/s^{i\ 1}$
A_d	Diffusional term	-
b	Coefficient	-
Bo	Bond number	-
c	Concentration	kg/m^3
Ca	Capillary number	-
C_H	(Higuchi) Constant	-
c_s, c_1	Saturation (equilibrium) solubility	kg/m^3
d	Diameter of the capillary tube	m
D	Diffusion coefficient	m^2/s
e_r	Extraction rate	-
g	Gravitational acceleration	m/s^2
h	Thickness of diffusion layer	m
Δh	Head difference	m
H^E	Enthalpy of mixing	J/mol
I_0, I_{z-1}	Imbibition mechanisms	-
$\mathbf{J}$	Diffusive flux	$kg/m \cdot s$
$J(s)$	Leverett J-function	-
k	Permeability	m^2
K	Rate constant (of dissolution)	m^3/s
K_h	Proportionality constant (hydraulic conductivity)	m/s
l_m	Mixing length	m
L, L_0	Length (of the capillary tube or filled with liquid)	m
m_g	Mass fraction of glycerol in the ejected fluid	-
m_i	Mass of glycerol injected into the capillary tube	kg

[1]The index i can have the following values in the expression of the unit of measurement for coefficients A_r and B_r: $2/3, 0.3, 1/3$ and 0.6, respectively.

M	Amount of drug released	-
Ma_s	Solutal Marangoni number	-
p	Pressure	Pa
p_c	Capillary pressure	Pa
Pe	Peclet number	-
$\mathbf{q}$	Seepage velocity vector	m/s
Q	Volumetric flow rate	m^3/s
r	Radius (of the capillary tube)	m
Ra_s	Analogue of Rayleigh number for solutal convection	-
Re	Reynolds number	-
s	Saturation	%
s_e	Solvent spent for extraction	-
S	Spreading parameter	-
t	Time	s
T	Temperature	K
v	Velocity	m/s
V	Volume occupied by the solvent	m^3
Δx	Displacement of particles	m
x_1, x_2	Coordinates of the interfaces positions	m
z	Coordination number	-

Greek symbols

α	Mobility coefficient	$kg \cdot s/m^3$
η	Dynamic viscosity	$Pa \cdot s$
μ	Chemical potential	J/kg
ϕ	Porosity	-
ρ	Density	kg/m^3
σ	Interfacial (surface) tension	N/m
τ_d	Diffusive time scale	s
θ	Contact angle	^{o}

Subscripts

$1, 2$	Phase 1, Phase 2
b	Bubble
d	Droplet
g	Glycerol
imb	Imbibition
la	Liquid/air
ls	Liquid/solid

nw	Nonwetting
sa	Solid/air
w	Wetting

Superscripts

α	Scaling exponent
n	Exponent of time dependence
ν	Exponent

Chapter 1

Introduction

Multiphase flows through porous media have been studied for decades but due to the great complexity of the natural porous media and thereby of the wide range of parameters that influence them, there are still many aspects of these types of flows that require investigation. An introduction to the field of miscible multiphase flows through porous media with an emphasis on dissolution dynamics is given in this chapter together with the motivation and the main objectives of this project. An outline of the entire thesis is also provided in this chapter.

1.1 Motivation and objectives

The dissolution process of miscible binary mixtures within a porous medium is a very challenging subject with great importance in several fields such as petroleum engineering, hydrogeology, biotechnology and medicine. The dissolution (i.e. mass transfer between the components of binary mixtures) is traditionally modelled as a process of inter-diffusion. The usual description of miscible liquid/liquid interfaces with zero interfacial tension neglects the slow diffusion process and the gradient stresses that mimic the effect of interfacial tension. Thus, for the case of miscible binary mixtures, the classical Fickian description of diffusion is a bad approximation because the interfacial diffusive flux is incorrectly defined and it neglects the gradient stresses that mimic the effect of interfacial tension [1].

When two miscible liquids are brought into contact, a clear interface endowed with a small interfacial tension is observed [1]. In the first moments of the dissolution process the shape of this interface can be no different from the shape of an interface between two immiscible liquids. The only difference is that due to a slow diffusion process the interfacial tension that characterizes a miscible interface decreases in time (dynamic interfacial tension) reaching a zero value once the components of the miscible binary mixture completely mix [1].

Historically the concepts of dynamic interfacial tension and capillary forces acting on miscible interfaces were noted around a century ago. Regarding the existence of dynamic interfacial tension for miscible interfaces, in 1926 Freundlich noted that *"...the dynamic tension of liquids, when first brought in contact, is to be distinguished from the static tension, when the two liquids are mutually saturated. Not only do liquids which are not miscible in all proportions have a mutual surface tension; even two completely miscible liquids, before they have united to form one phase, exhibit a dynamic interfacial tension. For we get by careful overlaying of any two liquids a definite meniscus, a jet of one liquid may be generated in another, and so on. The tension decreases rapidly during the process of solution, and becomes zero as soon as the two liquids have mixed completely."*. The influence of capillary forces present at the interface between miscible liquids was acknowledged in 1901 by M. Bosscha who in one of his letters wrote: *"The phenomena which I observed related to the slow flow of one liquid into another, however slow the flow, remains nevertheless phenomena of motion, and the states that I observed are always states of motion. It is only by way of approximation that one can think of them as states of equilibrium."* These extracts are taken from the historical introduction given by Joseph and Renardy in their chapter dedicated to dynamics

of miscible liquids [1]. Even though these concepts were mentioned for the first time around 100 years ago, nowadays there are still many researchers who ignore them in their studies involving miscible interfaces and who still treat slow diffusion problems in the classical way with vanishing interfacial tension[1, 2].

According to Joseph and Renardy different studies suggest that when two miscible liquids slowly interdiffuse, gradients of concentration, density and possibly temperature can induce stresses that can cause effects that mimic the interfacial tension [1]. Still, in many applications related to liquids mixing such as miscible displacements and dispersion these gradients are ignored, one of the most common approximations being that there is no density gradient and thus the simplified form of the continuity equation, $div\,\mathbf{v} = 0$ can be employed. However, density gradients can be present in an isothermal binary mixture due to pressure and concentration gradients, $\rho = \rho(p, c)$. The assumption of no density gradient, even for a mixture of two incompressible liquids, ignores the dependence of a mixture density on concentration and thus the physical effect of quasicompressibility.

Furthermore, the existence of the dynamic interfacial tension gives rise to a pressure difference across the interface which should also be considered. This pressure gradient is usually incorporated, if the gradient of chemical potential is considered to drive the diffusion flux instead of the gradient of concentration.

Diffusive transport and mixing problems are widely spread in many practical applications from various technological fields (e.g. miscible displacements in porous media). The flows in porous media are usually studied with the aid of the network approach and the porous medium can be roughly represented as a network of interconnected capillary tubes. Consequently, we define the principal aim of this experimental research project as to understand the dissolution dynamics of miscible binary mixtures first within a single capillary tube and then within a more complex porous matrix which can simulate the natural porous media up to a certain extent.

1.2 Thesis outline

This thesis contains in total 6 chapters.

Chapter 2 provides the reader with a few general concepts regarding multiphase flows in porous media, their main practical applications and the principal parameters that could define such flows. The literature on the subject is enormous

and thus this chapter represents just a summary by covering only the basic ideas relevant to this project. As this study is focused on dissolution in both capillary tubes and $2D$ network models a literature survey of previous studies which employed these geometries is also presented in this chapter.

Chapter 3 describes the experimental study of the dissolution process in capillary tubes with various dimensions and cross-sections. The experimental results obtained are discussed and put into context with other data published in the literature.

Chapter 4 presents the experimental study of the dissolution process within a micromodel designed as a network of interconnected capillary tubes and outlines the importance of the diffusive mass transfer in multiphase flows.

Chapter 5 summarizes all the experimental work completed during this project and presents the main conclusions of this thesis.

Chapter 6 provides a few recommendations of pathways that could be followed for a continuation of this study.

Chapter 2

Literature review

This chapter provides an overview on the research undertaken in the field of multiphase flows through porous media. A slow dissolution process of a binary mixture within a porous media is an essential part of several fields including petroleum engineering, hydrogeology, biotechnology and medicine. After providing a short introduction to the topic, the main applications will be reviewed. Some important concepts for porous media and the evolution of pore-scale models will also be included in this review. The most significant factors that influence the dissolution dynamics will be discussed in the sections regarding liquid/liquid binary mixtures and mass transfer. A literature survey of the most important studies involving capillary tubes and micromodels for studying flows in porous media is also included in this chapter.

2.1 Introduction

Over the past few decades an enormous amount of research has been undertaken in the field of multiphase flows in porous media. The aim of this chapter is to provide a short literature survey on the practical applications of flows in porous media, their current status and the potential progress that can be made based on advancing the fundamental understanding of these types of flows. In addition, a brief description of several relevant physical parameters and concepts regarding the mass transfer mechanisms is provided before embarking on the discussion of the experimental results. The aim is to have a clear overview of the implications of certain factors (e.g. the rate of solute/solvent dissolution, capillary pressure and wetting effects) and their interplay when characterizing the liquid/liquid dissolution process.

2.2 Applications

Petroleum engineering, hydrogeology and biotechnology are just some of the fields in which the importance of multiphase flows through porous media can be identified [3, 4, 5]. A better understanding of these flows is also essential in medicine (e.g. drug delivery in veins [6]) and in some other modern fields of chemical engineering [3, 6, 7]. Some of the most important applications for which dissolution and displacement processes in porous media play an essential role are detailed below.

2.2.1 Enhanced oil recovery

Enhanced oil recovery (EOR) refers to the recovery of oil trapped in oil fields when the methods of primary and secondary recovery (conventional methods) are proved to be either exhausted or no longer economical [8] and describes the set of techniques (i.e. the use of miscible and immiscible mixtures, chemical and thermal processes and biological operations [9]) utilized to increase the amount of oil that can be extracted from oil fields.

EOR is a tertiary recovery method but according to Donaldson [10] it can be used at any time or stage for an oil reservoir if the production needs to be stimulated by using some kind of chemical or thermal energy. EOR has been applied in

different situations ranging from new reservoirs to reservoirs that were on the point to be abandoned, but in all cases the objective was to obtain increased oil recovery in respect with the one provided by conventional means. In order to achieve higher recovery rates the recovery techniques have to be tailored to the reservoir and therefore, sometimes primary or secondary recovery are omitted due to the reservoir behavior and oil field economic reasons [10].

During primary recovery the natural pressure of the reservoir drives the oil into the well bore and lifts it to the surface. Even if this is the least expensive method to extract oil, since it uses natural forces, the amount of oil recovered is typically only 10% to 15%. Plus, oil production can be additionally diminished by physical constraints such as reduced well pressure and extensive oil trapping [9].

When the underground pressure is insufficient to move the remaining oil, the secondary recovery techniques need to be used. The most commonly employed technique is waterflooding. For this technique, a second (injector) well is required for injection of large water volumes into the hydrocarbon-bearing zone. The water will sweep along with it some of the encountered oil, so an additional 10% to 30% of the oil can be recovered. During common waterfloods the displacement of all oil in the reservoir is physically impossible due to the flow rates used and also due to the capillary forces which cause part of the oil to be retained between disconnected water-wet rock structures. The amount of trapped oil that remains in the reservoir after waterflooding is the most important factor for the economics of enhanced oil recovery. During secondary recovery, gas injection technique can also be used to increase the reservoir pressure. Usually, by combining the primary and secondary methods less than 40% of the amount of oil encountered in a reservoir can be recovered.

When the secondary recovery becomes no longer cost-effective the tertiary recovery techniques are considered. These additional methods are expensive but, in most cases, they allow for a $60 - 65\%$ of a field's total oil potential to be realized. EOR techniques are imperative to use because in addition to the economical reasons, technical ones could also be responsible for the existence of large amounts of residual oil after primary and/or secondary recoveries were employed. Hence, enhanced oil recovery methods were conceived in order to overcome the capillary forces usually responsible for the retention of such high amounts of residual oil in reservoirs [9] and target the recovery of more oil (residual oil) than the amount that could be extracted by conventional methods. Still, the initiation of EOR projects is strongly influenced by the willingness of investors to manage the risk

associated with this type of investments [11]. The employment of enhanced oil recovery methods can be risky but also rewarding if the implementation is based on a detailed knowledge of the oil field characteristics leading to the most suitable methods being utilized. The techniques used in all oil extraction stages are summarized in Figure 2.1.

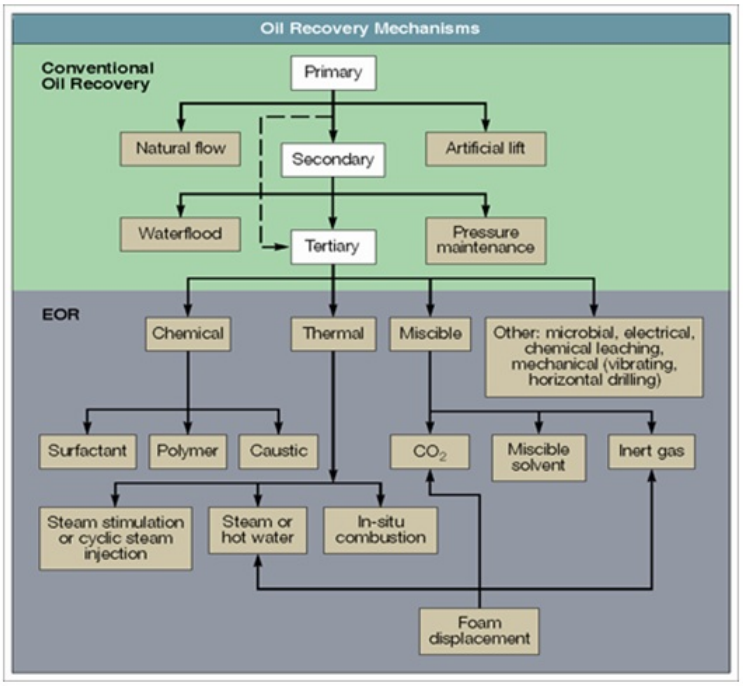

Figure 2.1: Oil recovery mechanisms [12].

There is a vast amount of publications in the literature which discuss various aspects of enhanced oil recovery in terms of efficiency and effectiveness but only a few of them will be mentioned herein. A thorough review for the case of tertiary enhanced oil recovery and the management of mature oil fields was presented by Babadagli [13]. He discussed the tertiary recovery techniques like miscible and immiscible gas injection and air and chemical injection (especially surfactant solutions) along with the strategies required and the economical criteria involved by their application. Hydrocarbon gases and CO_2 are the most commonly used agents for tertiary recovery processes. Usually, the gas injection techniques are applied when a large amount of remnant water exists in the reservoir due to the secondary recovery and therefore the efficiency of the process strongly depends on the existing pressure in the reservoir, miscibility and wetting effects. For example, wettability reversal represents a novel method being under current investigation which seems promising for the future of enhanced oil recovery. Another comprehensive review of EOR status and opportunities to increase oil recovery from mature fields is the one of Alvarado and Manrique [11]. Their review is organized

by reservoir lithology (sandstone and carbonate formations) and includes risks and rewards of EOR methods, economic aspects of EOR projects and their evolution in recent years. Thermal, chemical and miscible gas injection methods are discussed for both sandstone and carbonate type reservoirs with direct reference to oil fields around the world. Another recent work that evaluates the current status and future of EOR technology with emphasis on chemical methods especially using microemulsions is the one of Nazar et al. [9]. Besides the emphasis on chemical EOR (i.e. microemulsion techniques) basic concepts regarding other EOR techniques and their trend and the role of capillary and viscous forces in oil recovery can also be found in this review [9].

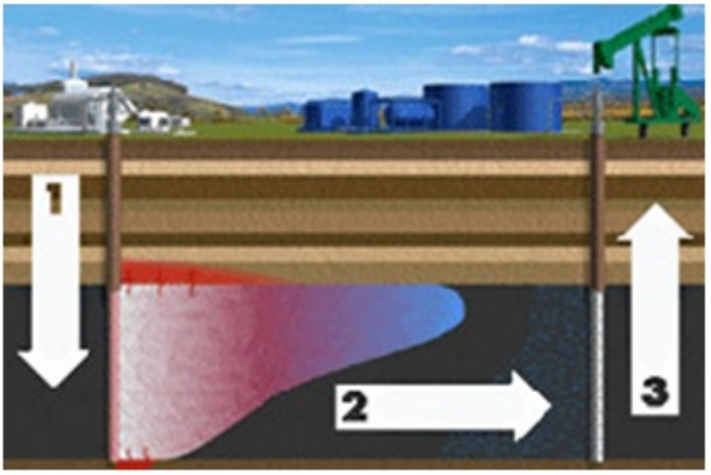

Figure 2.2: Miscible displacement process; 1. Injection of a miscible solvent into the reservoir; 2. Miscible displacement stage including the dissolution of oil; 3. Pumping out the mixture from the reservoir [14].

As stated in the previously mentioned literature, the techniques based on miscible processes (hydrocarbon gases and CO_2 injection) have seen an increasing trend in the recent years. As already known, the miscibility is highly beneficial from the recovery point of view as it affects the microscopic displacement efficiency in the gas injection processes. The minimum miscibility pressure is the minimum pressure needed for the oil and the injected gas to achieve miscibility at a certain temperature. The displacement process can take place above the minimum miscibility pressure or below it, in the so called near-miscible zone. In the latter case the recovery may be negatively affected. Displacement efficiency increases as high values of the capillary number are obtained. The capillary number represents the ratio of viscous forces to interfacial tension and is used to quantify their relative effect ($Ca = \eta v/\sigma$, where η represents the viscosity, v the velocity and σ the interfacial tension). Very high capillary numbers can only be obtained when the interfacial

tension is zero and miscibility is acquired [15]. The CO_2 flooding is a miscible displacement process (Figure 2.2) applicable to many reservoirs but the most feasible method is considered to be the alternate CO_2/gas and water injection. The number of CO_2-EOR projects has increased over the last few decades especially because of the vast and cheap sources of CO_2 found in US [11] and because of the interest of combining EOR projects with CO_2 sequestration [16, 17, 18, 19, 20].

To conclude, the miscible displacement is one of the main EOR techniques. The importance of dissolution in relation to EOR stems from the fact that the dissolution represents the inner core of a miscible displacement process. Enhanced dissolution rates can increase the efficiency of a miscible displacement process and thus can yield to enhanced oil recovery. Therefore, the results obtained in this study could find their practical applicability in the field of oil recovery.

2.2.2 Enhanced aquifer (soil) remediation

An aquifer is a layer of porous substrate that contains and transmits groundwater. An aquifer is unconfined when water can flow directly between the surface and the saturated zone of the aquifer. A confined aquifer is an aquifer that is overlain by a relatively impermeable layer of rock or substrate with so low porosity that is virtually impermeable to groundwater (Figure 2.3).

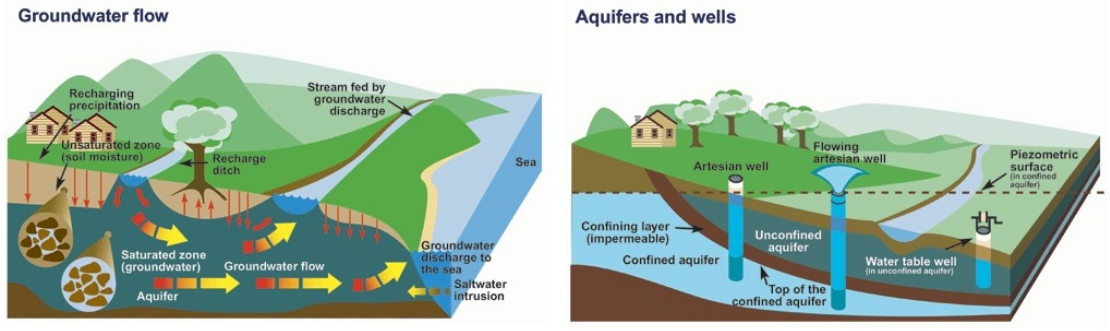

Figure 2.3: Groundwater flow and aquifers [21].

Improper storage and disposal of liquid contaminants represent the main causes of subsurface contamination [22, 23]. Non-Aqueous Phase Liquids (NAPLs) generally characterized by low solubilities represent a continuous groundwater contamination source because after their spillage or leakage to the subsurface they usually migrate toward the water table under the influence of gravity and capillary forces and are then distributed in the form of disconnected blobs or NAPL pool in the aquifer material [24]. NAPLs can be further classified function of their density in

respect to water density into: Light Non-Aqueous Phase Liquids (LNAPLs, less dense than water, e.g. gasoline) and Dense Non-Aqueous Phase Liquids (DNAPLs, denser than water, e.g. chlorinated solvents) [25]. The density of the contaminants is responsible for their various movement patterns through soils and aquifers.

Enhanced aquifer remediation (EAR) is usually accomplished by treating the groundwater using in situ methods involving the addition of chemical agents to an injection fluid during a miscible displacement to accelerate the displacement, dissolution or transformation of contaminants. The in situ methods (e.g. chemical flushing, chemical oxidation, gas and steam treatment) replaced the previously pump-and-treat method in which the groundwater was pumped out of the site, treated at the surface for contaminant removal and then re-injected [26]. The pump-and-treat method was the first one employed in the remediation of NAPLs contaminated aquifers but was ineffective mainly because of the low solubility of NAPLs and the high interfacial tension between contaminants and water [27, 23]. The limitations of the pump-and-treat method led to the investigation and development of alternative remediation techniques (e.g. in situ surfactants and cosolvents flushing, bioremediation). According to Soga et al. remediation strategies can be divided in two major groups: source zone remediation (removal of NAPL phase from within the ground) and plume remediation (treating the plume and controlling its concentration in groundwater to safe levels) [23].

A huge amount of research has been done over the past few decades in attempt to study various aspects of NAPLs removal from contaminated subsurface sites and progress in the field has been noticed [28, 25]. Subjects such as NAPLs dissolution in homogeneous and heterogeneous porous media have been extensively studied at both microscopic (studies employing micromodels) and macroscopic (laboratory experiments employing soil columns) scales but the up-scaling to megascopic scale (i.e the scale of contaminated sites) is still problematic and requires further investigation [28]. Other aspects related to accurate descriptions of NAPLs location (i.e source zone) and size in the subsurface [28, 23], mass transfer rates (i.e. dissolution rates) [26, 6], porous media characteristics (e.g. heterogeneity and wettability) and their influence on dissolution rates [22], up-scaling issues such as dispersion and flow by-passing [28], bioremediation clean-up strategies [29] and surfactants and muticomponent mixtures (i.e cosolvents) [30, 31, 24, 32, 27] have also been extensively investigated in both experimental and numerical studies.

The surfactants are known to enhance the removal efficiency of the contaminants through two mechanisms: micellar solubilization (the aqueous solubility of NAPLs

is increased many fold) and mobilization of entrapped NAPL (the interfacial tension between NAPL and water is reduced until gravitational or viscous forces overcome the capillary forces holding the contaminant in place). The mobilization occurs when the strength of the capillary forces responsible for the NAPL entrapment is sufficiently reduced and is known to remove a larger amount of contaminant than micellar solubilization in a shorter time. Still, in the case of DNAPLs removal the enhanced dissolution of contaminants is more favorable than the mobilization because in the latter mechanism the reduction of the interfacial forces can cause serious secondary effects (due to density differences) such as vertical movement of DNAPLs to unexpected areas farther down in the subsurface [31, 24].

One has to bear in mind that although very high levels of remediation efficiencies have been obtained at microscale, in most cases, the results were obtained in homogeneous conditions and based on a number of assumptions and therefore they are considered not to be representative for field scale due to the non-uniformities that characterize groundwater flow [23]. For example, in [23] is considered that complete source zone remediation is very difficult or impossible at field scale (especially for DNAPLs) due to complex entrapment and large scale issues in contaminant transport. Therefore the authors of this publication suggest that the effectiveness of remediation techniques should be assessed based on the reduction of entrapped NAPL from the source zone and the risk associated with possible recontamination after remediation [23]. However, a detailed description of all processes involved at microscale is essential for the design and implementation of any EAR technique.

Similar to the case of EOR, site specific strategies should always be employed with the target to at least minimize the risk of further (re)contamination (i.e. decrease NAPLs quantities/concentrations to acceptable levels) if complete remediation is not possible. For further reading on the topic of groundwater flow and contaminant transport the book of Bear and Cheng [25] is highly recommended.

2.2.3 Vegetable oil extraction

Vegetable oils have a large number of applications in many industries besides food industry. They are used as components in different cosmetic and pharmaceutical products, paints or lubricants, as drying agents or insulators and for biodiesel production [33, 34].

Solvent extraction is the most commonly used process for extracting vegetable oil from oleaginous materials, therefore much attention has been paid recently

towards improving solvent extraction efficiency and modelling the process in different type of extractors. Additionally, the attempt to find other suitable solvents beside hexane that can be used on industrial scale and are economically feasible also represents a major challenge. Hexane is the most widely used solvent for the vegetable oil extraction because is a very good solubilizing agent for oils, is chemically stable and it can be easily separated by stripping [33]. However, concerns regarding its toxicity and increased costs related to its recuperation determined researchers to seek for alternative solutions [33, 34].

To the author's best knowledge the first review on the topic of potential biorenewable solvents that could substitute hexane in the extraction process pertains to Hron et al. [35]. They reviewed the most important solvents that could be used as substitutes including water, alcohols, ketones and liquefied and supercritical gases and described the advantages and disadvantages that would result from this replacement. Some other solvents which contain aldehyde, ether, ester or cloro/fluorocarbon groups were also briefly discussed in their review [35].

Supercritical carbon dioxide (SC-CO_2) proved to be the best alternative for the extraction process as it is a non-toxic, inert, technically safe and readily available and affordable solvent [36]. Even though many experimental and theoretical studies have been published in the literature on the subject of oil extraction with SC-CO_2 [37, 38, 39, 40, 36] and the process seems very promising in comparison with the traditional technique, its implementation at industrial scale has encountered some difficulties and hence been hindered, mainly due to the inconvenience of batch processing [41]. Therefore efforts are still being directed towards improving the traditional hexane-based technique by reducing the costs and increasing the efficiency of the solvent recovery stage. For example, Martinho et al. studied the vegetable oil extraction from soybeans with special emphasis on the optimization of the solvent recovery stage [33] and Eller et al. studied the use of liquid carbon dioxide (L-CO_2 i.e. lower pressure and temperature) instead of SC-CO_2 to separate the hexane from the soybean oil/hexane mixture resulted from the extraction process [41].

At industrial scale the solvent extraction process usually occurs in reactors such as *Rotocell* or *DeSmet* which have been used in the food industry for more than 20 years. In general, these reactors operate based on the principle of counter-current crossed flows of the oleaginous material (i.e. a solid porous medium that contains oil) and the miscella (i.e. solvent/oil mixture) [42]. In this way at the end of the

extraction process the porous medium has a low oil content at the exit, whereas the miscella is highly enriched in oil.

Numerous mathematical models based on simplified equations have been developed to study the solvent extraction process in these types of reactors. Veloso et al. developed the first mathematical model applicable to *DeSmet* type extractors which incorporated the counter-current crossed flow of the porous material and miscella. Their numerical model considered the mass transfer between the flakes and miscella, the diffusion in the entire extraction field, the transport of miscella between various regions, the influences of loading and drainage zones and the transient operational regimes of the extractor [43]. Hence, the model was composed of various sub-models connected through the boundary conditions. Similar models for a *Rotocell* type extractor which is commonly used for coffee, oil and sugar processing have been developed by Thomas et al. [44, 45]. These two models were very similar to the one of Veloso et al. and incorporated the same counter-current crossed flow, oil diffusion in the extraction field, mass transfer between pore and bulk phases, oil losses and the variation of viscosity and density of miscella. Different methods were used in the two models to simulate the processes in the extractor. The novelty of the second model of Thomas et al. [45] was the description of the spatial concentration distributions of pore and bulk phases in the extraction field and the sensitivity to the raw material characteristics, section sizes and wagon parameters. Later, Carrin and Crapiste also developed a two-dimensional non-steady state mathematical model [46] for a *DeSmet* type extractor in order to account for non-equilibrium mass transfer between the phases and for different oil categories. They compared the results obtained with experimental data for sunflower oil extraction with hexane. Later on, their model was further expanded by Baumler et al. to account for the extraction of oil and its minor components [42]. Despite of the large number of theoretical models developed for the extraction of vegetable oils, experimental data are still required for verifying these models in the design and implementation of efficient solvent extraction techniques.

2.2.4 Drug delivery

The enhancement of dissolution rates and thereby bioavailability improvement of drugs administered through different routes in the body has been for many years a major concern in the pharmaceutical industry. There are two major administration categories: enteral (i.e. oral route) and parenteral (i.e. intravenous injection). The oral route is usually the method of administration preferred because of its

convenience [47], but it still has quite a few disadvantages. First, the drugs must be absorbed from their entrance point (stomach or intestine) into the bloodstream and for this to happen drugs must pass at least one cell membrane, process limited by diffusion. Second a suitable dosage is needed to ensure the drug will reach its site of action in a pharmacologically effective concentration and be maintained at this concentration for a certain period of time. The easier and most common method to introduce a drug (i.e liquid drug) in emergency cases is to inject it into veins straight into the systemic circulation. Due to the veins structure the blood found in veins is the one released when a rapid therapeutic response is required (e.g. cardiac arrhythmia). Hence, in this case the liquid/liquid dissolution plays a crucial role.

The historical evolution of drug dissolution is well described in [48] and it goes back all the way to the work of Noyes and Whitney in 1897 [49] which represents the theoretical foundation of solid/liquid dissolution research. The original Noyes-Whitney equation:

$$\frac{dc}{dt} = K(c_s - c) \tag{2.1}$$

describes the dissolution of a drug from a primary particle and incorporates the effect of solubility on the dissolution rate. In Equation 2.1 dc/dt is the rate of increase of the amount of drug dissolved, K is the rate constant of dissolution, c_s is the saturation solubility of the drug in the dissolution media and c is the concentration of drug at time t. Later theories accounted for a variable surface area [50, 48] and the Noyes-Whitney equation was rewritten in a different form, with a better defined rate constant [48] being:

$$\frac{dc}{dt} = \frac{DA(c_s - c)}{Vh}. \tag{2.2}$$

In Equation 2.2 A is the surface area of the drug undergoing dissolution, D is the diffusion coefficient of the dissolved drug molecules, V is the volume of the dissolution medium, h is the thickness of the diffusion layer and all the other variables are the ones already defined in Equation 2.1. The dependence of dissolution rate on the surface area may also be applicable in the case of liquids dissolution.

It has been estimated that approximately 40% of the newly developed drugs are poorly soluble or insoluble in water and this poor solubility represents one of the major challenges in drug development [47, 51, 52]. Hence, the study of

drug (solid/liquid) dissolution and drug release rates from various dosage formulations has received particular attention in the pharmaceutical industry. The most commonly studied and employed method to enhance dissolution rates and hence bioavailability is the decrease of particles sizes by preparing nanoparticles/microparticles in order to increase drug solubility [47, 51, 52]. According to Wong et al. the use of nanoparticles/microparticles to formulate poorly soluble drugs would not only enhance dissolution rates but would also improve the targeting capabilities of the drugs (e.g. in the case of intravenous injection) [51].

Besides enhancement of dissolution rates, drug release profiles constitute the second main area of interest in drug delivery. Different drug release profiles exist based on the difference of the drug concentration in the blood: usual single dose preparation, sustained/controlled release preparation and prolonged release preparation. The ideal one is considered to be the sustained release profile even though this is very difficult to achieve in practice. Intensive research has been focused on controlled and prolonged drug delivery systems and the use of biocompatible polymers to achieve better control of drug administration [53, 54, 55]. Polymers can be used to coat a drug to prevent it being released in the stomach or to produce a slow controlled release of the drug. The release rates of the drug are determined among others by the design system. Maintaining the drug in the desired therapeutic range with just a single dose still represents a challenge. A convenient classification of controlled release systems can be made function of the mechanisms that control the release of the drug: diffusion-controlled systems, chemical-controlled systems, and solvent-controlled systems [55]. Many theoretical models have also been developed for studying the kinetics of drug release [56, 54] and most of them model the rate of drug release based on Higuchi equation, $M = A_d t^{1/2} + C_H$, where M is the amount of drug released, A_d is a diffusional term, t is time and C_H is a constant.

When drugs are administrated via oral route the drug concentration in the blood is controlled either by the rate of drug dissolution from the dosage formulation or by the rate of absorption. Usually the dissolution rate of the drug is the rate-determining step of the overall process and therefore the intensity of the clinical response is influenced by controlling the dissolution process. The relative drug release rates function of the drug dosage form presented in Table 2.1 show that from the bioavailability point of view the use of liquid medicines is more advantageous.

However, aqueous solutions are rarely used due to various problems (e.g. solubility,

Ranking of dosage forms		
Aqueous solutions	↑	
Emulsions	|	
Soft gelatine capsules	|	
Suspensions	|	Increasing release rates
Powders	|	and bioavailability
Granules	|	
Hard gelatine capsules	|	
Tablets	|	
Coated tablets	|	

Table 2.1: The ranking of dosage forms in respect to the rate of drug release [57].

stability, taste and non-uniform dosing), but oils used as drug carriers provide efficient oral dosage formulations either as emulsions or in soft gelatine capsules. Such capsules represent convenient dosage formulations because of the rapid release of oil (i.e. short dissolution stage) and therefore exhibit very good bioavailability [57]. Thus, even though in the past drug dissolution research started with and included only solid/liquid systems nowadays, the applications of dissolution studies include both solid/liquid and liquid/liquid systems.

Dissolution research is still considered an essential part of drug development as poor water solubility of drugs, dosage formulations and the kinetics of drug delivery represent the major problems still encountered in drug design [47, 48].

2.3 Porous media

The porous media is usually described as a collection of particles of different shapes and sizes [58] or as a solid material that contains voids (pores) [59]. Many materials encountered in everyday life such as soils, building materials, clothes, food and even body components are porous materials. As a consequence porous media play an important role in many technologies from various engineering fields. Besides petroleum, chemical and biochemical engineering, hydrogeology and medicine are other major areas in which porous media properties have major influence.

There are two main types of pores that can be found in porous media: *interconnected* and *noninterconnected* pores. The flow of fluid phases through porous media is only possible in the interconnected pore space. The pores which are interconnected from one side only are referred to as *dead-end* pores and they have a negligible contribution to the mass transport process.

The pore geometry influences porous medium properties at both microscopic and macroscopic level. The pore size (pore diameter/radius) is considered the most important microscopic pore structure parameter [60], but is very difficult to assess in natural porous medium due to its irregularity. At macroscopic level some of the most important pore structure parameters are porosity, permeability and specific surface area.

Porosity is defined as the fraction of pore space volume to the total volume of the porous medium. Sometimes the term *effective porosity* is employed which denotes the fraction of the interconnected pore space volume to the total volume of the porous medium. Porosity values can vary between almost 0 and 1 function of the type of porous medium. Some typical values for porosities are given in Table 2.2.

Material	Porosity
Soils	$0.5 - 0.6$
Sand	$0.3 - 0.4$
Sandstone	$0.1 - 0.2$
Limestone	$0.01 - 0.1$
Gravel	$0.3 - 0.4$
Dolomite	$0.001 - 0.15$

Table 2.2: Typical porosity values of natural porous materials [25].

Permeability refers to the conductivity of the porous medium or in other words its capacity of allowing fluids to pass through it. This parameter provides information on porous medium properties such as homogeneity and isotropy and can vary for the same porous medium as it also depends on the fluid properties and its mechanism of transport. The specific surface area can be defined as the interstitial surface area (solid-pore interface) per unit mass of the porous material. The specific surface is related to permeability and is an especially significant parameter in surface phenomena such as absorption and ion exchange.

In order for various phenomena to be described at macroscale they should first be studied at microscale as they might have different manifestations. Jia et al. considered that for the study of contaminant transport in groundwater, mass transfer should be investigated at the following 4 scales:

a. pore scale or microscopic scale (order of tens of μm);
b. pore-network scale (order of mm);
c. laboratory scale (order of cm);
d. field or megascopic scale (order of m and higher) [26].

For other applications of flows through porous media such as EOR, soil remediation or vegetable oil extraction the typical scales defined above for EAR may have different orders of magnitude. More details about the theories employed to study flows in porous media at both microscopic and macroscopic scales will be given in Section 2.6.

2.4 Liquid/liquid binary mixtures

2.4.1 Thermodynamics of binary mixtures

When considering the statics of multiphase flows the phase equilibrium of mixtures and thus the thermodynamic parameters are very important in characterizing binary mixtures. The equilibrium state of a binary mixture[1] is described by the following relation:

$$\mu_1(p,T) = \mu_2(p,T), \tag{2.3}$$

which states that besides the equality of pressures and temperatures, the chemical potentials of the two phases in contact also have to be equal for equilibrium conditions to be fulfilled. Thus, the equilibrium of a binary mixture may be represented by a surface in a $3D$ coordinate system whose axes correspond to the quantities of p, T and μ. However, for convenience, $2D$ diagrams are usually used with (p, c) or (T, c) as coordinates[2]. On the equilibrium curves depicted in such diagrams there can be two types of points: critical points (i.e. at which all properties of the phases become equal and thus phases become identical) and points of equal concentration (i.e. when the two phases in contact simultaneously coexist). Several types of phase diagrams are depicted in Figure 2.4. Usually the phase diagrams are more complicated being combinations of the ones presented in Figure 2.4, but a few simple examples of mixtures characterized by some of these types of phase diagrams are: methanol/water (**c**), formic acid/water (**d**), and methane/propane (**e**)[61].

[1]Equation 2.3 is valid when the two solvent phases in contact contain no solute. By all means, if the two solvent phases also contain a certain amount of solute dissolved then concentrations also need to be included and Equation 2.3 becomes $\mu_1(p,T,c_1) = \mu_2(p,T,c_2)$ [61].

[2]The concentration of the mixture (c) is defined as the ratio of the quantity of one of the substances to the total quantity of both and hence has values between 0 and 1 [61].

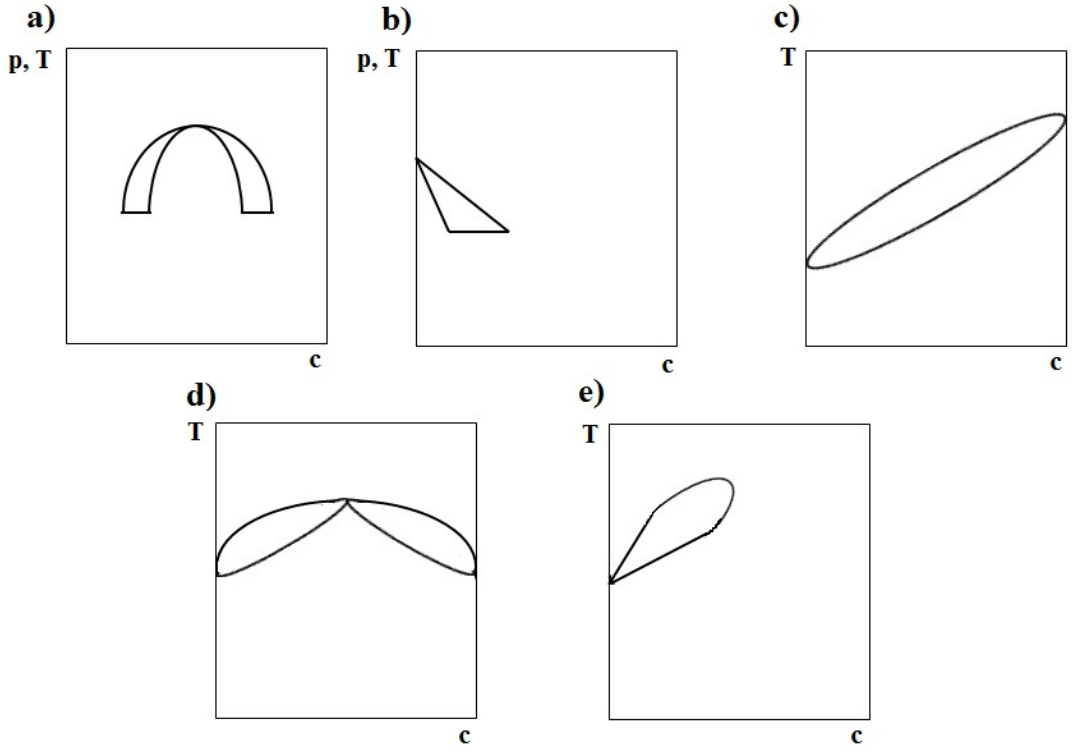

Figure 2.4: Different types of phase diagrams for binary mixtures: **a)** with point of equal concentration; **b)** for phases with low concentration at equilibrium; **c)** for components that mix in any proportion; **d)** for components that mix in any proportion and with a point of equal concentration (at the equal concentration point the mixture is called azeotropic); **e)** for liquid and gas that mix in any proportion and with a critical point [61].

The behavior of liquid binary mixtures near the critical point is very interesting. If the system has an upper critical solution temperature (UCST), when is below that, the two phases in equilibrium behave like immiscible liquids. If the temperature is suddenly increased to exceed the UCST but the system is not mechanically disturbed the interface will still remain visible for a certain time period as the mixing will occur due to diffusion which is a very slow process.

In this project the dissolution of the following binary systems: glycerol/water, soybean oil/hexane and isobutyric acid (IBA)/water will be investigated. Among these, isobutyric acid/water system is characterized by an UCST (i.e. is partially miscible at room temperature and completely miscible above $\sim 26^oC$). Glycerol/water and soybean oil/hexane are completely miscible at any temperature, in all proportions.

The phase diagram for IBA/water mixture is shown in Figure 2.5. This binary mixture is characterized by an UCST, at which the concentration and all other

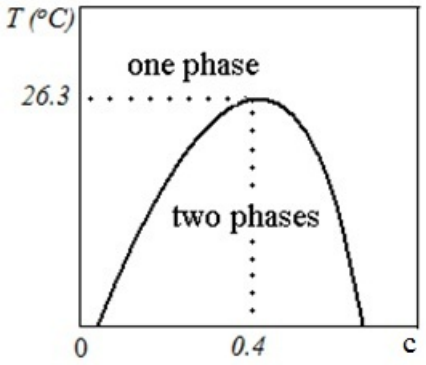

Figure 2.5: Phase diagram for IBA/water binary mixture.

properties of the two phases become equal (i.e. the phases become identical and $(\partial\mu/\partial c)_{p,T} = 0$). The critical (consolute) point of IBA/water mixture corresponds to $T \sim 26.3^oC$ and $c \sim 0.4$. More explicit phase diagrams for the IBA/water binary mixture can be found in [62] and [63]. Similar diagrams may have a minimum critical point (if the system has a lower critical solution temperature (LCST), e.g. polymers mixtures) or even two critical points, an upper and a lower one. Other partially miscible systems with phase diagrams similar to IBA/water are 1-butanol/water, 2, 6-lutidine/water and aniline/hexane.

2.4.2 Interfacial tension

The interfacial tension is a thermodynamic property that greatly influences the displacement process between immiscible and miscible fluids. When two immiscible fluids are brought into contact there is always a thin transition zone between the two phases. This transition zone can be regarded as a 'surface' near which fluids properties change due to different intermolecular interactions. In the interior of a liquid, molecules are attracted to each other equally, in all directions. The molecules found on the surface are attracted stronger by likewise molecules found towards the interior of the liquid and therefore they find themselves in unfavorable energy states. Due to this uneven attraction (Figure 2.6), molecules are continuously joining and leaving the interface and work has to be performed to increase the surface of the interface by bringing to the interface molecules from the liquid bulk. A liquid will always tend to expose the smallest possible surface area which corresponds to a state of minimum energy. The work required to increase the surface of an interface by one unit area is called interfacial tension. Usually, the interfacial tension is denoted by σ and for the case when a liquid is in contact

with its own saturated vapour the parameter σ is called surface tension. Still, the term surface tension is often employed to denote the interfacial tension between two immiscible liquids or a liquid and a gas [64, 65, 25].

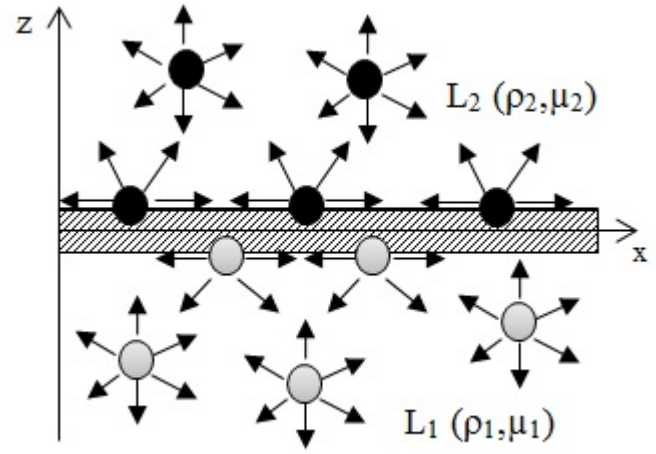

Figure 2.6: Interfacial tension between two immiscible liquids.

These differences in intermolecular forces existent in neighboring phases which explain the existence of interfacial tension on molecular level refer to both immiscible and miscible liquid mixtures and distinguish them from gaseous systems. In the case of gaseous systems the intermolecular forces are negligible and therefore no interfacial tension may appear. This idea was raised amongst others, by Korteweg [66], Zeldovich [67] and Joseph and Renardy [1]. Later, the interfacial tension between miscible liquids was measured for different binary mixtures [68, 63, 69, 70].

Because a thermodynamically stable (static) interface can only exist between immiscible fluids in the case of miscible ones the term of 'miscible interface' is used. When two miscible fluids are brought in contact, initially a sharp interface exists. In time, due to the gradients in the physical properties of the fluids the diffusion across the interface takes place and at the end of the transition the fluids finally mix (the interfacial tension decreases during the mixing process and in the end becomes zero) [1]. Several authors reported the existence of this 'miscible interface' and associated it with a dynamic interfacial tension also called effective interfacial tension (EIT). Petitjeans and Maxworthy estimated the EIT from the wavelength selection of the displacement of water into glycerine in a capillary tube [71]. Pojman et al. measured the EIT between miscible fluids (isobutyric acid/water and 1-butanol/water) using spinning drop tensiometry [63] and Zoltowski et al. used the same method for measuring the EIT between dodecyl

acrilate/poly(dodecyl)acrylate [69]. Pojman et al. [72] even set up an experiment with honey/water mixture onboard of the International Space Station.

Sometimes, due to variations in concentration or temperature that can result from dissolution processes or due to the presence of surface active molecules (surfactants) interfacial tension gradients can emerge at the interface between fluids which can lead to the developing of Marangoni instability. Further details about this type of instability can be found in Section 2.5.2 and in [73] and [64].

2.4.3 Wetting properties

The interfacial tension forces also exist at fluid/solid interfaces and they are very important because they provide information about the preferential wettability of the solid towards a certain fluid phase. For example, in petroleum reservoirs (water-wet, oil-wet or mixed wet) the interfacial tension forces between the rock and the oil are the primary reason of the increased difficulty in the recovery process [10].

When a fluid tends to spread over a solid is called a wetting fluid and if it tends to maintain a compact shape is referred to as a partial wetting or as a nonwetting fluid. When two fluids are in contact with a solid surface, the wettability of the surface depends on the chemical composition of the two fluids and of the solid. In most cases, one of the fluids will behave as the wetting fluid with respect to that solid and the other fluid will behave as the nonwetting one [25]. This situation can easily be reversed by chemical treatment of the solid surface. The parameter used to describe the wettability of a surface relative to different fluids is usually the contact angle, θ which represents the angle between the solid surface and the fluid/fluid interface [60]. If one considers a liquid/air interface like the one represented in Figure 2.7, at equilibrium, Young's equation:

$$\sigma_{la} cos\theta = \sigma_{sa} - \sigma_{ls} \tag{2.4}$$

can be applied. If $0^o < \theta < 90^o$ then the fluid is considered to wet the solid (wetting phase) and if $90^o < \theta < 180^o$ then the fluid is considered to be the nonwetting phase. In addition, there are two particular cases when $\theta = 0^o$ situation in which one of the fluids would spread completely on the solid and when $\theta = 90^o$ meaning that none of the fluids would have preferential affinity for the solid. In Figure 2.7 for example, the liquid is the wetting phase and the air is the nonwetting one.

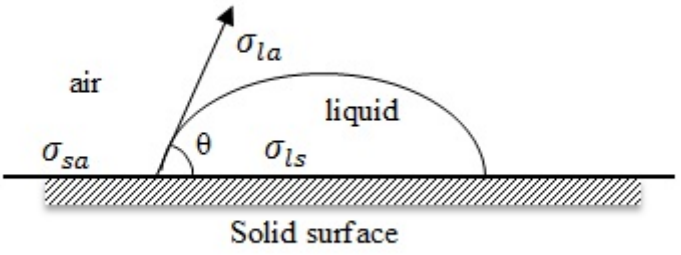

Figure 2.7: Wettability: $\theta < 90^o$, the liquid preferentially wets the solid; $\theta > 90^o$, air preferentially wets the solid.

De Gennes used a slightly different nomenclature to describe possible wetting regimes when spreading a liquid on a solid surface [65]. He described two major types of wetting based on the spreading parameter, (S): total wetting, $S > 0$ and partial wetting, $S < 0$. However, S represents a measure of the difference between the surface energy of the substrate in dry and wet conditions and in fact can be written based on the interfacial tensions between phases (i.e. $S = \sigma_{sa} - (\sigma_{ls} + \sigma_{la})$). If the spreading parameter is positive, the contact angle equals 0^o which means the spreading is complete. In the opposite case when the spreading parameter is negative a drop of liquid would not spread completely on the solid surface and it would be considered mostly wetting if $\theta < 90^o$ and mostly nonwetting if the contact angle would be between 90^o and 180^o (Figure 2.8).

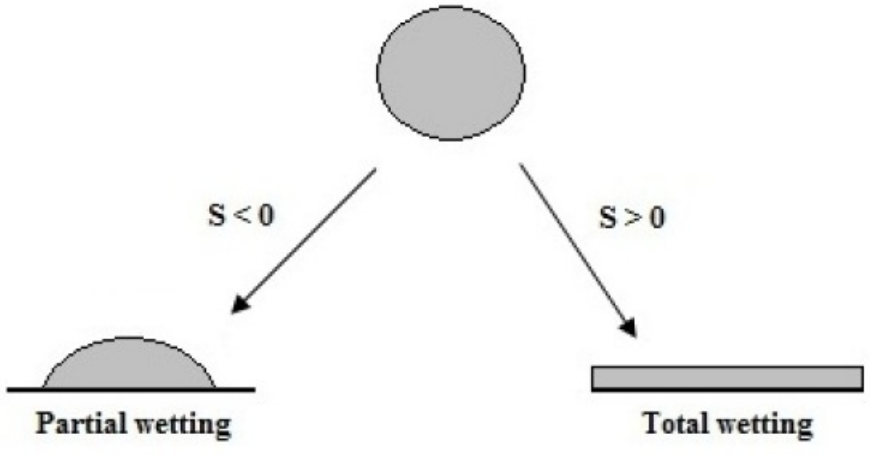

Figure 2.8: Wetting regimes characteristic to drops (redrawn from [65]).

If the interface is stationary the contact angle measured is also called static contact angle and needs to be distinguished from the dynamic contact angle, which is measured when the contact line is moving. The dynamic contact angle depends

on the velocity of the contact line and this dependence is especially pronounced in very small capillaries [74, 64]. The dynamic contact angle also depends on the direction of displacement and thus, difference must also be made between receding and advancing contact angles as they can be different for the same fluid if the fluid is the displacing or the displaced phase. The contact angle hysteresis concept was therefore employed to describe the dependence of the contact angle on the particularities of the system studied. Surface roughness and contamination of either the liquid or the solid are the main causes for which contact angle hysteresis is observed. The wettability of a surface can be greatly affected by its roughness. A hydrophilic substrate can become even more hydrophilic on a rough surface meanwhile a hydrophobic one can become super-hydrophobic [65]. Therefore when the surface involved is not smooth, the contact angle measured is often called 'apparent contact angle'. According to Dullien the measured value of the contact angle may also strongly depend on the time of exposure of the solid to both fluids [60].

There are various methods used to measure contact angles which were described by several authors [59, 60, 65, 25], but a simple prediction of a surface being or not being wettable can always be easily made based on Zisman's rule which categorizes the surfaces as high energy, on which nearly any liquid spreads (materials that are ionic, covalent or metallic) and low energy, hardly wettable (molecular crystals and plastics) [65]. In EOR for example, due to the fact that reproducible contact angles are difficult to measure in natural porous media, they can not be used as a measure of reservoirs wettability. There are three main types of systems encountered in EOR: wetted, intermediate and non-wetted systems [10]. According to Dullien, in reality the intermediate or neutral wettability regime in porous media corresponds to a range of contact angles of about 90^o, roughly $75^o \leq \theta \leq 105^o$. The wettability condition of the reservoir is very important for waterflooding and thereby for the amount of residual oil remained in the reservoir.

Wetting effects were emphasized in different studies [3, 75, 76] and the need to use square cross-section capillary tubes for simulating the porous medium from the wettability point of view was discussed by Spildo and Buckley [77] and Aguilera et al. [58].

The term of relative wettability is sometimes employed by different authors as the term of wettability is not characterized by a numerical value and therefore just a qualitative characterization is usually made by considering the relative permeability of two fluids over a solid [59].

2.4.4 Capillary pressure

Capillary pressure can be defined as the difference in the pressures of the nonwetting and wetting phases and represents a basic parameter in the study of immiscible flows through porous media [78, 60]. However, capillary pressure has to be considered even when miscible flows through porous media are investigated due to the fact that for such configurations at the beginning there are many interfaces between the fluids.

At equilibrium, the capillary pressure balances the resultant of the interfacial forces acting on a curved interface. Thus, the following equation:

$$p_c = p_{nw} - p_w \tag{2.5}$$

expresses a microscopic relationship satisfied by the pressures within the two fluids as the interface is approached from both sides [60].

Capillary pressure plays an important role when network models are considered to simulate flows of both immiscible and miscible fluids through porous media. For example, Aker et al. [79], performed numerical simulations focused mostly on the temporal evolutions of the pressure across the network and of the global capillary pressure. When the porous medium is represented as a network of capillary tubes, the capillary pressure for a tube with circular cross-section is given by the Young-Laplace equation:

$$p_c = \frac{2\sigma}{r} cos\theta \tag{2.6}$$

where θ refers to the contact angle between the nonwetting and wetting phases, r is the radius of the tube and σ denotes the interfacial tension between the two phases. Thus, the magnitude of the pressure difference at a point on the interface depends on both the radius of curvature of the interface and on the interfacial tension at that point [25].

The displacement process of a nonwetting fluid by a wetting one in a porous medium when only capillary forces account for this is referred to as spontaneous imbibition. The opposite displacement process of a wetting fluid by a nonwetting one is called drainage. In porous media for given pore shapes and wetting conditions the capillary pressure is known to vary inversely with the pore size [80], which

means that the pressure difference across the interface increases with the decrease of the radius of curvature (Equation 2.6). Hence, the penetration of a nonwetting phase will always take place in the direction of decreasing pore diameter.

At macroscopic level, the relation between the capillary pressure and the saturation of the porous media is given by the capillary pressure curves. Their shape can characterize the wettability of the pore-space as it depends on the contact angles. Furthermore, capillary pressure exhibits the effect of hysteresis, fact that can be explained by the hysteresis between the advancing and receding contact angles. According to Hassanizadeh and Gray the standard approaches for describing macroscale capillary pressure are simple extensions of microscale concepts and the equations used are not adequate for macroscale description. They propose an alternative approach in which they relate the capillary pressure with the change in free energy of the two fluid phases and all three interfaces that accompanies a change in saturation [81].

2.5 Mass transfer in binary mixtures

2.5.1 Diffusion

Diffusive mass transport is ubiquitous in several engineering fields and plays an important role in the study of multiphase flows in porous media. Diffusion is the process through which mass is being transported from one part of a system to another due to random molecular motions [82]. Diffusion is an irreversible process leading to equalization of the concentration by direct changes of composition [83].

In the past decades there have been a large number of theoretical and experimental studies on diffusion in porous media but most of them were concerned with gaseous diffusion [84, 85, 86, 87] and/or diffusion of minor impurities in a liquid saturated porous medium. Even though there have been also a reasonably high number of theoretical and experimental studies on dispersion in porous media, in all these studies the diffusion process was described based on the classical model of minor impurity. Hydrodynamic dispersion includes both convective and diffusive mass transports. At low fluid velocities, solute dispersion is determined by molecular diffusion and for high values of velocity convection dominates, but still the contribution of diffusion cannot be neglected [88]. In most dispersion studies, diffusion coefficients and velocities were measured by employing NMR techniques

[89, 90]. A thorough analysis of the data presented in the literature up to date to characterize dispersion in porous media can be found in [88].

For modeling miscible two-phase flows within capillary tubes many authors have also performed numerical simulations and developed different theoretical models by employing the diffusive interface approach [2, 91, 7]. The problem with these models is that they were all based on Stokes equations which means that in the equation expressing the balance of mass:

$$\frac{\partial c}{\partial t} = \nabla \cdot (D \nabla c) \tag{2.7}$$

the gradient of concentration is considered instead of the gradient of chemical potential.

The interfacial tension effects influence the dissolution dynamics both through the morphology of the interface and the rate of the mass transfer through the interface [92]. For immiscible liquids the interfacial tension is sufficiently high to exclude the co-diffusion of molecules. The mass transfer through the interface will be not zero for miscible mixtures but its rate will be limited by the surface energy effects. This results from Fick's law which states that the linear proportionality between the diffusive flux and the concentration gradient is invalid for strong solutions. Thus, equation:

$$\mathbf{J} = -D \nabla c \tag{2.8}$$

is only valid for ideal mixtures.

For example, for an equilibrated heterogeneous binary system there is a strong concentration gradient across the interfacial boundary, but no interfacial diffusion. An equilibrium state of a binary mixture is defined through the equality of the chemical potentials of the adjoining liquids. Therefore, when a binary system is taken out of its equilibrium the interfacial mass transport generated should be described based on the gradient of the chemical potential through the interface. For an isothermal system the diffusive flux can then be written as:

$$\mathbf{J} = -\alpha \nabla \mu, \tag{2.9}$$

where α is the mobility coefficient. In this case the expression for the chemical potential,

$$\nabla\mu = (\partial\mu/\partial c)_{p,T}\,\nabla c + (\partial\mu/\partial T)_{c,p}\,\nabla T + (\partial\mu/\partial p)_{c,T}\,\nabla p, \tag{2.10}$$

will already include the effects of thermo- and barrodiffusion [83]. These effects would then be taken into account when dissolution rates are being calculated. For isothermal systems, temperature gradients could only be generated in the system due to the enthalpy of mixing. For example, the enthalpy of mixing for glycerol/water mixture is approximately $-100\,J/mol$ for very small and very large concentrations of glycerol and reaches a minimum value (i.e. $H^E \sim -600\,J/mol$) around a molar fraction of glycerol in the mixture of 0.4 at 25^oC [93, 94]. However, the temperature gradients possibly induced by mixing should be rather small and the amount of heat released due to mixing should not be significant.[3] Thus, in this case the second term of Equation 2.10 can be neglected. The last term of Equation 2.10 should be taken into account when there is a considerable pressure gradient in the fluid [83]. Variations in pressure field can be induced for example, by gravity and capillary forces. A set of governing equations for slow dissolution processes was recently obtained by Vorobev [92].

The diffusive dissolution of a drop in a capillary has been studied theoretically by Ugrozov et al., who developed a model for the rate of dissolution of drops and the time of complete dissolution function of physico-chemical parameters such as solubility concentration and diffusion coefficients [6]. They treated the problem as one-dimensional and derived the expression for the dissolution rate of a poorly soluble liquid droplet in a capillary tube obtaining:

$$\frac{dL_d}{dt} = -\frac{c_1}{\sqrt{3-2c_1}}\sqrt{\frac{D}{t}} \approx -\frac{c_1}{\sqrt{3}}\sqrt{\frac{D}{t}}, \tag{2.11}$$

where L_d is the length of the droplet, and c_1 is the solubility. The mathematical model of Ugrozov et al. was also reduced to Fickian diffusion process, and hence, the predicted dissolution rate followed the classical diffusion $t^{-1/2}$ time dependence, but in real porous media the dissolution process is more complex.

[3]Enthalpy of mixing is considerably smaller in comparison to enthalpies of vaporization or fusion. For example, the enthalpy of vaporization of water (at its boiling point) is greater than $4 \cdot 10^4 J/mol$.

Despite an apparent simplicity of the dissolution it is difficult to provide a simple estimate for the typical dissolution time in porous media. In this case, even if the simple Fickian diffusion law (Equation 2.7) is accepted, which is frequently done [2, 95], it is unclear which length scale should be associated with the porous media. Natural porous media are very complex and could have many length scales associated with them [96].

In numerous contexts anomalous diffusion (also referred to as 'restricted diffusion') is more adequate for describing fluid dynamics in porous media (i.e. both for hydrodynamic dispersion and in the absence of flow (pure diffusion) [96]). Anomalous diffusion is usually divided into two different regimes: subdiffusive (slower than Fickian diffusion, $n < 1$) and superdiffusive (faster than Fickian diffusion, $n > 1$). In these cases the root-mean-square value of the displacement of the particles is not proportional with time:

$$(\Delta x)^2 \propto t^n, \tag{2.12}$$

as in the case of Fickian diffusion ($n = 1$) [97]. Both regimes of anomalous diffusion can be identified in natural porous media due to their very complex microstructures.

Fomin et al. also reinforced the idea that the conventional diffusion equation based on Fick's law is not appropriate to model diffusion in porous media as the diffusive mass transport observed in experiments has an anomalous character and they provide new equations that can be used for describing anomalous mass transport [98]. Glimm and Sharp have also shown that the mixing length between two fluids in heterogeneous media has an anomalous diffusion behavior $l_m = O(t^\alpha)$ for $1/2 \leq \alpha \leq 1$, where α is a scaling exponent which characterizes the mixing behavior [99]. They obtained $\alpha \approx 0.875$ but stated that α is not a universal constant and depends on the heterogeneity of the porous media. They also mentioned that in various contexts besides the heterogeneity of the porous medium anomalous diffusion could also arise from a nonlinear diffusion equation and due to random velocity fields. More details on modeling anomalous diffusion in heterogeneous porous media can be found in [100] and [101].

2.5.2 Hydrodynamic flows (Convection)

The mass transfer in binary mixtures can also be driven by convective flows. For isothermal systems, as the ones studied in the current work, the convective flows are induced by variations in concentration. There are two types of convective flows, the buoyancy-driven ones generated in the bulk and the flows induced at the interface by the interfacial tension gradients.

At the interface between two liquids, interfacial tension gradients can generate convective flows, thus affecting the evolution of the interface. These interfacial tension gradients can arise due to heat and mass transfer processes occurring at the interface (i.e. differences in temperature and concentration leading to thermocapillarity and solutocapillarity as forms of the Marangoni effect.) The flows generated by these gradients are also known as Marangoni-driven flows [64]. Their role can be estimated by the Marangoni number, which for the case of solutocapillarity can be written as follows:

$$Ma_s = \left|\frac{d\sigma}{dc}\right| \frac{L\Delta c}{\eta D}. \tag{2.13}$$

The solutal Marangoni effect and thus the role played by dissolution in interfacial instabilities was studied experimentally in [102, 103, 73, 104]. In [102] was studied the motion of a nitroethane lens located at the surface of an aqueous solution of surfactant. The motion of the lens was generated by a solutal Marangoni effect induced by the transfer of the surfactant from one phase to the other. In [103] the same system nitroethane/water/sufactant was investigated, but in this case the focus was on the interfacial instabilities caused by the dissolution of nithoethane and its effect on the lens behaviour. The dissolution of nitroethane into the aqueous solution induced the distortion and the motion of the lens. Nitroethane and water are partially miscible liquids and thus as long as the system is not in thermodynamic equilibrium transfer of each constituent can occur across the interface. In this case the role of the surfactant was only to decrease the aqueous surface tension and to prevent the spreading of the lens on the aqueous surface. The spreading of a nitroethane drop on the free surface of a water layer was investigated in [73] and [104]. In [73] particular emphasis was placed on the pattern formation and its evolution (surface waves and their interactions) meanwhile, in [104] the focus was on the spreading process. In the latter work it was found that the spreading of partially miscible liquids follows power laws and their values are largely influenced by dissolution.

Buoyancy driven convection or solutal convection is the second type of convective motion and is generated by density differences in the bulk phases. The role of the solutal convection, for instance, can be estimated by the following analogue of the Rayleigh number,

$$Ra_s = \frac{g\Delta\rho L^3}{\eta D}, \tag{2.14}$$

where $\Delta\rho$ is the density contrast between the liquids, η is the mixture viscosity, D is the diffusion coefficient and g is the gravity acceleration. Ra_s is constructed similar to the classical Rayleigh number and should be considered as the ratio between the diffusive and convective time scales. Still, the typical size L is not well defined in Equation 2.14, but it is generally presumed that the hydrodynamic flows are suppressed or at least significantly dampened in capillary tubes due to their small diameters. The occurrence of solutal convection in the bulk can also indirectly give rise to interfacial tension gradients at the interface leading to Marangoni-driven flows.

The flows induced by the above-defined bulk- and surface-mechanisms occur in general, simultaneously. Traditionally, however, in the terrestrial conditions, the solutal convection dominates, except in the cases of very thin film layers and of zero buoyancy (e.g. for two liquids with matched densities).

In some sense, the effect of solutal convection can also be interpreted as the gravity current, also called the lock-exchange flow [105, 106, 107]. Such a flow is induced if two liquids of different densities are initially separated by a vertical barrier, which is then removed. For instance, Zukoski [105] examined the motion of an air bubble in long closed tubes of different diameters ($> 0.5\,cm$) and with different inclinations. It was found that the bubble moved with a time-independent velocity,

$$v_b = b\left(\frac{\Delta\rho}{\rho} gd\right)^{1/2}. \tag{2.15}$$

In Equation 2.15, the coefficient b depends on the angle of inclination, viscous effects, and on the ratio between the gravity and capillary forces. In tubes of small enough diameter, when the effect of surface tension increased, the bubble motion ceased. The interplay between the gravity and capillary forces can be defined by the Bond number,

$$Bo = \frac{\Delta \rho g d^2}{\sigma}. \tag{2.16}$$

In [105], the bubble motion ceased completely for $Bo < 1.5$.

2.5.3 Capillary motion (Imbibition/Drainage)

Capillary forces can also induce the motion of a liquid/liquid interface. Capillary forces are determined by the capillary pressure defined for the tubes of circular cross-section as in Equation 2.6. The equation is written assuming that the meniscus is axisymmetric, but this symmetry may be broken by the gravity effect, i.e. when $Bo < 1$.

The speed of the interface driven by the capillary pressure is defined by the simple formula of Washburn [108],

$$v_{imb} = \frac{p_c}{32} \frac{d^2}{\eta L_0} \tag{2.17}$$

where L_0 is the length of the capillary tube. It should be also taken into account that for a miscible system which is not in its thermodynamic equilibrium, the values of both the interfacial tension coefficient and the contact angle in Equation 2.6 are time-dependent. The ratio between the diffusion rate and the speed v_{imb} determines whether this time-dependence is important.

There are two types of immiscible two-phase displacement that can occur in porous media due to capillary forces: imbibition and drainage. When a nonwetting phase is being displaced by a wetting phase solely due to the capillary pressure the process is called *spontaneous imbibition*. If the displacement of the nonwetting phase by the wetting phase occurs under the influence of an external pressure gradient applied, then *forced imbibition* is the right term to use for this process. In the opposite case, when a wetting phase is displaced by a nonwetting one the process is called *drainage*. Drainage can also be forced or spontaneous. Most of the time, in the literature, the simple term *imbibition* is employed and used for either spontaneous or forced imbibition [60]. Another term frequently encountered in the literature is the one of *controlled imbibition* which is assumed by many to correspond to spontaneous imbibition. This assumption is considered to be wrong and according to Rose this process should be seen as a hybrid between spontaneous and forced imbibition [109].

The huge amount of research focused on imbibition and drainage in porous media consists of studies in which two-phase fluid displacements in capillary tubes, columns filled with different types of glass beads or sand and/or micromodels were analyzed theoretically and experimentally. There are a large number of studies on controlled/forced imbibition/drainage in all three systems (i.e. capillary tubes, packed columns and micromodels), but only very few dealing with spontaneous imbibition/drainage especially for capillary tubes and micromodels. Capillary driven flows in glass beads models [110], cores and sand pack models made of glass beads [111] or sands [112] are only briefly mentioned herein. The most relevant studies for imbibition/drainage in capillary tubes and micromodels are discussed in Section 2.7.1 and Section 2.7.2.

In general, there are two main mechanisms which characterize fluid displacement at the pore level in both imbibition and drainage: piston-like displacement and snap-off [113, 75]. Snap-off and piston-like mechanisms are different and mutually exclusive [110, 114]. It is considered that snap-off can only occur if piston-like displacement is topologically impossible [75].

The piston-like displacement describes the advancement of the displacing fluid in a connected front occupying the center of the pore space yielding to a complete sweeping from the pore of the displaced fluid (i.e. the displacing fluid enters the pore by pushing the displaced fluid in front of it). During an imbibition type displacement the filling of pores through this mechanism is more complex as it depends on the number of nearest neighbours that are already filled with the wetting phase [75]. The way a pore may be filled depending on the number of surrounding throats already filled with wetting fluid was first described by Lenormand et al. [113]. For example, if a lattice has a coordination number z, there are z imbibition mechanisms possible (i.e. I_0 to I_{z-1}) which represent filling of a pore when 0 to $z-1$ connecting throats contain nonwetting fluid. The capillary pressures decrease in the following order: $p_c(I_0) > p_c(I_1) > ... > p_c(I_{z-1})$. The I_0 mechanism can only occur if the nonwetting phase is compressible and the I_z mechanism is impossible if the pores are larger than the throats as in capillary equilibrium the wetting fluid must occupy at least one of the attached throats before the pore is filled [75]. Later, Al-Gharbi and Blunt described three different types of piston-like displacement: invasion of a single pore branch or throat side, invasion of a pore center and menisci fusion [115].

In the second mechanism, snap-off, a thin film of wetting phase flows along crevices in the pore space, pinching off the nonwetting phase in the middle of the pore

throat and filling pores in advance of the connected front [75, 114]. Snap-off can occur in both imbibition and drainage [115] but, according to [114] is more likely to happen in imbibition. The snap-off capillary pressure depends on the pore geometry, contact angle and interfacial tension as well as on the fluid occupancy in the neighbouring pores. As a consequence the dynamics of the system can greatly influence the snap-off occurrence. Snap-off dominates at small capillary numbers and the probability of its occurrence decreases with the increase of the capillary number. Capillary numbers between $10^{-8} - 10^{-7}$ are considered to be a transition between snap-off and piston-like mechanisms and in general, the possibility of snap-off is higher with longer aspect ratio [114].

Trapping of the displaced fluid is possible in both imbibition and drainage when clusters disconnected from the moving part are formed. However, according to [114], the trapping is more significant during imbibition and is usually caused by the snap-off mechanism yielding to the entrapment of the nonwetting phase. Phase trapping which is also referred to as residual saturation depends significantly on the dynamic parameters that characterize the displacement including the capillary number, viscosity ratio, aspect ratio, interfacial tension and contact angle. Phase trapping (residual saturation) can be reduced by either suppressing the snap-off mechanism or by mobilizing the disconnected blobs. Snap-off can be suppressed by decreasing the capillary forces in comparison with viscous forces. Thus, this entails the increasing of the capillary number, decreasing of the interfacial tension and decreasing the wettability for the probability of snap-off to be decreased [114].

2.6 Description of mass transport in porous media on macro- and pore-level scales

The evolution of multiphase systems can be described by two different approaches. The first approach entails a microscopic (pore-level) description. The second approach entails a macroscopic description in which the fluids and the porous medium are treated as continuum media. Hence, in this case, the behaviour of the phases within the porous medium is described by the averaged values of variables and material properties. Thus, two-phase flows in porous media are described by macroscopic equations which usually represent various generalizations of Darcy's law for single-phase flow in porous media [60].

2.6.1 Macroscopic theory

Macroscopic theories are employed to study multiphase flows through porous media when is impractical to use a microscopic description due to the great complexity of the natural porous media and thereby of the difficulty of describing the complex solid/liquid boundaries at microscale. However, it must be considered that various macroscopic manifestations can result from different aspects of the flow at microscale [10].

All the analysis of multiphase flows through porous medium at macroscopic scale start with Darcy's empirical law which is a fundamental building block for modelling flow through porous media for both immiscible and miscible fluids [25]. Darcy's equation is used rather successfully to investigate macroscopic phenomena without considering the microscopic variations involved.

The original form of Darcy's law $Q = K_h A \Delta h / L$ was obtained by examining experimentally the laminar flow of a single fluid through homogeneous porous media. In this expression K_h is a proportionality constant (also called hydraulic conductivity), A is the cross-sectional area of flow, Δh is the head difference, L is the length of the sample and Q is the volumetric flow rate [116, 25]. In its original form, Darcy's law is highly restricted hence various differential forms were obtained that can be used to characterize different types of flows through porous media [59]. Admittedly the extension of Darcy law to account for multiphase flows is more problematic.

For single phase flow the differential form of the law can be written as:

$$\mathbf{q} = -\frac{k}{\eta}\nabla p \tag{2.18}$$

and together with the continuity equation and the relationship between density and pressure:

$$-\phi\frac{\partial \rho}{\partial t} = div(\rho \mathbf{q}) \tag{2.19}$$

$$\rho = \rho(p) \tag{2.20}$$

can be used to characterize any single phase flow problem. Obviously, the boundary conditions also need to be considered in order to have a complete description of the problem. In these equations $\mathbf{q}$ is the seepage velocity vector, k the permeability, η the viscosity, p the pressure, ρ the density of the fluid and ϕ the porosity. The law is considered to be valid as long as the Reynolds number ($Re = \rho v L/\eta$) does not exceed a value of about 1 but, sometimes can still remain valid for Re numbers as high as 10 [25].

This macroscopic form of Darcy's law (Equation 2.18) can be derived starting from the momentum balance equation at microscale by employing an averaging approach (i.e. the representative elementary volume (REV) averaging approach, the homogenization approach or the mixture-theory approach) and making use of various simplifying assumptions. Any resultant macroscopic counterpart obtained from a microscopic physical law by any averaging technique will always be dependent on the set of simplifying assumptions introduced [25].

For the case of two-phase immiscible flows, these equations can be extended by denoting the two phases with subscripts and assuming the validity of Darcy law for each phase. The following set of equations is then written:

$$\mathbf{q_1} = -k\frac{k_1}{\eta_1}\nabla p_1 \tag{2.21}$$

$$\mathbf{q_2} = -k\frac{k_2}{\eta_2}\nabla p_2 \tag{2.22}$$

$$-\phi\frac{\partial(\rho_1 s_1)}{\partial t} = div(\rho_1 \mathbf{q_1}) \tag{2.23}$$

$$-\phi\frac{\partial(\rho_2 s_2)}{\partial t} = div(\rho_2 \mathbf{q_2}) \tag{2.24}$$

$$s_1 + s_2 = 1; \quad \rho_1 = \rho_1(p_1); \quad \rho_2 = \rho_2(p_2); \quad p_2 - p_1 = p_c(s_1). \tag{2.25}$$

In these expressions k is the total permeability, k_1 and k_2 are relative permeabilities, s_1 and s_2 are saturations and p_c is capillary pressure. This non-linear system is very difficult to be solved analytically, because too many functions need to be introduced and defined depending on various porous media. Moreover, the

key weakness of the model described by Equations 2.21–2.25 is the use of infinitely many phenomenological parameters which are hidden in the functions $k_1(s)$, $k_2(s)$, and $p_c(s)$. In some special cases, however, solutions were still obtained.

One solution was obtained by Buckley and Leverett by using the assumptions of neglecting gravity, capillarity and variations in density. Further details about solving the system and the solution obtained can be found in [59]. For the specific case when imbibition of a porous media is considered the relation between capillary pressure and saturation is given by the so called "Leverett J-function":

$$J(s) = \frac{p_c}{\sigma}\left(\frac{k}{\phi}\right)^{1/2}. \tag{2.26}$$

Its expression is used to modify accordingly Darcy's law for the case considered. According to Scheidegger, this extension of Darcy's law to multiphase flow is just a heuristic procedure suggested by the analogy with single phase flow has the same limitations as the law for single phase flow and can not provide a good understanding of the physics of multiphase flow [59]. Still, the law must be at least partially correct as there were experimental results with which it could be correlated [59].

In the case of miscible two-phase flows, the equation derived from Darcy's law was proved to be inadequate by experiments even with the assumption that the mixture can be considered as a single phase fluid for which the change in concentration is due to diffusion when complete miscibility is achieved. Hence, miscible multiphase flows cannot be described by equations obtained from the generalization of Darcy's law for single phase flow [59].

The current macroscopic theory used to describe miscible flows in porous media is the dispersion theory. Hydrodynamic dispersion includes both convection and molecular diffusion with a more significant effect of the latter at low velocities. The influence of convective and diffusive effects can be evaluated with the aid of Peclet number (i.e. $Pe = Lv/D$). In time, several researchers have concluded that a Fickian-type law cannot characterize the dispersion, not even in a relatively homogeneous porous medium and thus, non-Fickian dispersion models began to be considered [25].

The advantages of using a macroscopic theory to analyze different phenomena in porous medium (e.g. dispersion) were emphasized by Sahimi along with the associated mechanisms and models (i.e continuum and discrete) used to describe

these phenomena [3]. In time, various mathematical models have been developed in order to attain an accurate quantitative description of two-phase flows in porous media: capillaric models, statistical models, empirical models and network models. Even though the empirical models were considered the practically useful ones, the network models have proven to have the best potential in achieving a better understanding and a more accurate quantitative description of two-phase flow phenomena in porous medium [60].

2.6.2 Pore-scale models

The description of two-phase flows in porous media at macroscale does not always account for important microscale effects (e.g. capillary, viscous and gravitational forces) with consequences at macroscale and thus, these effects must be studied first at microscale. This is usually achieved by employing pore-scale models.

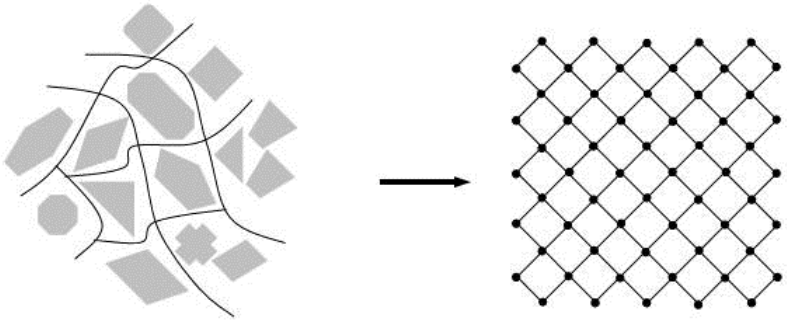

Figure 2.9: Modelling of porous medium by a network of pores and throats.

Pore-scale models allow the evaluation of some important dynamical properties of porous medium and transport coefficients at microscale and are usually either mathematical models used mostly for computer simulations of flow phenomena or physical models used for flow visualization studies [3]. In recent years pore-scale modeling has become one of the most popular approaches for studying the physics of flow and transport in porous media. With the aid of the network approach (Figure 2.9), the porous medium can be roughly represented as a network of interconnected capillary tubes [79, 117, 118]. Thus, in the last few decades the number of publications that use pore-level modelling to describe various important characteristics of multiphase flows like capillary pressure, interfacial area or mass transfer coefficients has significantly increased. This is mainly due to the advances made in visualizing the pore space and the increase in computational power [119].

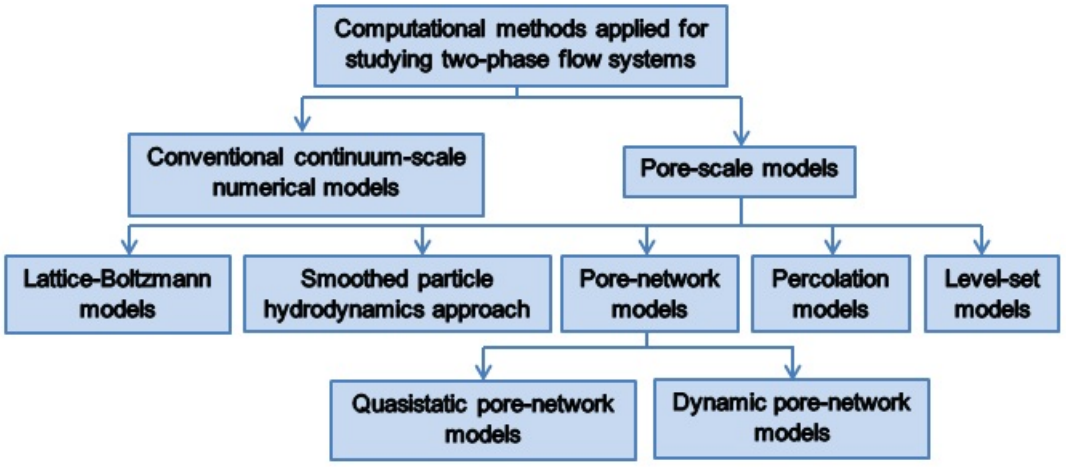

Figure 2.10: Classification of computational methods applied for studying two-phase flow systems according to Joekar-Niasar and Hassanizadeh [114].

All the analysis of two-phase flows through porous media started with theoretical studies and the development of many network models or/and experimental studies of flows in simple geometries like Hele-Shaw cells, capillary tubes or/and micromodels. According to Petitjeans and Maxworthy the flows in Hele-Shaw cells are regarded as the limiting models for two-dimensional motion in extended porous medium and the flows in capillary tubes are considered to represent the simplest model of displacement in just one pore of such a medium [71]. However, laboratory experiments can be expensive and time-consuming and thus, theoretical and computational approaches are increasingly used as complementary or substitute tools for the study of two-phase flows in porous media [114]. According to Joekar-Niasar and Hassanizadeh the computational methods employed for studying two-phase flow systems can be classified as shown in Figure 2.10. In [114] the advantages and disadvantages of each method are discussed with the most representative studies also being referenced. Yet, in this review the emphasis is placed on the dynamic pore-network models which are discussed in more detail. In comparison with quasistatic pore-network models which can only simulate equilibrium states [120], dynamic pore-network models are adequate for studying the transient behavior of multiphase flows.

Since the first network model developed by Fatt in 1956 many other pore-scale network models were developed to study a multitude of diverse phenomena including various aspects of dissolution processes (e.g. dissolution rate coefficients [121], nonequilibrium NAPL dissolution [122], mass transfer between two fluid phases [123], dissolution of entrapped NAPL and the connection between microscale

and macroscale phenomena [124] and effective diffusion coefficients [95]), capillary pressure-saturation and capillary pressure-interfacial area relationships [125], imbibition and drainage displacements [79, 118, 115], wettability [75, 126, 127, 128] and multiphase flows [117, 115]. Other topics studied with the aid of pore-scale models were related to single phase permeability, relative permeability and capillary pressure hysteresis and hydrodynamic dispersion [122, 117].

Most of the results obtained from the development of pore-network models, both quasistatic and dynamic were compared with results of displacement experiments within micromodels or columns packed with various materials such as glass spheres or sand. For more detailed information about any of the pore-network models mentioned and more, the two excellent reviews of Blunt and Joekar-Niasar and Hassanizadeh are highly recommended [120, 114]. Experimental pore-scale studies employing micromodels are described in Section 2.7.2. The large number of studies on pore-scale experiments and modelling of multiphase flow dynamics emphasizes the importance of understanding the complexity of these types of flows not only at microscale, but also when applied to practical applications.

2.7 Current research of multiphase flows within capillaries and micromodels

2.7.1 Theoretical and experimental studies employing capillary tubes

Usually, both theoretical and experimental investigations of flows in natural porous media are too complicated due to the complex geometry of such media and therefore simpler geometries have to be employed for their simulation. Capillary tubes are among the simplest geometries widely used to simulate the channels of a porous medium and thus to simplify the studies of flows in porous media.

The imbibition in capillary tubes has been experimentally studied by Washburn [108] and Chertcoff et al. [129]. They found that Equation 2.17 correctly predicts the propagation of a more wetting liquid into a capillary tube.

In other related studies, Taylor [130] and Cox [131, 132] examined the displacement of a liquid by air from the capillary tube driven by external pressure difference. Similar experiments were also fulfilled by Soares et al. [133] with the use of two

immiscible liquids. They noted that air (or an injected liquid in the case of Soares et al.) breaks through the central part of the tube, and some amount of the liquid, that initially occupied the tube, remains on the walls of the tube. Later, Soares et al. also studied theoretically the gas-displacement of non-Newtonian liquids in capillary tubes [134]. Imbibition experiments with oil displacing air into independent tubes and groups of capillaries were also performed by Unsal et al. [135, 136]. Other experimental observations of spontaneous imbibition in square capillaries were reported by Spildo and Buckley [77].

Zorin and Churaev [137] also studied immiscible liquid/liquid spontaneous displacement and the displacement under external pressure gradients in thin quartz capillaries. They used both hydrophilic quartz capillaries and hydrophobized ones and studied the influence of viscosity, flow rate, formation of equilibrium and nonequilibrium wetting films, contact angles and the lyophilicity of the capillaries surface. They used mixtures of different hydrocarbon liquids and water and concluded that at very low rates of spontaneous displacement, when water displaces various hydrocarbon liquids the advancing contact angles are not disturbed by the slow motion of the meniscus (i.e. the contact angles are almost constant and equal to the static contact angle for water on quartz). In the case of forced displacement, thick nonequilibrium wetting films were formed behind the retreating meniscus. When flow rates were increased the displacement efficiency decreased due to the capillary instability which caused coalescence of the thick films. In the case of hydrophobized capillaries the results of the forced displacement were different due to the fact that the hydrocarbon liquids completely wet the walls of the capillaries and thus no dynamic wetting films of water are formed after the retreating meniscus [137].

Other theoretical and experimental works in which the motion of bubbles in capillary tubes was considered are the ones of Bretherton [138], Levich [139] and Starov et al. [140]. Bretherton studied the motion of a long bubble in a capillary tube both theoretically and experimentally and found that the bubble moves with a slightly higher velocity than the fluid in the tube. The fractional correction of the velocity was found to be proportional to $3Ca^{2/3}$ [138]. In [140] the motion of a long oil bubble under the action of an imposed pressure difference was investigated theoretically in a thin capillary filled with another immiscible fluid. In this work the velocity of the drop was calculated as a function of the pressure difference (including the disjoining pressure) and the thickness of the film between the bubble and the capillary walls. The solution obtained was in good agreement with Bretherton's equation [138] at high velocities but it was substantially different at

low velocities due to the action of the disjoining pressure in the thin film. The concept of disjoining pressure was introduced by Derjaguin around 80 years ago [141] and the disjoining pressure isotherms form a fundamental basis for understanding and controlling practically important phenomena such as wetting, spreading, capillary condensation and mass transfer in porous bodies partly saturated with liquid [142]. Derjaguin's equation is usually employed to describe the profile of the transition zone that forms between a wetting film coating a surface and the meniscus of the bulk liquid. Within this transition zone the surface forces and the capillary forces act simultaneously [143].

The research on the displacement of a viscous fluid by a less viscous one was extended to also address the displacement of miscible liquids in both experimental and theoretical studies [71, 2, 91, 144, 145, 7]. Experiments with miscible interfaces were carried out with mixtures of glycerol/water [71, 145] and of two different silicone oils [144]. In these studies the tube was initially saturated with a more viscous liquid, which was then displaced by a less viscous liquid by applying an external pressure gradient. The velocity of the induced hydrodynamic flow substantially exceeded the diffusion rate with the typical Peclet numbers (Pe) of about 10^4. The liquid/liquid dissolution was not considered in these works [71, 144, 145]. For example, in [71] the main focus of the work was the investigation of the amount of fluid left on the wall of the tube function of Pe number and viscous and gravitational effects. The results obtained were compared with Taylor's experimental results for immiscible displacement [130] and with the numerical simulations of Chen and Meiburg [2]. The instability of miscible interfaces in a cylindrical tube was studied experimentally by displacing a less viscous liquid by a more viscous one (silicone oils) in vertical capillary tubes [146]. Even though capillary tubes were predominantly used for studying immiscible and miscible displacements, they were also frequently employed for wettability related studies [74, 147, 148, 149].

Only a few works could be found in the literature in which diffusion in capillary tubes was considered. Enhanced CO_2 diffusion in hydrocarbons (i.e gas/liquid system) was studied by Aguilera et al. in both circular and square cross-section capillaries [58]. They found substantial differences in the rates of mass transfer function of the type of capillary used (diffusion coefficients calculated from experimental data were one order of magnitude larger for square capillaries than for circular ones). Furthermore, the different behavior of a liquid bridge in square and circular capillaries was accounted on the lack of the liquid film on the walls of the circular capillary. In the experiments of a shrinking bubble they also considered

that the enhancement of diffusion in square capillaries is due to the density gradient and the increased surface of the interface (because of the liquid filaments in the corners) and thus the appearance of convective diffusion in comparison to the circular capillary in which the length of the bubble could be plotted function of the square root of time with diffusion being the only mechanism present [58]. The only other theoretical work that describes the diffusive dissolution of a poorly soluble droplet in a capillary tube is the one of Ugrozov et al. [6] which was described in more details in Section 2.5.1.

More recent studies involving capillary tubes are the ones of Bouzid et al. and Foroughi et al. [150, 151]. In the former work observations were made on the NaCl precipitation in capillary tubes which increased the heterogeneity of the system and apparently closed the capillary at the two liquid/air interfaces. After 3 months the authors observed the cavitation of a vapor bubble behind the NaCl plugs and deduced that the plugging was almost complete with a very small annular space (i.e. invisible with an optical microscope) remaining open between the capillary tube and the NaCl plugs [150]. In the latter study the immiscible displacement of a silicone oil by water was investigated in a circular capillary tube. This viscous fingering phenomenon has been extensively studied before in order to predict the thickness of the oil film left on the walls of the tube. The correlations developed did not always predict accurately the film thickness in part because of stability problems. In this study a film thickness of 3 μm could be identified for higher flow rates, but for the lowest flow rate tested corresponding to a capillary number equal to $2 \cdot 10^{-6}$ the oil film could not be observed [151].

2.7.2 Theoretical and experimental studies employing micromodels

Micromodels are $2D$ transparent networks of pores and constrictions widely used for the study of flow processes at the pore level. Micromodels can simulate the complexity of natural porous media just up to a certain degree [24]. Still, they allow tracking the interfaces position and movement through the porous network, which makes them valuable utensils for multiphase flows studies. Micromodels applications result from their important role in understanding some of the effects that pore geometry and topology, fluid properties and the interplay of capillary, viscous and gravity forces have on the flow dynamics at the pore scale.

In the past few decades numerous experimental studies have been reported in the literature which employ micromodels for studying a large variety of pore-scale mechanisms characteristic to EOR and EAR processes. Besides petroleum engineering and geological applications there are many other fields in which micromodels find their applicability, as for instance drying technology [152].

Even though the first who ever employed an etched glass network model (i.e. micromodel) in his study was Kyte in 1961 [153], the use of micromodels increased continuously after 1980 and exploded after 2000 when better techniques became available for their manufacturing. The most commonly employed technique to fabricate micromodels is the etching. In time the technique was improved and resulted in the developing of micromodels with a wide variety of regular and irregular patterns and very accurate dimensions. Detailed fabrication techniques of both silicon and glass micromodels can be found in [153, 154, 155, 152, 156, 157]. Some of the successes and limitations of micromodels in illustrating the mechanisms of multiphase flows as well as the early approaches employed to design and fabricate micromodels are described in Buckley's review [153]. The author divided the network models in two categories: initially water-wet glass and silicon models (high energy surface) and resin models (low energy surface). Aside from the network models, Buckley also described different other types of models under the name of micromodels such as bead packs, single pore and rock models. More details about fabrication techniques, examples of various micromodels with regular and irregular patterns and several applications can be found in the reviews of Buckley and Blunt [153, 120].

As previously mentioned the most commonly studied applications for which micromodels are being increasingly used are enhanced oil recovery and soil and aquifer remediation. Micromodels have been extensively used for investigating ways of recovering additional oil via different enhanced oil recovery techniques such as alkaline flooding, surfactant and polymer injection processes [158, 159, 160, 161, 162, 163, 164], CO_2 and other gas injection processes [126, 128, 165, 166, 167], foams, gels and microbial EOR [168]. In addition, other processes related with petroleum engineering such as critical phenomena [169] and kinetics of calcium carbonate precipitation [170] have also been studied using visual observations within micromodels. Topics related with aquifer and soil remediation including three-phase flow of NAPL-water-air at the pore scale [171], enhanced removal of NAPLs by surfactant foam flooding [24, 27, 163] and DNAPLs by concurrent injection of cosolvent and air [32, 172], residual NAPLs solubilization/dissolution [26, 173, 174], colloids dispersion and transport [175, 176, 177], bioremediation

clean-up strategies involving dispersion of bacteria within subsurface [29] and in situ concentration determination of contaminants [156] have also been amply studied. Aside from these two major fields, micromodels applications have also been exploited in other scientific studies regarding for example: immiscible displacements and imbibition processes in porous media [178, 113, 179, 180, 181, 182], flow and transport in fractured porous media [154], gas-condensate flow in pores [183], hydrodynamic solute dispersion [184], vacuum impregnation of porous media with applications in food industry and wood science [185], gas-hydrate formation with potential cementing effect on sediments with major implications for subsea slope stability and interpretation of seismic data [186], moisture transport (drying) in softwoods [152], transport phenomena in the gas diffusion layer (GDL) of a polymer electrolyte membrane (PEM) fuel cell [155] and wettability related matters [126, 187, 161, 162]. Since most of these studies are very specific, a large variety of silicon or glass micromodels with different characteristic shapes and sizes were employed to better correspond to the purpose of each specific study.

Glass micromodels are considered to be more advantageous from many points of view including optical [182] and mechanical properties, chemical and thermal resistance, surface coatings, design flexibility, durability, reusability and cost effectiveness [188]. On the other hand silicon micromodels have the advantages of being disposable (very important for microbial enhanced oil/aquifer remediation studies) and more suitable for small-scale pore structures as they allow a more controllable and precise etching process [159, 157]. The large number of papers published containing results of microvisual experiments shows that despite their limitations micromodels are very useful and continue to find new applications. Still, their contribution is mostly qualitative rather than quantitative. The disadvantage of larger models is that they are more difficult to manufacture but, on the other hand they might have the advantage of reducing boundary effects and they could provide better statistical samples for comparison with simulations data. Still, it remains a challenge to create more realistic models of the porous media while retaining visibility. The literature includes an exhaustive number of studies in which micromodels were used from which, only a few were mentioned in this section to provide the reader with an idea of the large applicability of micromodels.

2.8 Summary

All applications mentioned in the beginning of this chapter have as a central point the dissolution process in a porous medium and/or the immiscible or miscible displacement of a solute (liquid) by a solvent (liquid) from a porous medium. In all cases the achievement of enhanced dissolution rates and high displacement efficiencies is targeted in order to attain a good understanding of the governing physical phenomena and to improve current technologies that rely on these processes.

Even if the literature concerning with each of these applications in which dissolution and immiscible and miscible displacement processes play essential roles is already very wide, the interest of many researchers in this field is kept active by the complexity of the problems that need to be understood and solved at both microscopic and macroscopic scales in order for a viable implementation of newer technologies to be realized.

Traditionally, one would expect that the dissolution of slowly miscible liquids is solely governed by diffusion, meanwhile the displacement process is merely driven by convection and the problem of multiphase flows in porous media can be simplified and treated based on these assumptions. In fact, in order to fully describe the evolution of multiphase systems during dissolution and/or displacement processes both convective and diffusive effects have to be taken into account, as their interplay will actually define the evolution of the system. Despite this seeming a simple task, the definition of convective and diffusive time scales is not so straightforward, especially when flows of slowly miscible liquids through porous media are considered. In this case, for example, it is very difficult to estimate typical dissolution times as even if the process is reduced to Fickian diffusion and the diffusive time scale is defined as L^2/D it is still unclear what should be used as the typical size L in this formula, as usually the porous medium has many length scales associated with its topology.

Since the focus of this project is on the experimental study of slow dissolution dynamics of binary mixtures within a single capillary tube and in network models which simulate the porous media, first the most important phenomena and physical parameters that influence the dissolution process were introduced followed by a brief description of the mass transport mechanisms. Afterwards, some of the most relevant experimental and theoretical studies that employed the same or similar geometries in previous studies were reviewed. Some of these studies will be

discussed in more detail in the following chapters in accordance to the discussion of the results obtained in this study.

Chapter 3

Dissolution dynamics of liquid/liquid interfaces in capillary tubes

In this chapter are reported optical observations of the dissolution behavior of glycerol/water, soybean oil/hexane, and isobutyric acid (IBA)/water binary mixtures within horizontal capillary tubes. Glass capillary tubes with diameters as small as $0.2\,mm$ were initially filled with one component of the binary mixture (solute) and then immersed into a solvent-filled thermostatic bath. Both ends of the tubes were open, with no pressure difference being applied. In the case of glycerol/water and soybean oil/hexane mixtures, the dissolution could be isolated from the hydrodynamic motion. Two phase boundaries moving from the ends into the middle section of the tube with the speeds $v \sim D^{1/3}t^{-2/3}d^2$ were observed. The boundaries slowly smeared but their smearing occurred considerably slower than their motion. The motion of the phase boundaries could possibly be explained by the effect of barodiffusion. The shapes of the solute/solvent boundaries are defined by the balance between gravity and interfacial tension effects. The contact line moved together with the bulk interface: no visible solute remained on the walls after the interface passage. Changes in temperature and in the ratio between gravity and capillary forces altered the apparent contact angles. The IBA/water system had different behavior. Below the critical point, no dissolution was observed: IBA and water behaved like two immiscible liquids, with the IBA phase being displaced from the tube by capillary pressure. Above the critical point, two IBA/water interfaces could be identified, however the interfaces did not penetrate much into the tube.

3.1 Introduction

Numerous engineering processes such as vegetable oil extraction [189], enhanced oil recovery [10, 13], aquifer and soil remediation [30, 190], etc. [3, 7] are variations of the solvent-based (or miscible) displacement of a solute from a porous medium. Even an intravenous drug delivery could be considered as the dissolution of a liquid miscible droplet through porous body tissues [48]. The pore sizes are typically small, which makes the hydrodynamic flows within porous media being rather slow and as a result the diffusion and capillary effects play essential roles in the overall mass transport. The porous medium can be roughly represented as a network of interconnected capillary tubes [79, 117]. Using this so-called network approach, the aim of the work described in this chapter is defined as to understand the dissolution dynamics of binary mixtures within a single capillary tube, which is a necessary step to understand the miscible flows through a more complex porous matrix. The principal aim was to investigate the dissolution in capillary tubes of very small diameters, when it is expected to be a diffusion-driven process. We managed to visualize the dissolution in capillary tubes with diameters as small as $0.2\,mm$, which are already comparable with the typical pore sizes in geological applications frequently assumed to be $0.1\,mm$ and smaller. The pores however could be larger in the case of vegetable oil extraction.

In the experiments described in this chapter, the capillary tubes saturated with the solute phase were horizontally immersed into a solvent-filled thermostatic bath. When the pure components of a binary mixture are brought into contact a non-equilibrium binary system is obtained. Equilibration of the mixture to a thermodynamically stable state involves diffusive and hydrodynamic processes and usually occurs very slowly (visible phase separation exists for hours after the initial contact of two completely miscible liquids). An example would be the dissolution of a honey droplet in water: honey is miscible in water in all proportions, but the droplet of honey remains visible in water for a rather long time period; the honey droplet even retains its original shape while being agitated. It was concluded that the concept of interface needs to be employed to describe the dissolution in such a miscible system, and the interface should be endowed with dynamically variable surface tension [1].

The majority of studies up to date in which capillary tubes were utilized covered mostly the subject of displacement, especially immiscible displacement. The most important studies employing capillary tubes were reviewed in Section 2.7.1. In addition, the interface smearing rates were measured by Viner and Pojman [191],

who examined the evolution of the IBA/water mixture in a vertical cuvette heated to supercritical temperatures by using the laser line deflection technique. They noticed that the homogenization of IBA/water mixture (the components were taken in equal volumes of $0.6\,ml$ each) lasts for about 25 hours at the temperature of 30^oC, and reported that the transition zones that separate the water and IBA phases (the interphase boundaries) slowly grew into the IBA volume with $t^{0.06}$ time dependence. Similar experiments were undertaken by Petitjeans and Maxworthy [71] in order to measure the diffusion coefficient at the glycerol/water interface. They found that the transition zone slowly grew into the glycerol phase and fully disappeared after at least 6 hours under room temperature. Dambrine et al. [192] studied the interdiffusion of pure water and 40% glycerol/water mixture within a microchannel using Raman imaging and found that the interface thickness grows as $(Dt)^{1/2}$, but they also noted shifting of the phase boundary into glycerol phase.

3.2 Materials and methods

3.2.1 Binary mixtures

Glycerol/water, soybean oil/hexane and IBA/water binary mixtures were used in this project. These binary mixtures were chosen due to their importance in industrial applications and because of their physical and chemical properties. For example, glycerol is a widely used cosolvent for aqueous solutions in pharmaceutical and cosmetic industries. Glycerol and water are both polar substances with a reasonable density difference and a large viscosity ratio. Soybean oil/hexane is one of the most widely encountered mixtures in vegetable oil extraction. Soybean oil and n-hexane are both nonpolar substances with a density difference similar to glycerol/water mixture. However, in comparison with glycerol/water mixture, soybean oil/hexane has a smaller viscosity ratio. IBA/water mixture was chosen mainly because is characterized by an UCST (i.e. is partially miscible at room temperature and completely miscible above $\sim 26^oC$). Another main reason for choosing this mixture was the fact that IBA and water have almost matched densities and viscosities. All chemicals having high purities were purchased from Fisher Scientific or Sigma Aldrich and were used as received.

Glycerol and water and soybean oil and hexane are miscible in any proportions under all temperatures. The IBA/water mixture is characterized by the upper critical solution temperature, $T \sim 26.3^oC$ [193, 62, 63]. At temperatures above

the critical point, the mixture components are miscible in any proportions. Below the critical point, only small amounts of IBA are completely miscible in water, and if a larger droplet of IBA is added, then IBA and water phases will inter-diffuse until the equilibrium concentrations, c_1 and c_2, are established. The values of c_1 and c_2 are temperature dependent and can be obtained from the phase diagram available e.g. in the paper of Pojman et al. [63].

Substance	$\rho, g \times cm^{-3}$	$\eta, Pa \times s$
Glycerol	1.26	1.41
Soybean oil	0.917	0.069
IBA	0.95	$1.1 \cdot 10^{-3}$
Water	1.00	$1.01 \cdot 10^{-3}$
n-Hexane	0.659	$0.326 \cdot 10^{-3}$

Table 3.1: Density and viscosity coefficients for pure glycerol, soybean oil, IBA, water and n-hexane at 20^oC [1, 194, 195].

The values of density and viscosity coefficient for the pure substances are summarized in Table 3.1. The mixture densities are concentration dependent, but it is known that a 'simple mixture' approximation,

$$\frac{1}{\rho} = \frac{1-c}{\rho_1} + \frac{c}{\rho_2}, \tag{3.1}$$

usually works well. For instance, this approximation has an 1% accuracy for the glycerol/water mixture [1], which has also been confirmed by our measurements. In Equation 3.1, ρ is the mixture density, while ρ_1 and ρ_2 are the densities of the pure substances, and c is the concentration defined as the mass fraction of solute. The mixture viscosity also depends on concentration. For the glycerol/water mixture measurements of the viscosity as a function of concentration can be found in the works of Segur and Obestar [194] and Kim and Ju [196]. The values of viscosity of the IBA/water mixture at supercritical conditions are available in the work of Ouerfelli et al. [195].

The values of diffusion coefficient for the glycerol/water mixture under different temperatures and for different compositions can be found in the works of Petitjeans and Maxworthy [71], Rashidnia and Balasubramaniam [197], and D'Errico et al. [198]. For reference, the mutual diffusion coefficient at room temperature equals $1.6 \times 10^{-10} m^2 s^{-1}$ at an interface between pure glycerol and water, the magnitude of diffusion coefficient linearly drops for interfaces between glycerol/water mixture and pure water and gets ten times smaller in pure glycerol [71, 198]. The

IBA/water mutual diffusion coefficient is zero in the critical point and above the critical point the diffusion coefficient grows as $D = D_0 \left(\frac{T-T_c}{T_c}\right)^{\nu}$, where $\nu = 0.664$ and $D_0 = 5.9 \times 10^{-10} m^2 s^{-1}$ [193, 199, 200, 201, 202]. Thus, the diffusion coefficient equals $1.3 \times 10^{-11} m^2 s^{-1}$ at $27^o C$ and $2.8 \times 10^{-11} m^2 s^{-1}$ at $30^o C$. These values will be used further for the analysis of the experimental observations. However, in [68] and [70], smaller values (i.e. one or two orders of magnitude) of the IBA/water diffusion coefficient can be found. Likewise, the work of Melzer et al. [203] reports considerably higher values (by one order) both below and above the critical temperature. Furthermore, [203] is the only work that could be found in the literature in which values of the IBA/water diffusion coefficient for temperatures below the critical point are mentioned. The values reported in [203] are however too different from the results of other researchers and hence were not used. Nevertheless, the mutual diffusion coefficient of the IBA/water mixture is at least one order lower than the ones of glycerol/water and soybean oil/hexane mixtures which signifies considerably weaker diffusion mass transport in such a mixture.

The interfacial tension coefficient is traditionally defined only for the equilibrium states of a binary mixture. Glycerol and water form a homogeneous solution at equilibrium, and no interfacial tension coefficient is traditionally associated with miscible interfaces. The dissolution is however a very slow process and the phase separation could be observed for long time periods, so the effective interfacial tension could be introduced. The estimations of Petitjeans and Maxworthy [71] show that the interfacial tension coefficient to be associated with the glycerol/water interface is approximately $0.4 - 0.5\, dyn \times cm^{-1}$. In the case of IBA/water mixture, the equilibrium heterogeneous states can exist at temperatures below the UCST. The IBA/water interfacial tension coefficient depends on temperature, decreasing as the mixture temperature approaches the critical point. For instance, the interfacial tension coefficient equals $0.06\, dyn \times cm^{-1}$ at $T = 24^o C$ [200, 204]. The equilibrium interfacial tension is zero at and above the critical temperature. Since thermodynamic equilibration occurs slowly the dynamic interfacial tension could be introduced. These dynamic values were measured by Pojman et al. [63] using the spinning droplet tensiometry technique. Values of the order of $0.01\, dyn \times cm^{-1}$ were reported for temperatures slightly above the critical point.

We could not find in the literature the above-mentioned material coefficients for the soybean oil/hexane mixture. Only in the paper of Wu and Lee [205] the theoretical estimations of the mutual diffusion coefficient for the mixture of soybean oil and hexane are given, being $9.1 \times 10^{-10} m^2 s^{-1}$ at $25^o C$.

3.2.2 Experimental setup

In the experiments the capillary tubes were filled with solute (glycerol, soybean oil or IBA) and then immersed into a thermostatic transparent solvent-filled (water or hexane) bath of dimensions $100 \times 20 \times 20\, cm$. The capillary tubes were placed horizontally with both ends being open. No pressure gradient was applied between the ends of the tubes. The capillary tubes had circular and square cross-sections, different inner $(0.2 - 1.6\, mm)$ and outer diameters $(0.33 - 7\, mm)$, various lengths $(2 - 50\, cm)$ and were made of fused quartz or borosilicate glass. The capillary tubes were purchased from Vitrocom Inc and Fisher Scientific.

The experiments were performed at various temperatures in the range of $20^oC - 50^oC$. The temperature in the water bath was controlled with a Grant digital thermostat (GD100, stability at 37^oC is 0.05^oC); the homogeneity of the solvent temperature was checked in several reference points with a Checktemp1 thermometer by Hanna Instruments (accuracy is 0.3^oC). Solute and solvent temperatures become equal at the time the capillary tube is immersed into the bath. Simple estimations show that the thermal equilibration takes less than 1 minute even for the thickest capillary tubes used, i.e. almost instantly in comparison with the duration of the experiments.

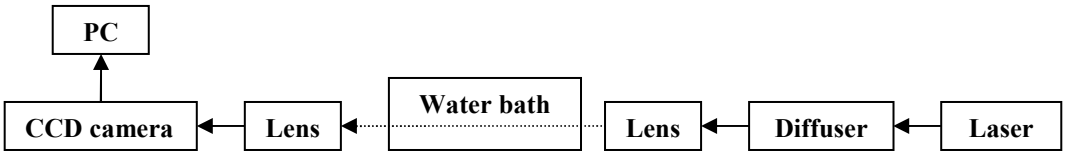

Figure 3.1: A schematic view of the experimental setup.

The shape and the position of the solute/solvent interfaces were recorded with a system including a CCD camera with Questar lens, a diffuser and a diode laser used for illumination. A schematic view of the experimental setup is presented in Figure 3.1 and all pieces of equipment are described in the following subsections. To improve the image contrast the solute-liquids were colored with methylene blue, Sudan IV, or eriochrome black T dyes purchased from Sigma Aldrich. In some experiments solid microparticles were dispersed in the solute phase to detect any hydrodynamic flows in the tube. The whole capillary tube is schematically depicted in Figure 3.2.

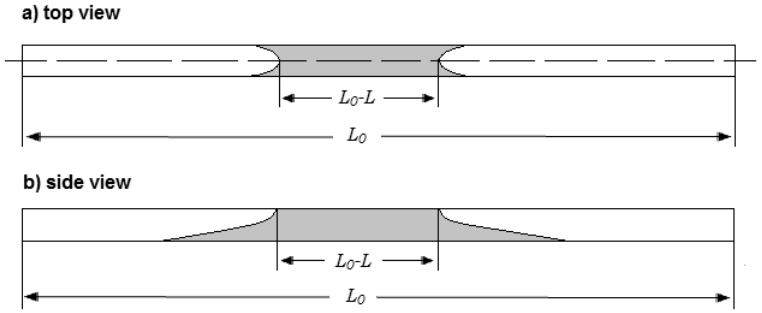

Figure 3.2: A schematic view of the solute/solvent mixture saturating the capillary tube.

3.2.2.1 CCD camera

Charge-coupled devices (CCD) are used in many scientific applications for digital imaging, especially where high-quality image data are required. A CCD camera (Figure 3.3), LaVision Imager 3S (1280x1024 pixels) was used to record the images in this project [206]. In order to control the camera and acquire the images, DAVIS software version 7.2 was used. The camera was internally triggered by the internal timer of the laser thus allowing the acquisition of sharper images [207]. The field of view of the measurement area is determined by the focal length of the lens, the size of the CCD of the camera and the distance between camera's CCD and lens [208]. A series of calibration experiments were done by Dr. D. Ju in order to establish the acceptable depth of field for this system. All details about the calibration method can be found in [208].

Figure 3.3: LaVision Imager 3S CCD camera.

3.2.2.2 Questar lens

In order to view the shapes of the interfaces in greater detail a high magnification lens was needed together with an adequate light source. The Questar QM100 lens (Model #30003) was utilized for visualization as it has a magnification of 34 times at the image plane at working distances in the range $15-35\,cm$, and a field of view

of $2\,mm$ x $1.6\,mm$. The QM100 (Figure 3.4) is very suitable to use for applications which require high magnification and resolution but also a high degree of flexibility [209].

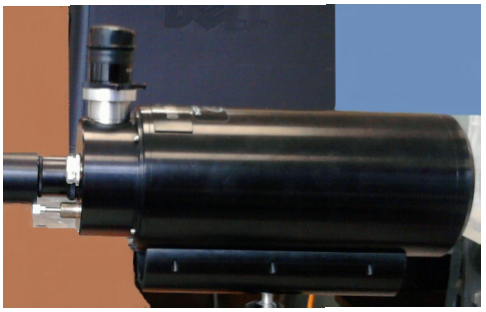

Figure 3.4: Questar lens.

3.2.2.3 High efficiency diffuser

The end diffuser of the LaVision high efficiency diffuser package designed for strobe background illumination purposes was used to diffuse the laser light [210]. The end diffuser (Figure 3.5) was mounted to the laser and in this way the presence of speckles could be considerably diminished.

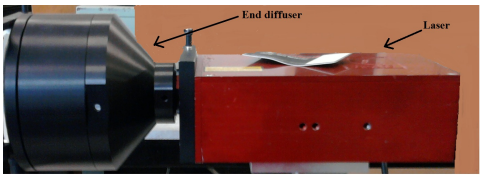

Figure 3.5: LaVision high efficiency diffuser head mounted to the Firefly laser.

3.2.2.4 Firefly high speed imaging laser

The illumination source utilized in these experiments was a Firefly diode laser from Oxford Lasers. Firefly high speed imaging laser is a semiconductor class 4 $300\,W$ laser that provides pulses of infrared laser light (wavelength of emission is $808-815\,nm$) with variable pulse durations and frequencies. The laser is designed to be used with high speed and/or high resolutions cameras for high speed image capture [211]. The diode laser system has 2 components, the laser head and the control unit (Figure 3.6). The laser head produces the light for illumination and the control unit regulates the pulse repetition frequency and the exposure time. The output light can be adjusted between light sheet and area illumination. In this case the light sheet illumination was used. This type of output light is usually

suitable for applications such as particle image velocimetry, flow visualization, measurement of spray pattern and plume geometry [211].

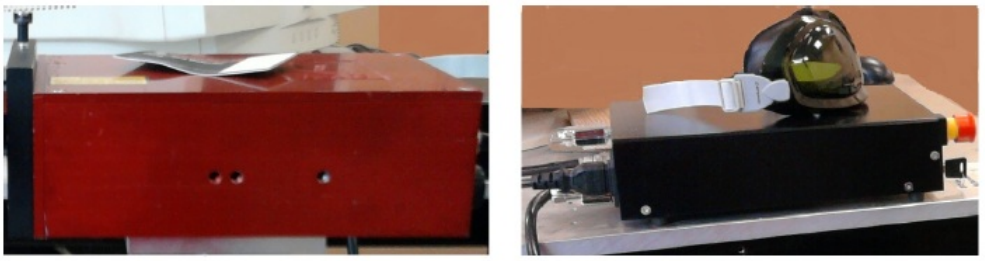

Figure 3.6: Firefly high speed imaging laser system.

3.3 Experimental results

3.3.1 Glycerol/water mixture

Glycerol and water are miscible in any proportions. One would expect that a glycerol/water interphase boundary would slowly smear in time due to inter-diffusion, while the boundary itself should remain stationary in the absence of hydrodynamic flows. In the experiment we observe that water penetrates into the capillary tube forming two clear glycerol/water interfaces at the ends. The interface smearing occurs at considerably lower rates than the interface propagation speeds. Generally, the interfaces remain visible for time periods up to 10^4s. Their time evolution is shown in Figure 3.7 and Figure 3.8. In shorter capillary tubes, the experiment could be carried out until the two opposite interfaces meet (Figure 3.8c). The interfaces of the shown shape remain stable for quite long time periods and experience shape changes only when they become too diffusive or at their point of fusion.

Figure 3.7a shows the initial evolution of the glycerol/water boundary. This stage lasts for about 1 minute. Diffusion is negligible at this stage, and glycerol being heavier than water is displaced from the capillary tube due to gravity. The interfacial boundary never breaks up in the sense that no new glycerol or water droplets are formed. When the contact line is closed up within the capillary tube the interface shape stabilizes (gravity and capillary forces are balanced).

For the glycerol/water binary mixture the Bond number defined by Equation 2.16 is less than 1 (i.e. when $d = 0.4\,mm$ or smaller), which indicates the dominance of

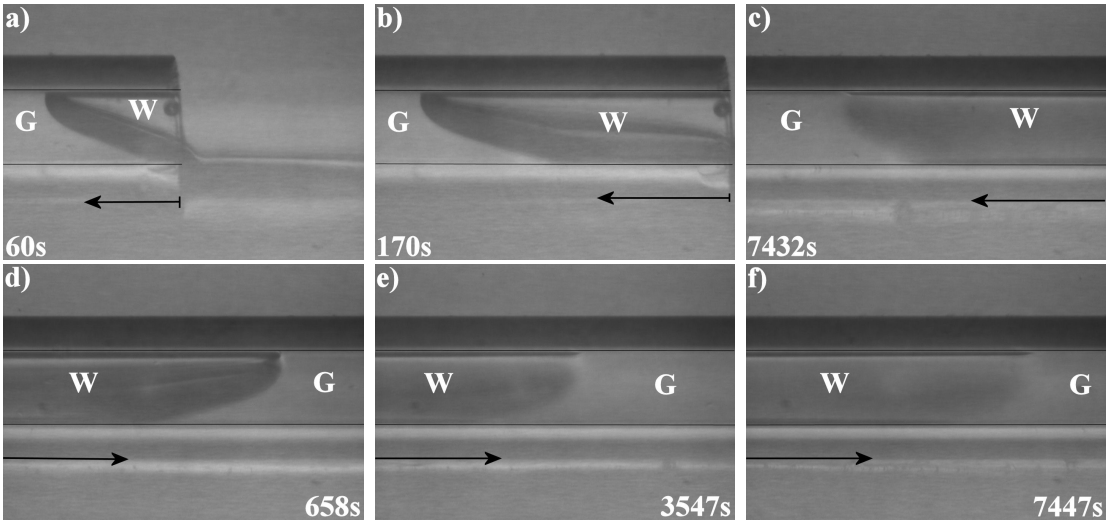

Figure 3.7: The shapes of glycerol/water interphase boundaries within a capillary tube with square cross-section at different time moments. **(a-c)** and **(d-f)** sequences show the two interfaces propagating from opposite ends of the capillary tube. The tube has diameter $d = 0.4\,mm$ and length $L = 10\,cm$; the mixture temperature is $T = 20^oC$. The exact time moments are shown in the pictures. 'W' and 'G' letters indicate the water and glycerol phases, respectively. The arrows indicate the directions of the interface motion.

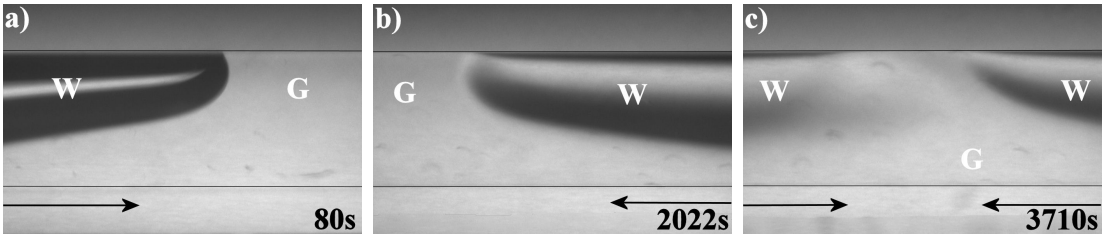

Figure 3.8: The time progression of the glycerol/water interface into a capillary tube of circular cross-section. The diameter of the tube is $d = 0.6\,mm$ and the length is $L = 5\,cm$. The temperature is maintained at $T = 30^oC$. Only the tips of the interfaces are shown, but the contact lines are closed within the capillary tube. All notations as in Figure 3.7.

capillary over gravity forces. Nevertheless, Figure 3.7 and Figure 3.9 show menisci are affected by gravity, which could signify that the glycerol/water interfacial tension coefficient of Petitjeans and Maxworthy [71] is an over-estimation. The gravity forces become less important for menisci in the capillary tubes of smaller diameters, which could be noted by comparison of Figure 3.7 ($d = 0.4\,mm$) with Figure 3.8 ($d = 0.6\,mm$). The interface becomes less inclined in capillary tubes of smaller diameters, but the gravity effects remain important even in the tubes of $0.2\,mm$ diameter (Figure 3.9). We found no dependence of the interface shape on temperature at least not for the investigated range of $20^oC - 50^oC$. Another conclusion that can be drawn from Figure 3.7 is that the more diffusive the phase

boundary becomes the less inclined it is. One could interpret this as the increase of capillary forces over gravity forces, but this is not possible because during any spontaneous process interfacial tension can only decrease in time, which means that capillary forces should decrease as well.

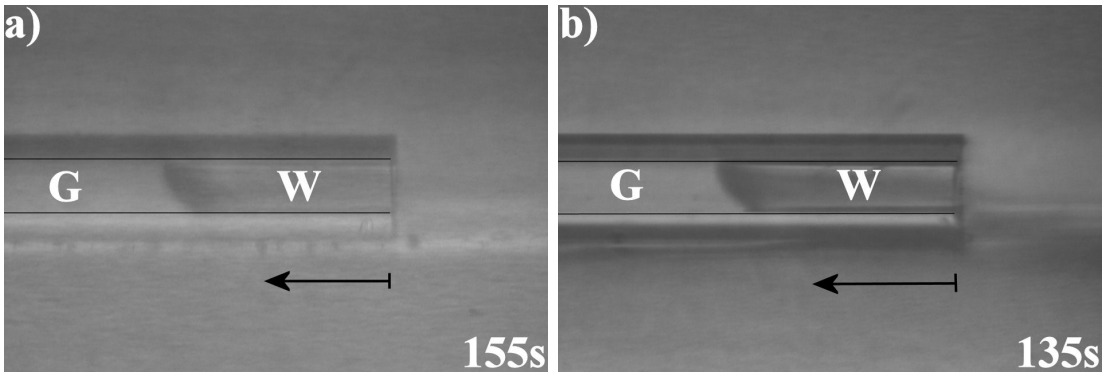

Figure 3.9: The shape of glycerol/water interface within a capillary tube of square cross-section. The diameter of the capillary tube is $d = 0.2\,mm$ and the length is $L = 10\,cm$. The temperature is maintained at: **a)** $T = 20^oC$; **b)** $T = 30^oC$.

In Figures 3.7–3.9 it appears that glycerol is a more wettable liquid than water. The apparent contact angles measured in glycerol phase at the upper and lower parts of the interface are different, but their values are still smaller than 90^o (e.g. values are in the range of $60^o - 80^o$ at the upper part and in the range of $10^o - 20^o$ at the lower part). By all means contact angle values depend on the cross-section of the capillary tubes and on the tubes diameters. The shape of the contact line does not change while the interface moves into the capillary tube indicating that no visible glycerol phase remains on the tube walls after the passage of the interface.

The rate of the glycerol dissolution can be defined as the rate of glycerol removal from the capillary tube. The water phase in the tube obviously contains some dissolved glycerol, an amount which we cannot measure by using the current experimental setup. For this reason, the dissolution rate was defined as the propagation speed of the glycerol/water phase boundary. We measured the length of the capillary tube occupied by the water phase L, calculated as $L = L_0 + x_1 - x_2$, where L_0 is the length of the capillary tube and x_1 and x_2 are the coordinates of the first and second interfaces (the reference point for the x-coordinate is at one of the tube's ends). Initially the capillary tube is filled with the solute, and L is zero, later water diffuses into the capillary tube, and L grows (see Figure 3.2). These measurements were obtained without the use of the optical rig and are shown in Figure 3.10. In this case a stopwatch was started when the tubes were placed on the bottom of the bath along its labelled section. The position of the tip of

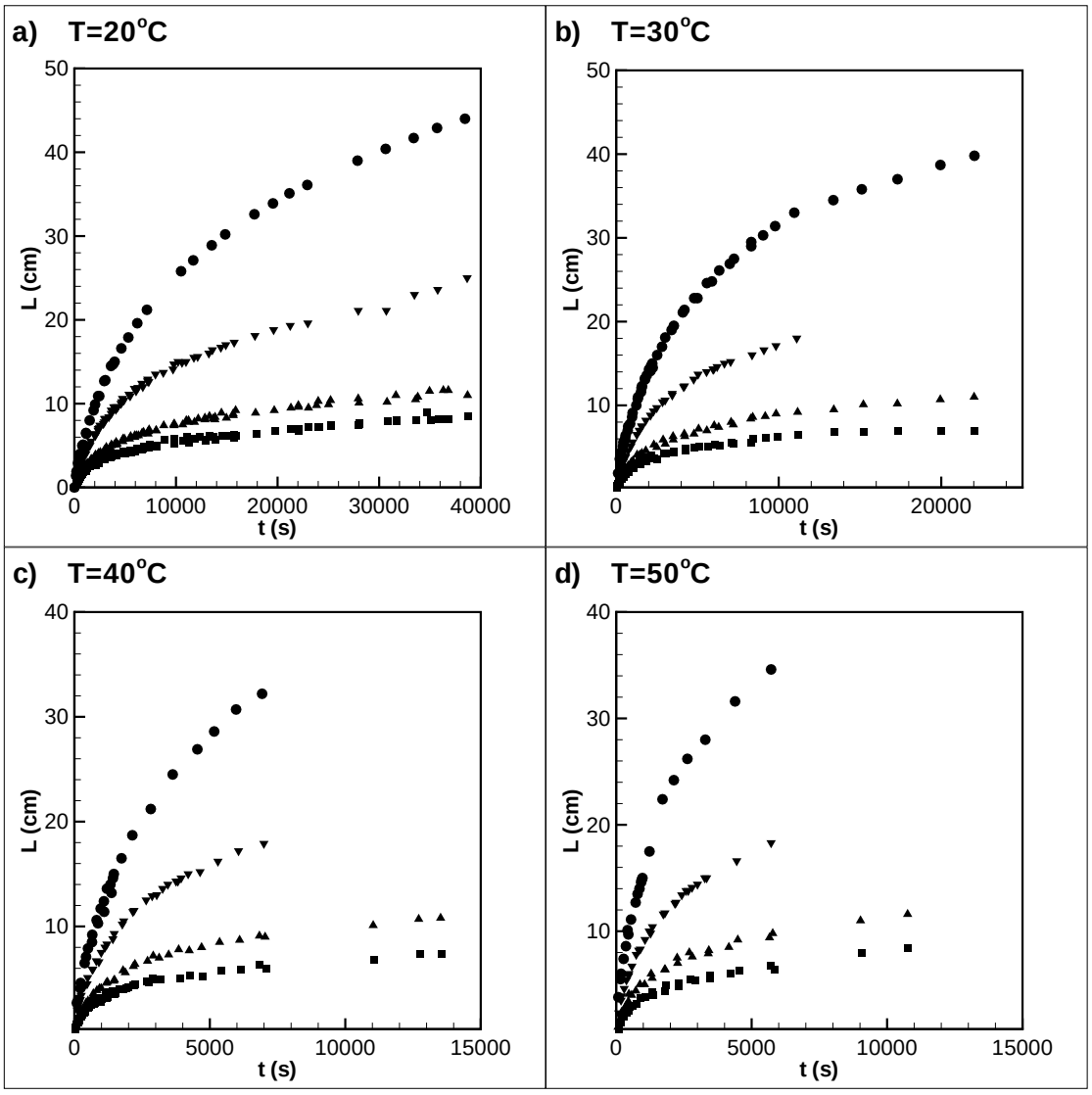

Figure 3.10: The length of the capillary tube occupied by the water phase as a function of time. Capillary tubes with circular cross-sections and diameters of $0.6\,mm$ (■), $0.8\,mm$ (▲), $1.2\,mm$ (▼) and $1.6\,mm$ (●) were used. The experiments were conducted at different temperatures: **a)** $T = 20^oC$, **b)** $T = 30^oC$, **c)** $T = 40^oC$ and **d)** $T = 50^oC$.

the interface was recorded at certain time periods for as long as the tip was still clearly visible. In Figure 3.10 each curve cumulates the data from several experiments carried out with capillary tubes of different lengths. We found that the rate of water propagation is independent on the length of the capillary tube. This is clearly shown in Figure 3.12 where data from several experiments with circular cross-section capillary tubes of the same diameter but different lengths are plotted for the same temperature. In Figures 3.10–3.11 it can be seen that the interfaces propagate faster in the capillary tubes of larger diameters and the dissolution rates grow with the increase of temperature.

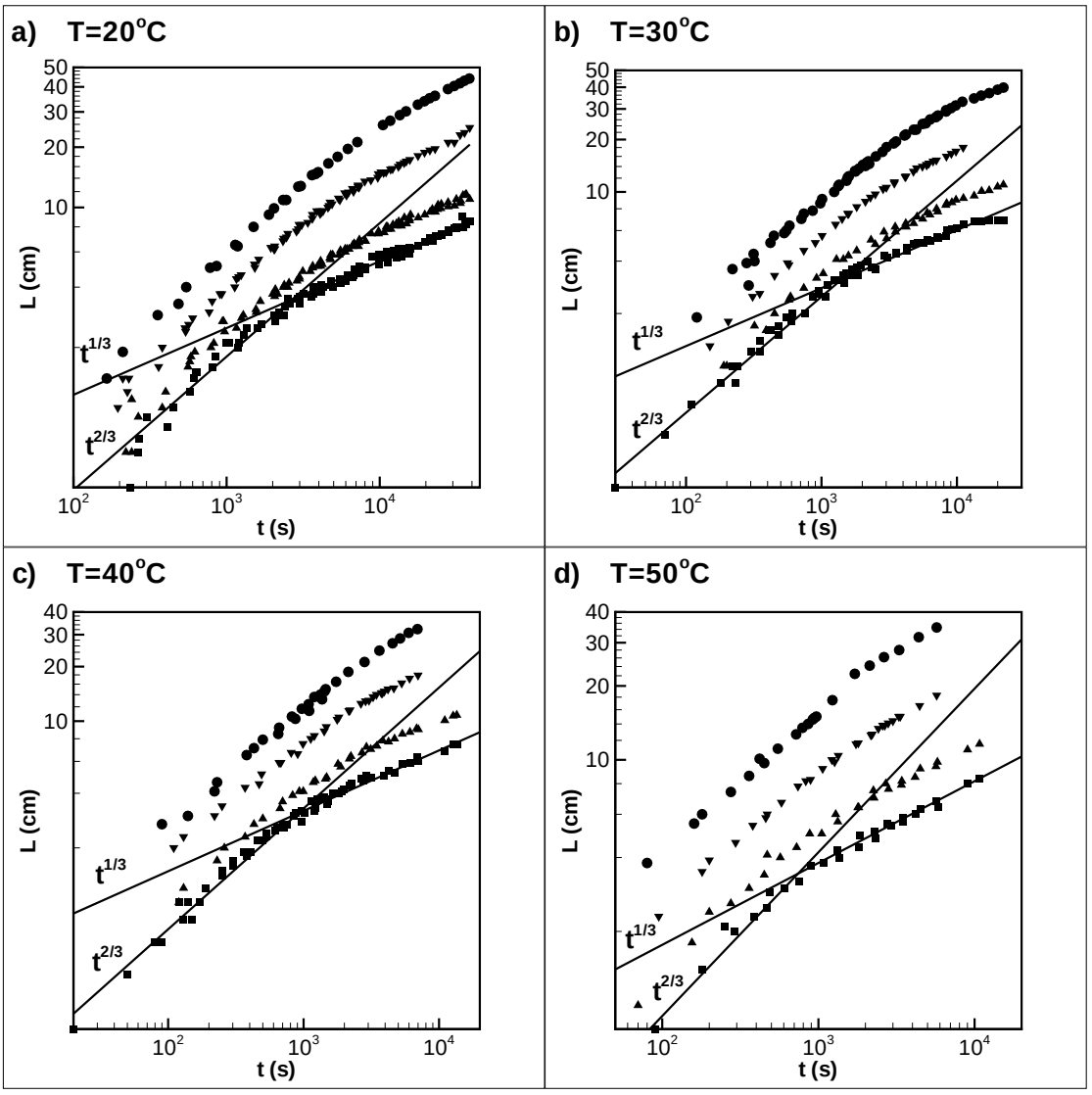

Figure 3.11: The length of the capillary tube occupied by the water phase as a function of time in logarithmic coordinates. Capillary tubes with circular cross-sections and diameters of $0.6mm$ (■), $0.8mm$ (▲), $1.2mm$ (▼) and $1.6mm$ (●) were used. The experiments were conducted at different temperatures: **a)** $T = 20^oC$, **b)** $T = 30^oC$, **c)** $T = 40^oC$ and **d)** $T = 50^oC$.

The propagation of the interface slows down upon its penetration into the capillary tube. The plots in Figure 3.10 have been re-drawn in logarithmic coordinates in Figure 3.11. The new figure shows that the time evolution of L can be approximately represented by two power laws, $t^{2/3}$ in the beginning and $t^{1/3}$ starting from some point. The time moments when the dependence is changed depend on the capillary tube diameter and temperature, but their values of about 100 s for a capillary tube with $d = 0.4mm$ indicate that the $t^{2/3}$ dependence most likely corresponds to the initial gravity-driven displacement of the glycerol phase (Figure 3.7a), while the later $t^{1/3}$ dependence should characterize the motion of the

stabilized interfaces. In larger capillary tubes ($d \geq 0.6\,mm$), the $t^{2/3}$ dependence is observed for longer time periods (i.e. $\sim 1000\,s$, see Figure 3.11), while in smaller capillary tubes ($d \leq 0.4mm$) the dissolution rate is solely defined by the $t^{1/3}$ power law (see Figure 3.13b).

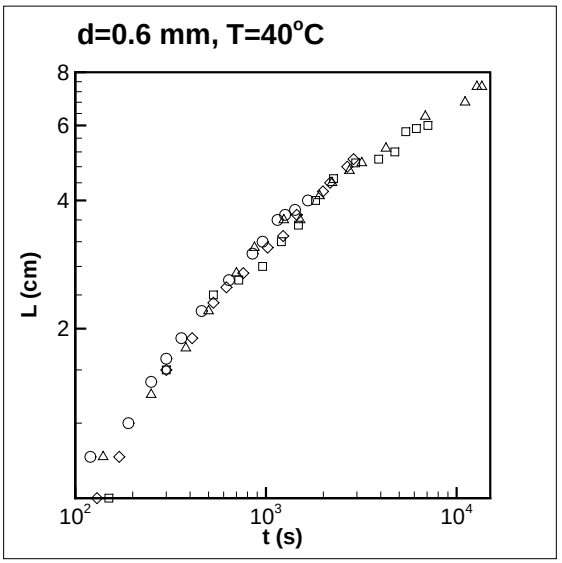

Figure 3.12: The length of the water phase as a function of time in capillary tubes of circular cross-section with $d = 0.6\,mm$ and various lengths; $T = 40^oC$; ($\circ$) $4\,cm$; ($\diamond$) $5\,cm$; ($\triangle$) $15\,cm$; ($\square$) $49\,cm$; The data are plotted in logarithmic coordinates.

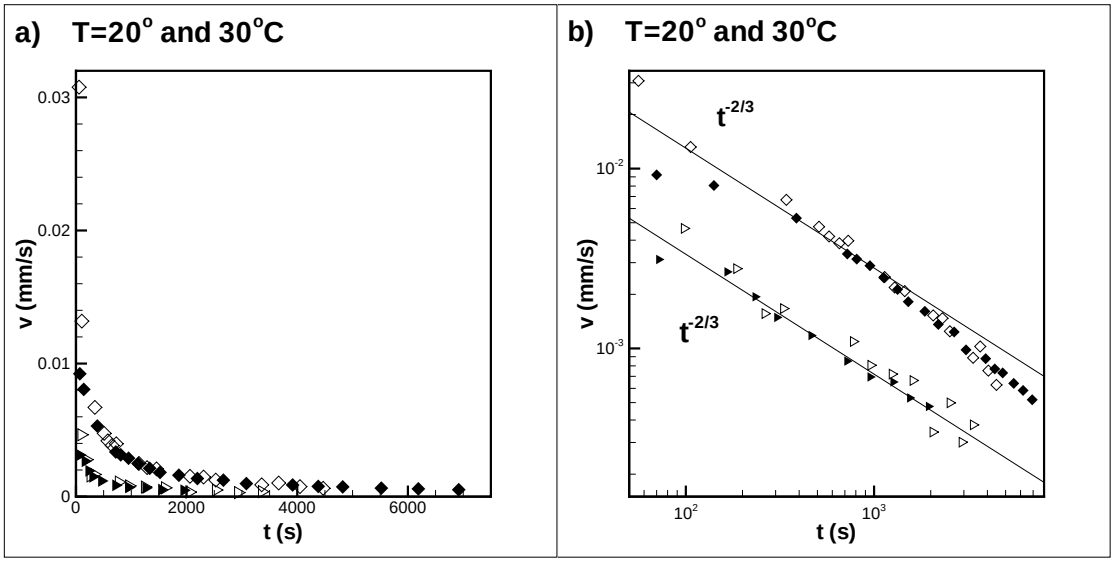

Figure 3.13: The speed of the interface propagation as a function of time in capillary tubes of square cross-section with diameters $d = 0.2\,mm$ ($\blacktriangleright$) and $d = 0.4\,mm$ ($\blacklozenge$) at temperatures of $T = 20^oC$ (filled symbols) and $T = 30^oC$ (empty symbols). **a)** The data are shown in normal coordinates. **b)** The same data are plotted in logarithmic coordinates.

The data in Figure 3.10 could be used to obtain the interface speeds derived as $v = \frac{1}{2}\frac{dL}{dt}$. In addition to the data in Figure 3.10, the speeds of the interface propagation within the smaller capillary tubes were obtained from the analysis of the image sequences. The interface speeds could be approximated by $t^{-1/3}$ at initial moments and by $t^{-2/3}$ at later stages. In the smallest capillary tubes, with diameters of $d = 0.2\,mm$ and $d = 0.4\,mm$, only one time-dependence, $t^{-2/3}$, could be identified, which is shown in Figure 3.13b.

The physical mechanisms that define the glycerol removal from the capillary tube need to be clarified. There are two interfaces formed moving towards each other; obviously, their propagations cannot be explained by spontaneous imbibition. Estimates of the Bond number are less than 1 for the capillary tubes with diameters smaller than $0.4\,mm$. Furthermore, once the solute phase is locked by the interfaces gravity currents should not drive the motion either. No pressure difference was imposed between the ends of the capillary tube, consequently, no externally generated hydrodynamic flow should develop. The internally generated convective flows may be induced due to density contrast (the solutal convection) and due to the dependence of the interfacial tension on concentration (the Marangoni convection). For instance, the intensity of solutal convection is characterized by the analogue of Rayleigh number (Equation 2.14), that can be estimated as $Ra_s \sim 10^2$ for the glycerol phase and $Ra_s \sim 10^5$ for the water-rich phase by using the smallest tube diameter ($0.2\,mm$) as the typical size. That means the solutal convection is more likely to exist in the water-rich phase.

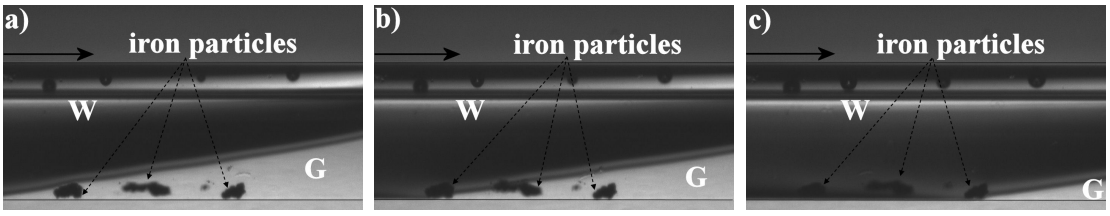

Figure 3.14: The evolution of the interface shape within a capillary tube with $d = 0.6\,mm$. The temperature is $T = 25^oC$. The glycerol phase contains metallic (iron) particles. The time interval between the shown snapshots **(a)** and **(b)** is $120\,s$; the interval between **(b)** and **(c)** is $310\,s$. Several small droplets appearing in the upper parts of the images are air bubbles in the water bath outside the tube.

The initial gravity-driven penetration of the water phase could also be interpreted as the solutal convection (or as the gravity current). To experimentally assess the role of hydrodynamic flows at later time moments, experiments were set up with the use of small metallic (iron, 99%) particles with diameters $< 212\,\mu m$ dispersed

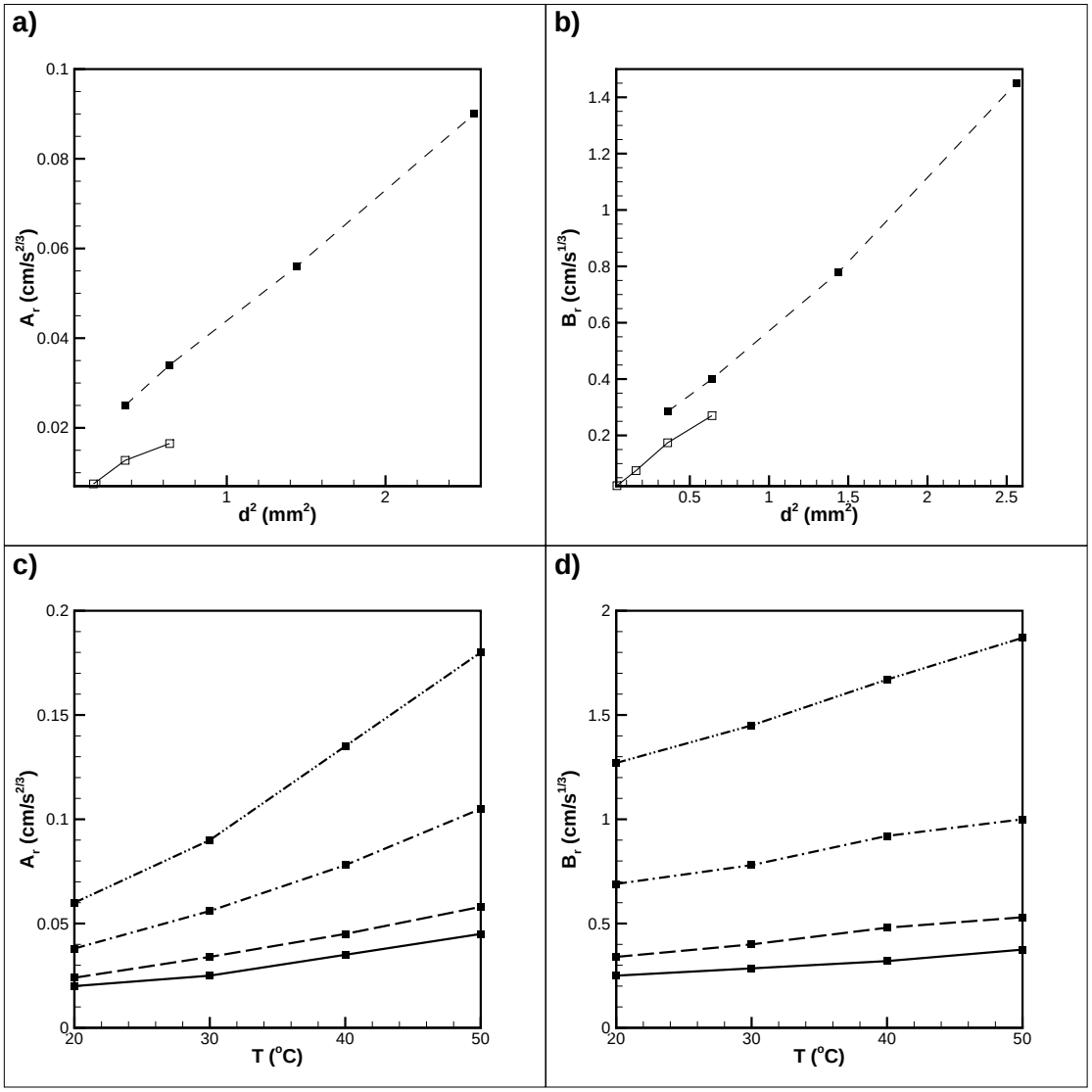

Figure 3.15: **(a,b)** Coefficients A_r and B_r versus the square diameter of the capillary tube. The filled symbols correspond to the data derived from Figure 3.10 (larger capillary tubes); the empty symbols correspond to the data obtained from the set of optical measurements (smaller capillary tubes). These data are obtained for the experiments conducted at the temperature $T = 30^oC$. **(c,d)** Coefficients A_r and B_r for different temperatures for the larger capillary tubes: $d = 0.6\,mm$ (solid line), $d = 0.8\,mm$ (dash line), $d = 1.2\,mm$ (dash-dot line), and $d = 1.6\,mm$ (dash-dot-dot line).

in the glycerol phase. Since the studied processes are rather slow, all particles aggregated and settled on the bottom of the capillary tube (Figure 3.14). It was observed that while the interface is passing through the section of the capillary tube with particles, the particles remain immovable. The interface shape remains almost unperturbed by the obstacles. No hydrodynamic flows were detected in these experiments.

Thus, the motion of the interfaces should be explained by the interfacial mass transport, which should be a diffusion-based process, but cannot be reduced to sole Fickian diffusion. Firstly, because the rate of the interface propagation does not follow the classical time dependence of the diffusion theory, $t^{1/2}$. Secondly, the use of the standard estimate for the diffusive time-scale gives an enormous value, $\tau_d = \frac{L^2}{D} \approx 10^8\ s$, if L is taken as the length of the capillary tube. The phase boundaries move considerably faster for the duration of these experiments.[1] However, it has to be considered that the experiments within longer capillary tubes were stopped before the fusion of the two interfaces, at the moment the tips of the interfaces were too diffused for their position to be accurately measured. Thus, it is not excluded that in longer capillary tubes at considerably later time moments the dissolution would not reduce to a Fickian diffusion based process.

Next, we analysed how the interface speed depends on the diameter of the capillary tube and temperature. For this, we introduced the coefficients A_r and B_r defined by the expressions, $L = A_r t^{2/3}$ and $L = B_r t^{1/3}$. The dissolution rate is obviously proportional to these coefficients. Figure 3.15 clearly shows that A_r and B_r grow with the increase of the tube's diameter and temperature. We found that the dissolution rate is proportional to the square of the tube's diameter. This is a surprising result, that also contradicts the assumption that the interface motion is driven by Fickian interdiffusion, for which the dissolution rate should be independent of the value of the diameter of the capillary tube.

To conclude, the phase boundaries could possibly be driven by the effect of barodiffusion. It could be seen that the solute/solvent interfaces are inclined, i.e. their

[1] The diffusion coefficient of glycerol/water binary mixture strongly depends on concentration. The mutual diffusion coefficient in glycerol-rich phase is about ten-fold lower than in water-rich phase [71, 198]. Such a strong dependence allows the front-type penetration of a solvent into a solute-saturated capillary tube to be mathematically reproduced on the basis of the Fickian law, but the resultant front speed would be always proportional to $t^{1/2}$ if only Fickian transport is taken into account [82]. The front-type dissolution in polymer mixtures with the front's speeds different from $t^{1/2}$ is known, see e.g. [212]. In [212] such a behaviour is associated with viscoelastic properties of polymers, but such an explanation and a developed mathematical model are not relevant for glycerol/water mixture.

shapes are affected by gravity. As the capillary tube diameter decreases, the gravity influence weakens and the motion of the interface is slower. A strictly vertical interface is not affected by gravity, and hence does not move due to barodiffusion. The inclined interfaces seen in these experiments could possibly be driven by barodiffusion, while their smearing is defined by Fickian diffusion.

3.3.2 Soybean oil/hexane mixture

Experiments were also carried out with the soybean oil/hexane binary mixture. Hexane and soybean oil are miscible in any proportion. Currently hexane is the most commonly used solvent for the vegetable oil extraction. The dissolution of soybean oil from the capillary tube occurred similar to the one of glycerol. The time progression of the soybean oil/hexane interphase boundaries is shown in Figure 3.16. By comparing Figures 3.16d and 3.8a it can be observed that the soybean oil/hexane interface is inclined twice stronger than the glycerol/water interface in the same capillary tube. This signifies that the gravity effects are stronger in this mixture and that the interfacial tension is lower, which is to be expected due to the non-polar nature of soybean oil and hexane.

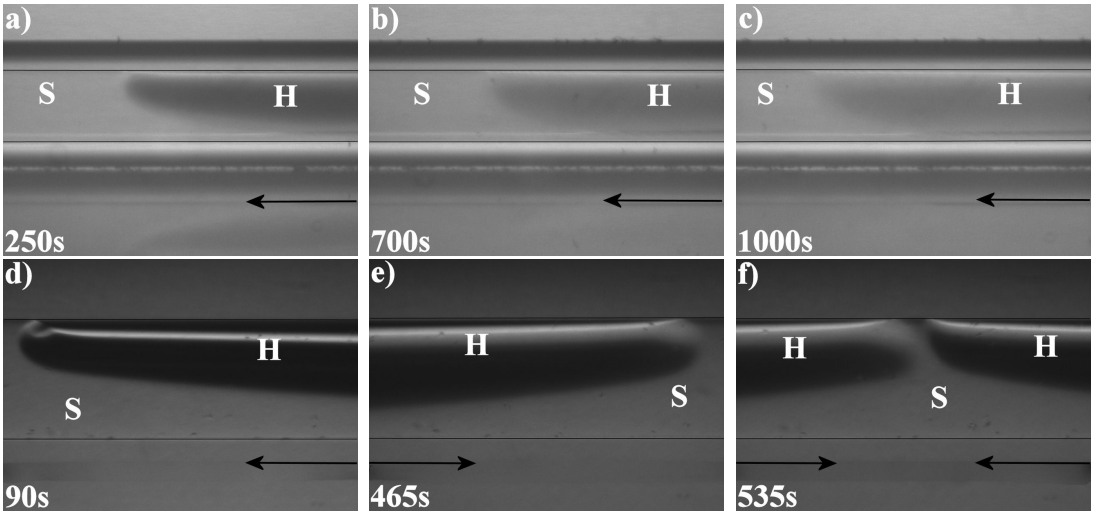

Figure 3.16: The soybean oil/hexane interphase boundaries at different time moments. The snapshots are obtained for the experiments conducted with a capillary tube of square cross-section with diameter $d = 0.4mm$ and length $L = 10cm$ **(a-c)** and with a capillary tube of circular cross-section with diameter $d = 0.6\,mm$ and length $L = 4\,cm$ **(d-f)**. In **(d-f)** only tips are shown, but the contact lines are closed within the capillary tube. Temperature is $T = 20^oC$. 'H' and 'S' letters indicate the soybean oil and hexane phases, respectively.

Similar to the glycerol/water interfaces, the phase boundaries between soybean oil and hexane diffuse in time but at considerably slower rates than the speeds of the interfaces motion. The propagation speeds of the phase boundaries are shown in Figure 3.17a. Again, we found that the speed of the interface propagation follows $t^{-1/3}$ and $t^{-2/3}$ power laws at the initial (convective) and later (diffusive) evolutions, and that the interface speed is proportional to the area of the cross-section of the capillary tube. The latter statement is confirmed by Figure 3.17b where the ratio of the interface speed over the square of the capillary tube's diameter is plotted versus time; the curves for the capillary tubes of different diameters are merged by this modification.

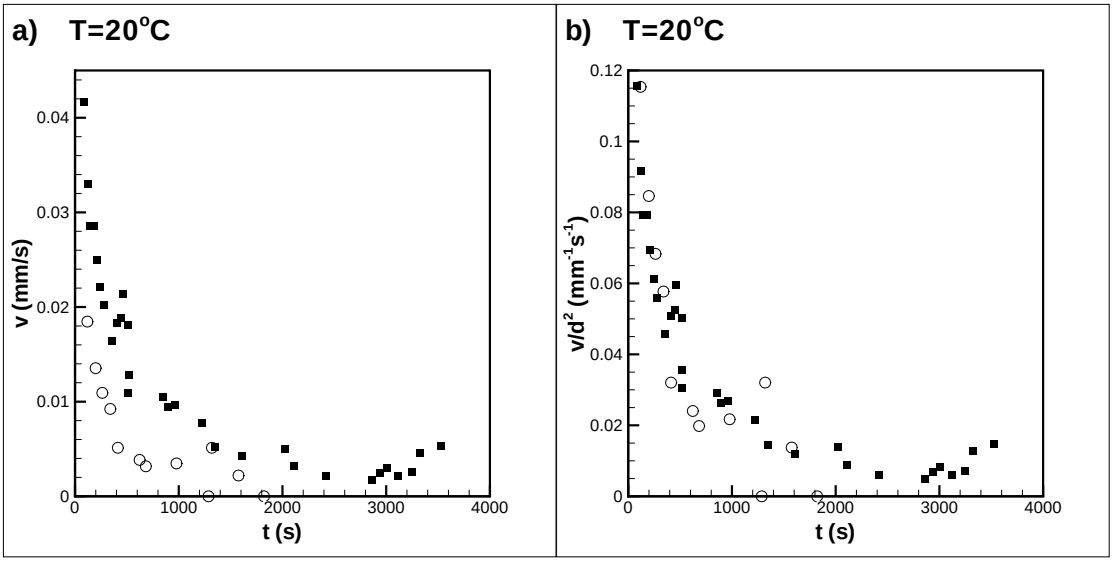

Figure 3.17: **a)** The time evolution of the speed of propagation of soybean oil/hexane interfaces in capillary tubes of different diameters. **b)** The interface speed divided by the square diameter of the capillary tube versus time. The data are collected from the experiments with the capillary tubes of diameter $d = 0.4\,mm$ ($\circ$) and $d = 0.6\,mm$ ($\blacksquare$). Temperature is $T = 20^oC$.

The diffusion coefficient for the soybean oil/hexane mixture is higher than for the glycerol/water interface (for similar solute concentrations), and both smearing and motion of the phase boundaries occur faster. This confirms that the observed dissolution of binary mixtures is a diffusion-based process. We also found that the propagation speeds of the soybean oil/hexane interface are about 1.7 times faster (e.g. for $d = 0.4\,mm$ and $T = 20^oC$) than the corresponding speeds of the glycerol/water phase boundaries. This indicates that the interface speed is proportional to the cubic root of the diffusion coefficient, $v \sim D^{1/3}$.

3.3.3 Isobutyric acid/water mixture

The experiments were also conducted with the use of isobutyric acid (IBA)/water binary mixture. This binary mixture has a phase diagram with an upper critical solution temperature, $T \sim 26.3^oC$. In our experiments, IBA volumes contained in the capillary tubes are negligibly small in comparison with the volume of the solvent, and all immersed IBA is finally dissolved even if the mixture temperature is below the critical (consolute) point.

It was found that the components of the binary mixture are separated by a visible interfacial boundary; below the critical point the interface is always sharp; above the critical point the interfaces become quickly diffusive. The dissolution scenario is different in the experiments conducted at temperatures below and above the critical point. At undercritical conditions, the propagation of only one phase boundary into the capillary tube was always observed with the second interface remaining attached to the opposite end. In the experiments conducted at supercritical temperatures, both interfaces start moving into the capillary tube at the initial moments. At some time moment one interface, being still quite close to the end of the capillary tube, stops, while the second interface continues its motion further into the tube.

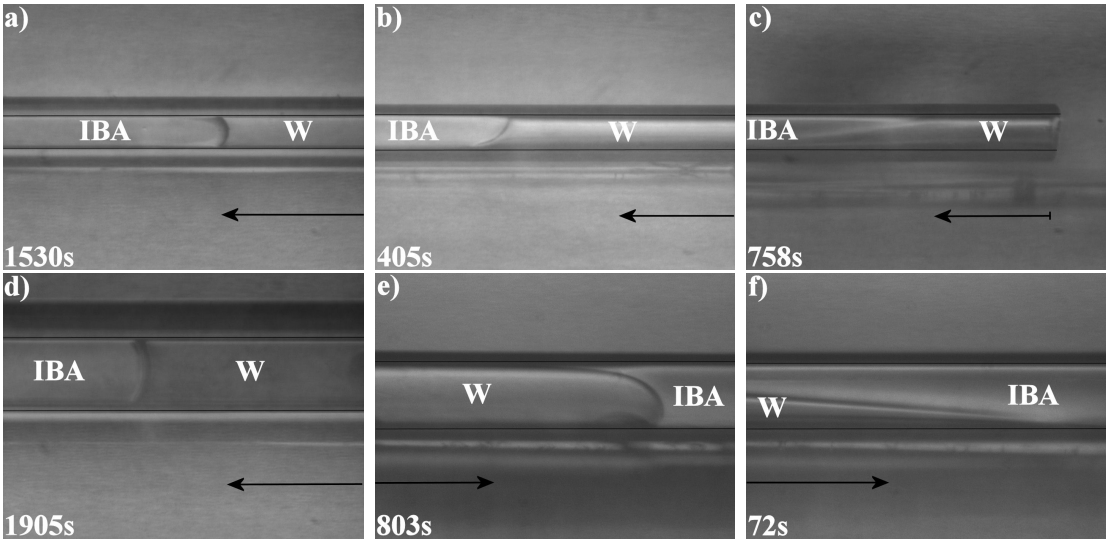

Figure 3.18: The shape of the IBA/water interface in capillary tubes of square **(a,d)** and circular **(b,c,e,f)** cross-sections with diameters of 0.2 mm **(a-c)** and 0.4 mm **(d-f)** and lengths of 10 cm at different temperatures: **a,d)** $T = 20^oC$, **b,e)** $T = 26^oC$, and **c,f)** $T = 30^oC$. 'IBA' and 'W' designate the IBA and water phases, respectively.

The shapes of the stabilized IBA/water interfaces strongly depend on the mixture temperature, as it can be seen in Figure 3.18. Below the critical point the role

of capillary forces is sufficiently strong to make the interface being vertical at least in the capillary tubes of smaller diameters (see Figure 3.18a,d). The effect of gravity is non-visible, the meniscus having axisymmetric shape (the density difference between IBA and water is also very small). For these temperatures, the estimation of Bond number (Equation 2.16) also indicates the dominance of the capillary effects ($Bo < 1$). In the capillary tubes with diameter of $0.6\,mm$ and larger, the apparent contact angles get slightly different at the upper and lower parts of the capillary tube. The gravity effects also become apparent in the smaller capillary tubes but at near-critical temperatures when the interfacial tension decreases (Figure 3.18b,e). At higher temperatures, higher than 30^oC, the interfacial tension becomes negligible and therefore the IBA phase is displaced due to gravity (Figure 3.18c,f). The wetting properties of the IBA/water mixture seem to be also temperature dependent. At undercritical conditions water looks to be more wettable than IBA. Closer to the critical temperature and above, the visible contact angles have different signs at the lower and upper sides of the capillary tube.

A discussion about how the IBA becomes removed from the capillary tube is required. It was observed that at temperatures below the critical point the interface always propagates from one side of the capillary tube only, being obviously driven by the capillary pressure, i.e. representing the process of spontaneous imbibition. As in the glycerol/water experiments, the contact line moves together with the main interface, and no IBA phase seems to be left on the walls of the capillary tube after the interface passage.

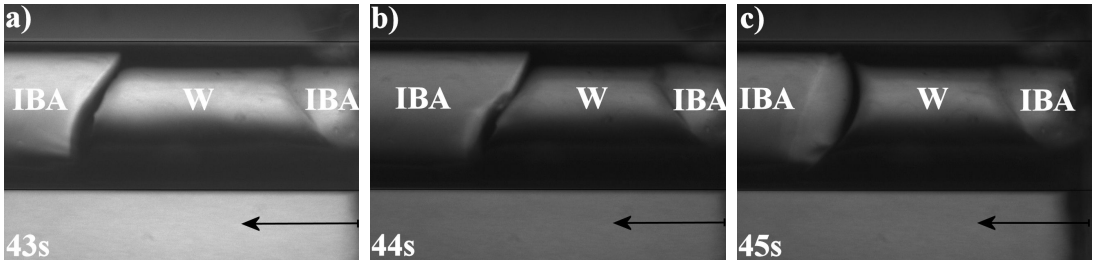

Figure 3.19: The initial evolution of the IBA/water interface in a capillary tube of circular cross-section with diameter of $0.8\,mm$ and length $10.3\,cm$ at temperature $T = 20^oC$.

In the capillary tubes with larger diameters, $d \geq 0.6mm$, the propagating interface experiences quite complex modifications of its shape at the time of the initial IBA/water contact as shown in Figure 3.19. The initially vertical IBA/water boundary is unstable and breaks down: the water phase under-rides IBA forming a new isolated droplet of IBA phase at the end of the capillary tube; the new

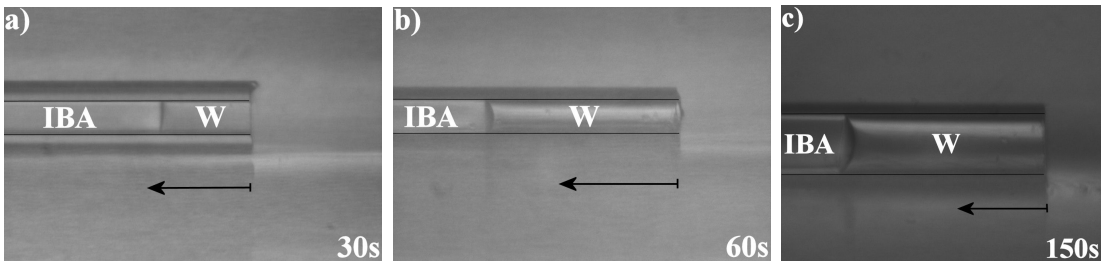

Figure 3.20: The initial evolution of the IBA/water interface in smaller capillary tubes at undercritical temperatures; **a)** square cross-section capillary tube with diameter of $0.2\,mm$ and length $10\,cm$ at temperature $T = 20^oC$; **b)** circular cross-section capillary tube with diameter of $0.2\,mm$ and length $10\,cm$ at temperature $T = 20^oC$; **c)** circular cross-section capillary tube with diameter of $0.4\,mm$ and length $10\,cm$ at temperature $T = 24^oC$.

IBA/water interface propagates further in the tube. This initial evolution, during which two IBA/water interfaces could be noticed at one end, typically takes about $\sim 10\,min$. Finally, the under-ridden IBA droplet is displaced/dissolved from the capillary tube. The newly formed IBA/water interface is more stable and does not experience any further instabilities. The complex evolution at the time of entrance of the water phase into the capillary tube was more evident at near-critical temperatures when the interfacial tension is lower. The interface never breaks in the capillary tubes with diameters $\leq 0.4\,mm$, at temperatures lower than 25^oC, when the interfaces were always stable from the start of the experiment (Figure 3.20).

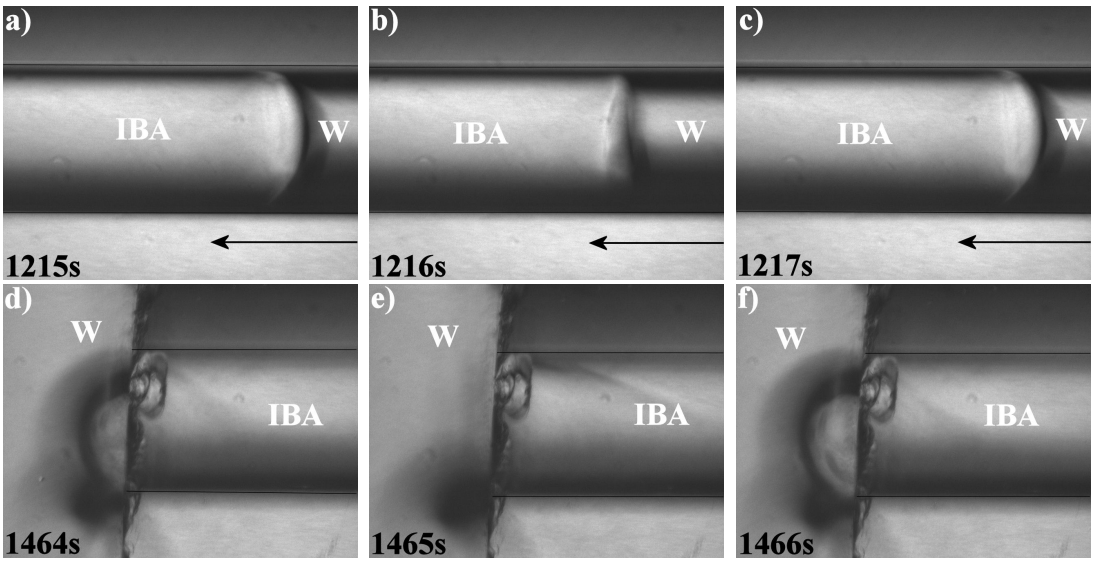

Figure 3.21: **(a-c)** Oscillations of the stabilized interface in a capillary tube of circular cross-section. **(d-f)** The formation and detachment of the IBA droplet at the opposite end of the capillary tube. The tube has a diameter of $0.8\,mm$ and length $10.3\,cm$. The temperature is maintained at $T = 20^oC$.

It was also observed that the meniscus shape experiences oscillations as demonstrated in Figure 3.21a-c. The amplitude of meniscus oscillations is larger in the capillary tubes of larger diameters and also in experiments conducted at near-critical temperatures. The time-resolution of the used visual rig was sufficient to estimate the period of oscillations which was found to be of the order of $2\,s$ in the capillary tube with diameter of $0.8\,mm$. It was also found that the penetration of the solvent from one end of the capillary tube was accompanied by the visible displacement of the solute from the opposite end (Figure 3.21d-f), where the droplets of IBA are periodically displaced and detached from the end of the capillary tube with the period equal to the period of the meniscus oscillations. The droplets are seemingly being detached when the buoyancy force overcomes the adhesion between the IBA droplet and the outer wall of the capillary tube, which defines the period of meniscus oscillations. Thus, it seems that the formation and detachment of the IBA droplets at the opposite end of the capillary tube are responsible for the appearance of the meniscus oscillations observed within the capillary tube.

Another question is when the symmetry of the experiment is broken. Two ends of the capillary tube are equivalent, two identical IBA/water interfaces should be expected at the ends of the capillary tube similar to the glycerol/water experiment, and the tubes are sufficiently long for the interfaces not to feel each other. Completing several test experiments, it was found that the symmetry is broken at the time of immersion of the capillary tube into the water bath: the IBA/water interface always starts moving into the capillary tube from the end that first touches the water. It should be underlined that the same initial conditions were realized in all experiments with all binary mixtures. The fact that the removal of the IBA phase occurs differently is explained by different material constants of the IBA/water mixture (lower viscosity, diffusivity, and density difference).

The spontaneous imbibition process involves the hydrodynamic flow driven by the capillary pressure. To figure out the role of hydrodynamic flows we fulfilled the experiment with spherical glass particles with diameters in the range of $100 - 400\,\mu m$ dispersed into the IBA phase. The spheres were settled on the bottom of the capillary tube. The evolution of the interface shape passing over the spheres is shown in Figure 3.22. The interface shape is affected by the imposed obstacles but the interface regains its normal shape and continues its normal run in the section of the capillary tube without particles. From Figure 3.22, one concludes that the particles are generally not engaged by the flow. Having watched the full video it may be concluded that each particle is being moved only when the interface passes over the particle. The second particle is smaller, obviously has less

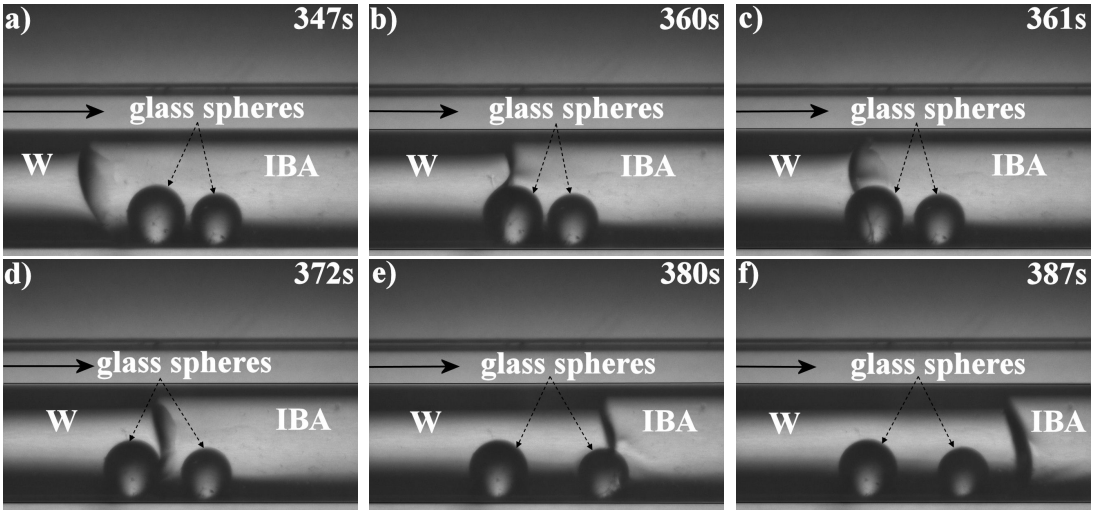

Figure 3.22: The shape of the IBA/water interface within a capillary tube of circular cross-section with diameter of 0.6 mm and length 10 cm. The IBA phase contains spherical glass particles. The temperature is $T = 23^oC$.

inertia, and moved farther. Each particle moves first forwards, when the interface approaches the particle from the left, and then backwards, when the interface leaves the particle. Thus, particles moved only when in contact with the interface and they did not move as a result of the IBA phase being displaced (pushed) by the water phase. This could mean that each glass bead is in equilibrium as long as is surrounded by only one phase (i.e. either before being in contact with the interface or after the interface past over it). However, when the glass bead is in contact with the interface, the system is not in equilibrium because of the different forces acting on the two sides of the bead (i.e. the side which is in contact with the water phase and the side which is in contact with the IBA phase). This could cause the movement of the glass bead, which would tend to reach again the equilibrium state.

Finally, based on the sequence of snapshots the speeds of the interface propagation were derived. Some values for the velocities of the interface within the smallest capillary tubes ($d = 0.2\,mm$ and $d = 0.4\,mm$) are shown in Figure 3.23. In the initial moment the interface speed increases up to a limiting value that remains constant while the interface is moving through the middle section of the capillary tube; the interface speed drops when the interface approaches the opposite end. The constant speed of the interface agrees with Equation 2.17. The use of Equation 2.17 allows one to estimate the capillary pressure in the capillary tube of diameter $d = 0.2\,mm$ being equal to $1\,Pa$. However, according to Equation 2.17 and Equation 2.6, the speed of the interface should be proportional to the diameter of the capillary tube, which was not observed. At the moment we do not know

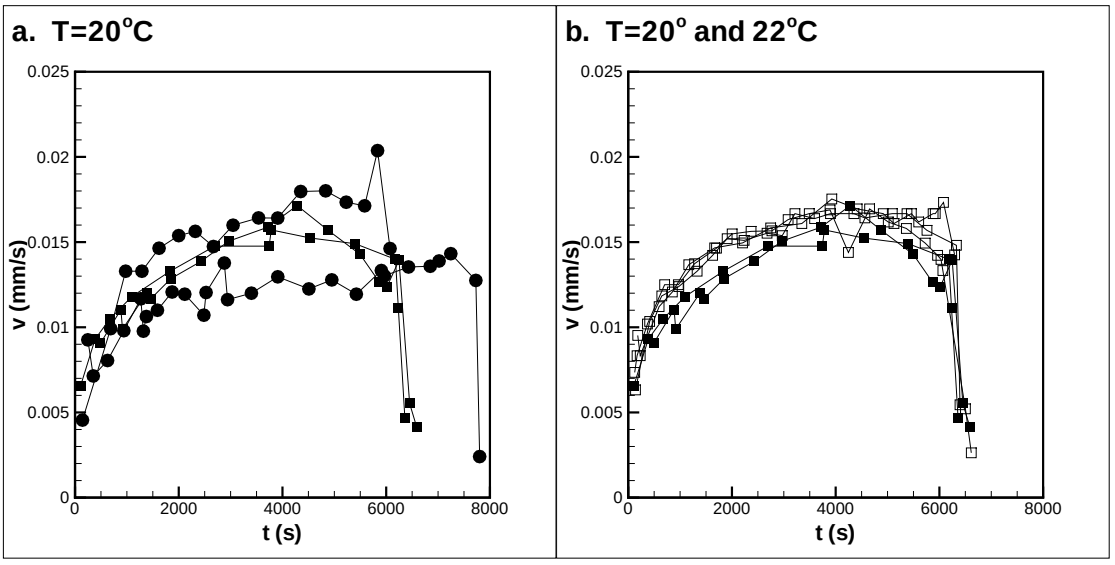

Figure 3.23: The speed of the IBA/water interface at undercritical conditions. **a)** Results for capillary tubes of different diameters are shown, $d = 0.2\,mm$ (■) and $d = 0.4mm$ (●); the capillary tubes have the length $L = 10cm$, and the temperature is $T = 20^oC$. **b)** The results are for the same capillary tube (diameter $d = 0.2\,mm$ and length $L = 10\,cm$) but at different temperatures, $T = 20^oC$ (■) and $T = 22^oC$ (□). Data from several different experiments are shown for each case.

the reason for this discrepancy. The speed of the interface grows with the increase of temperature (see Figure 3.23b). In Figure 3.23b, the temperature difference is not very big but is sufficient to demonstrate the increase of the speed of the interface with the increase of temperature. The experiments were carried out at these temperatures in order to avoid the possible influence of additional effects at values of temperature closer to the critical one.

Unfortunately, accurate measurements of the interface speeds at near-critical temperatures could not be obtained. The snapshots obtained for these conditions (e.g. Figure 3.18b,e) indicate that the gravity effects become more important in driving the fluid flow. The diffusivity is low, and the interface motion is complex representing the interplay between the spontaneous imbibition and gravity current effects.

At supercritical temperatures the interfacial tension effects decrease, and the capillary force is not capable of displacing the IBA phase. The time evolution of the interfaces at supercritical conditions is shown in Figure 3.24. Initially, the water phase moves into the capillary tube from both ends under-riding the IBA phase. Being quite close to the capillary tube ends, one of the interfaces stops moving (Figure 3.24d and Figure 3.24f show the immovable interface). The other interface continues its motion (Figure 3.24a-c,e), it diffuses faster and disappears

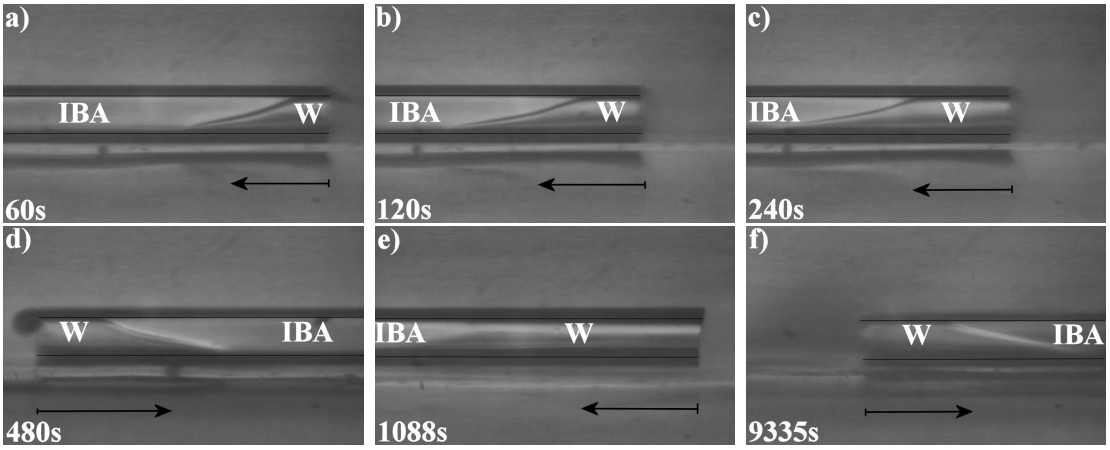

Figure 3.24: The interface shapes at different time moments within a capillary tube with diameter of $0.2\,mm$ and length $10\,cm$. The temperature is $T = 27^oC$.

much earlier than the second immovable interface (Figure 3.24e shows one of the latest moments when the moving interface can still be distinguished; Figure 3.24f depicts the clearly visible immovable interface at a much later time moment). The observed diffusion of the phase boundaries is not uniform along its length with the visible smearing starting at the tip.

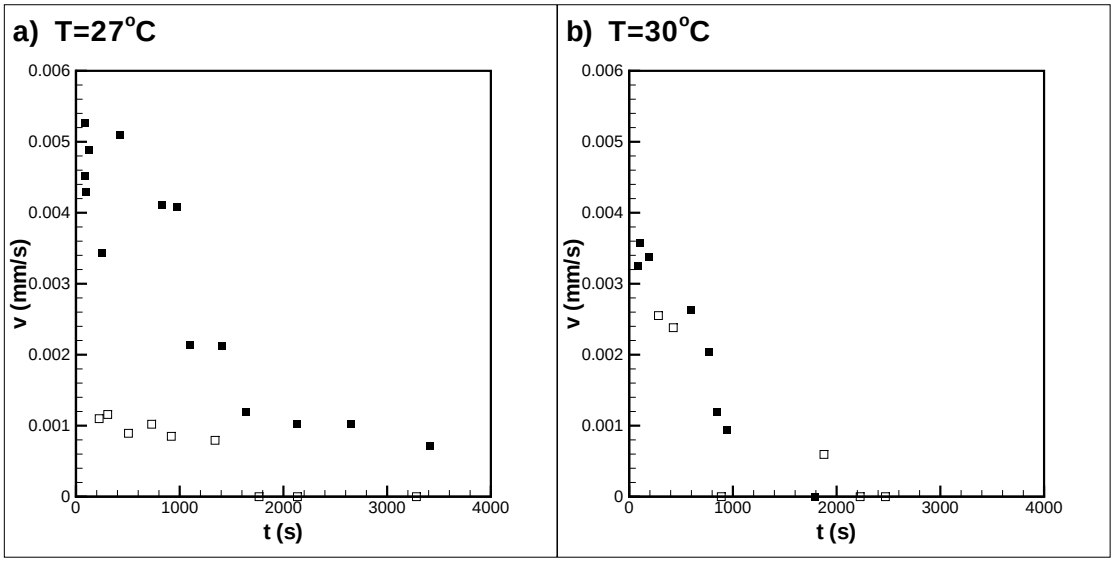

Figure 3.25: The speeds of the IBA/water interfaces in capillary tubes with diameter of $0.2\,mm$ and length $10\,cm$. The experiments were conducted at temperatures: **a)** $T = 27^oC$ and **b)** $T = 30^oC$. The filled symbols define the motion of one interface (which moves for longer time), while the empty symbols define the motion of the second interface from the opposite end of the capillary tube.

At supercritical conditions IBA and water are miscible in any proportions. The way in which water penetrates into the capillary tube is different from the observations outlined above for the other binary mixtures and for undercritical conditions.

From one hand, the observed behaviour is non-symmetrical, similar to the under-critical observations, which might point out that the capillary or gravity forces can be important (the hydrodynamic motion initiated by the capillary/gravity forces is still significant due to the lower viscosity of the IBA/water mixture compared to the viscosities of glycerol/water and soybean oil/hexane mixtures). From the other hand, two interfaces at the opposite ends are observed, similar to the mixtures of glycerol/water and soybean oil/hexane. The observed motion of the IBA/water interfaces is quite irregular. The speeds of the two interfaces derived from the image sequences are shown in Figure 3.25. The measurements show that the speed of the first (moving) interface is comparable with the speed of glycerol/water interface in capillary tubes of the same diameter. This suggests that the propagation of this interface is not driven by diffusion, since the diffusion coefficient of the IBA/water mixture is generally one order smaller than the diffusion coefficient for glycerol and water. The evolution of the second (immovable) interface is likely to be defined by diffusion but owing to low diffusivity it evolves very slowly.

3.4 Summary

The shapes and dynamics of solute/solvent phase boundaries of three different binary mixtures were examined in open horizontal capillary tubes. No pressure gradient was applied between the ends of the tube. Capillary tubes of different diameters, as small as $0.2\,mm$ were used. The task was to separate the interfacial diffusion from the hydrodynamic flows driven by either Marangoni or solutal convection, or by the capillary pressure (the spontaneous imbibition). Traditionally, the dissolution process is reduced to a simple interphase diffusion. A classically expected scenario for the dissolution of a solute droplet from a capillary tube would be as follows: two solute/solvent interfaces are formed at the ends of the capillary tube, if no external pressure gradient is applied, no flows should be generated and hence the phase boundaries should not move, and the boundaries will smear and finally disappear due to diffusion. It was found that removal of solute phase occurs differently. Firstly, numerous physical phenomena are involved at different stages of these seemingly simple experiments. Secondly, even diffusion dynamics of the solute/solvent interfaces differs from general expectations.

We managed to isolate the pure dissolution process in the experiments with glycerol/water and soybean oil/hexane mixtures. The short initial evolution (for about

1 *min*, when diffusion is negligible) is gravity driven; the observed motion represents a gravity current also called a lock-exchange flow [105, 106, 107]. The contact lines are not closed within the capillary tube and the solvent phase displaces small portions of the solute at both ends. But when the interfaces fully enter the capillary tube and the contact lines become closed within the tube, the solute phase becomes locked. At this moment the gravity force is balanced by the capillary force, which ends the initial 'mechanical' displacement of the solute phase. From this moment, whole interfaces with almost steady shapes move into the center of the capillary tube, which obviously cannot be interpreted as a gravity current. These phase boundaries smear in time seemingly due to mutual interphase diffusion, but the smearing rate is very small, considerably smaller compared to the speed of the boundary movement as a whole. The observed motion of the phase boundaries resembles the evaporation or solidification process: the interfacial mass transfer results in shrinking of the solute droplet, but the solute/solvent boundaries remain visible (if not sharp). The two interfaces move with equal speeds. The speeds of the interfaces slow down following the $t^{-2/3}$ power law in the capillary tubes of smaller diameters, i.e. do not follow the predictions of the diffusion theory, $t^{-1/2}$. The dissolution rate increases with growth of temperature, which was expectable, but it was also found that the rate of decrease of the droplet's length is proportional to the area of the cross-section of the capillary tube, which is a surprising result. Finally, it was concluded that the phase boundaries could possibly be moving due to barodiffusion.

By comparing the interface speeds, we may also conclude that the diffusion coefficient of the soybean oil/hexane mixture is obviously higher than the diffusion coefficient of the glycerol/water interface, which agrees with theoretical predictions [205]. Moreover, the values of the diffusion coefficients reported in the literature allowed us to conclude that the speed of the interface is proportional to $D^{1/3}$.

The behaviour of the IBA/water mixture was different. Below the critical point the mixture can be heterogeneous in equilibrium. But the amount of IBA enclosed in the capillary tube was negligible in comparison with the volume of the water bath, and consequently was fully dissolvable. Nevertheless, it was found that IBA and water behaved like two immiscible liquids in the experiments carried out below the critical temperature. Water penetrated into the capillary tube from one side; from another side IBA droplets were displaced. The droplets were detached when their size was sufficient to overcome the adhesion to the outer wall of the capillary tube. The speed of the interface propagation grew in the beginning up to a constant value, then the speed remained constant for the main part of the

experiment and sharply decreased when the interface approached the second end of the capillary tube. The motion of the interface was explained by spontaneous imbibition. In the experiments with microparticles dispersed in the IBA phase, it was observed that the interface was able to move the particles, but the IBA phase which was displaced by the water phase did not force the particles to move.

Above the critical point, IBA and water are miscible in all proportions. The observed meniscus shape was defined by the balance of the capillary and gravity forces, which seemed comparable. The capillary pressure was not sufficiently strong to initiate the spontaneous imbibition. The initial evolution of the interfaces could be explained by the gravity action. Two interfaces were observed within the capillary tube. One of them was initially moving but quickly became very diffusive and indistinguishable. The other interface was observed for considerably longer time periods but it remained stationary.

The diffusion and viscosity coefficients and density difference between mixture components for the IBA/water binary mixture are considerably lower in comparison to those of glycerol/water and soybean oil/hexane mixtures, both below and above the critical point. Below the critical point, the interfacial diffusion at the IBA/water boundaries was not observed at all. The interface speed is comparable to the initial speeds of glycerol/water and soybean oil/hexane interfaces, but the solute is removed faster as the speed of the undercritical IBA/water interface remains almost constant for the duration of the experiment. Above the critical point, two IBA/water interfaces penetrate into the capillary tube, and their motion should be driven by mechanisms similar to those that govern the motion of glycerol/water and soybean oil/hexane interfaces. However, apparently owing to smaller diffusion and viscosity coefficients and smaller density difference the supercritical IBA/water phase boundaries move differently.

Finally, it should be noted that the interface shapes and dissolution dynamics were qualitatively the same in capillary tubes with different cross-sections, in tubes made of different materials, and in new tubes and tubes previously used for the experiments and then washed with water and acetone and dried out. Bulk interfaces and contact lines always moved with the same speeds.

Chapter 4

Dissolution dynamics of liquid/liquid interfaces in a micromodel

In this chapter are reported optical observations of the dissolution behavior of glycerol/water, soybean oil/hexane, and isobutyric acid (IBA)/water binary mixtures within a glass micromodel built as a $2D$ regular network of capillary tubes with diameter of $0.2\,mm$. The micromodel is initially filled with solute and then is horizontally immersed into a thermostatic solvent-filled bath. The micromodel is open at its corners for solute dissolution to occur with no pressure gradients being applied. The results obtained show that the solvent penetration into the micromodel is diffusion-dominated in completely miscible binary mixtures (glycerol/water and soybean oil/hexane). This is however non-Fickian diffusion with the dissolution rate, dV/dt, being proportional to $D^{1/3}t^{-0.4}$ for almost the entire duration of the experiment (V is the volume occupied by the solvent, D is the diffusion coefficient, and t is time). For the partially miscible IBA/water mixture the experiments performed at undercritical temperatures revealed that the diffusive transport was negligible despite the mixture being out of its thermodynamic equilibrium. The water phase penetrated into some of the channels, but IBA was never completely displaced/dissolved from the micromodel and numerous interfaces remained visible after very long time periods.

4.1 Introduction

Multiphase flow phenomena in porous media have been extensively studied through both experiments and numerical simulations. A lot of attention has been paid to this topic in the last few decades and pore-network modelling has become one of the main approaches to study flows in porous media. Their large scale applications [3, 7] in enhanced oil recovery [10, 13], enhanced aquifer (and soil) remediation [30, 190], solvent extraction [189] and drug delivery [48] determined both industrial and academic researchers to focus on this topic. The pore sizes are typically small, which makes the hydrodynamic flows within porous media being rather slow and as a result the diffusion, wetting and capillary effects play essential roles in the overall mass transport. As pore-network modelling on its own cannot provide all the detailed information needed for practical problems to be solved at macroscale, the necessity of completing the theoretical studies brought forward the experimental use of micromodels for visualizing flow patterns at the pore level.

Making use of the so-called network approach, the aim of the experiments reported in this chapter is defined as to understand the dissolution dynamics of liquid/liquid binary mixtures within a regular flow-path micromodel, which represents a step further from the experiments reported in Chapter 3, in which the dissolution behavior of liquid/liquid miscible interfaces was investigated in single capillary tubes. The glass micromodel used in this work has dimensions comparable with the typical pore sizes in geological applications frequently assumed to be 0.1 mm and smaller. The pores however could be larger in the case of vegetable oil extraction.

Numerous experimental studies which employ micromodels for studying a large variety of pore-scale mechanisms characteristic to EOR and EAR processes have been reported in the literature in the last few decades. Besides petroleum engineering and geological applications there are many other fields in which micromodels find their applicability. A comprehensive literature survey on the subject can be found in Section 2.7.2.

In this study the micromodel saturated with the solute phase was immersed into a solvent-filled thermostatic bath. When the pure components of a binary mixture are brought into contact a non-equilibrium binary system is obtained. Equilibration of the mixture to a thermodynamically stable state involves diffusive and hydrodynamic processes, and usually occurs very slowly. The diffusive mass transport in a liquid/liquid system saturating a porous medium is the key interest of this chapter. Despite an apparent simplicity of the diffusion it is difficult to provide

a simple estimate for the typical dissolution time of a solute droplet surrounded by solvent even in simpler geometries [213], and the problem becomes even more challenging if a liquid/liquid system saturates a porous bulk.

In addition, liquid/liquid interfaces should be endowed with capillary properties, while liquid/solid interfaces posses wetting properties [1, 68, 63, 213], which can introduce additional mass transfer mechanisms. In the experiments with single capillary tubes reported in Chapter 3 was found that the mass transfer is predominantly diffusion defined in liquids miscible in any proportion, and is driven by the capillary pressure in IBA/water binary mixture below its critical temperature. Even though a high number of studies involving capillary driven displacements within micromodels can be found in the literature (see Section 2.7.2), to date, the only other studies known to the author that describe spontaneous (free) imbibition/drainage visual observations within micromodels are the ones of Chatzis and Dullien [178] and Jamaloei et al. [182, 160]. Furthermore, the author is unaware of any experimental work in which the diffusion-driven dissolution of miscible liquids within micromodels has been studied. Therefore the principal aim of the experimental study reported in this chapter is to advance the fundamental understanding of the liquid/liquid dissolution process at microscale with the expectancy that later this will convey to more reliable models at macroscale. The development of predictive pore-network models is not possible without reaching a clear understanding of pore-level transport mechanisms which is usually achieved experimentally by visual observation of flows in porous media.

4.2 Materials and Methods

4.2.1 Binary mixtures

In this chapter, the evolutions of glycerol/water, soybean oil/hexane and isobutyric acid/water binary mixtures were examined within a micromodel. All chemicals having high purities were purchased from Fisher Scientific or Sigma Aldrich and were used as received.

Glycerol and water and soybean oil and hexane are miscible in any proportions at all temperatures. The IBA/water mixture is characterized by the upper critical solution temperature, $T \sim 26.3^oC$ [193, 62, 63]. At temperatures above the critical point, the mixture components are miscible in any proportions. Below the

critical point, only small amounts of IBA are completely miscible in water, and if a larger droplet of IBA is added, then IBA and water phases will inter-diffuse until the equilibrium concentrations, c_1 and c_2, are established. The values of c_1 and c_2 are temperature dependent and can be obtained from the phase diagram available e.g. in the paper of Pojman et al. [63]. Values of diffusion coefficients for the mixtures at different temperatures and for different compositions and other physical properties for the pure substances can be found in Section 3.2.

4.2.2 Micromodel design and fabrication

The regular pore-shape glass micromodel used for the experiments described in this chapter (micromodel A) was manufactured by the Dolomite Centre Ltd. UK. Once the chip was designed in AutoCAD the drawing file (Appendix A) was translated into an appropriate format for mask fabrication. The isotropic wet-etching technique was used to fabricate the micromodel (Figure 4.2) [188]. As the isotropic etching results in widening of features exposed from a mask the shape of the resulting channels corresponds to a near circular profile (with width 210 μm and depth 200 μm) [188]. We considered this to be acceptable for our purpose as in the experiments performed within capillary tubes similar results were obtained for circular and square cross-sections [213]. The length of the mutually perpendicular channels connecting the pores is 2 mm. The coordination number of the pores is equal to 4. The dimension of the micromodel is 45x45x4 mm and it contains 361 pores and a larger channel (500 μm) on the edge to allow fluid to enter the porous media at any point (Figure 4.1). All micromodel characteristics are summarized in Table 4.1. The optical glass $B270$ used for the micromodel fabrication offers excellent optical properties and chemical resistance allowing a broad range of solvents and chemicals to be used [188].

Table 4.1: Micromodel characteristics

Characteristic	Value
Length	4.5 cm
Width	4.5 cm
Etched depth	200 μm
Pore and channel width	210 μm
Coordination number	4
Aspect ratio	1
Areal porosity	17%

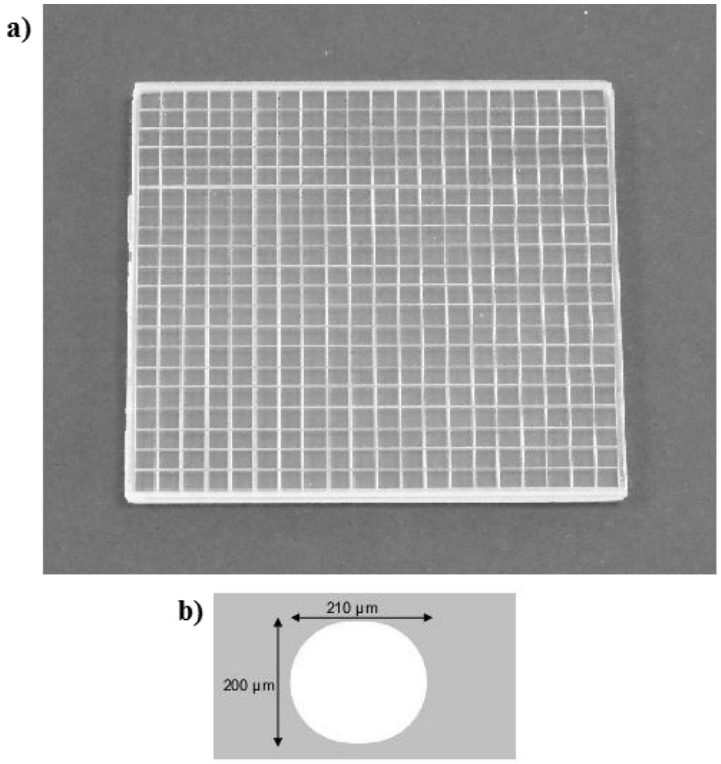

Figure 4.1: Micromodel A with dimensions of 45x45x4 mm, containing 19x19 channels with near-circular profile (0.21 mm width and 0.2 mm depth) spaced at 2 mm distance and a larger inlet channel on the edge (0.5 mm width and 0.2 mm depth). **a)** Empty micromodel; **b)** Section view of the channels (as supplied by the manufacturer [214]).

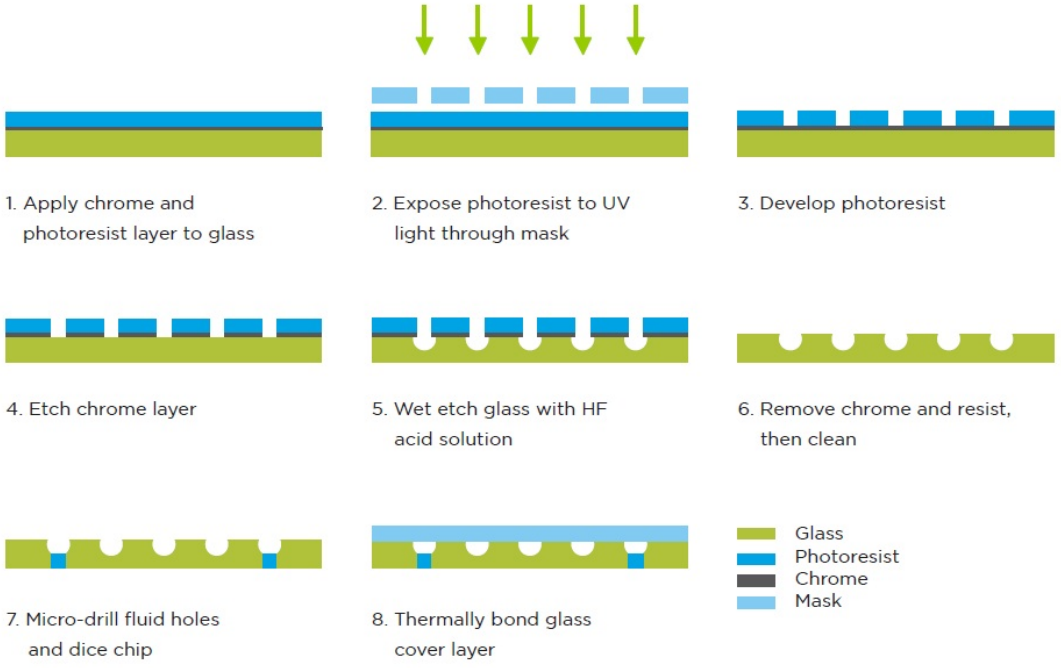

Figure 4.2: The basic process used for fabrication of glass microfluidic chips [188].

4.2.3 Experimental setup

First, the micromodel was saturated with the solute phase (glycerol, soybean oil or IBA) and then was immersed into a thermostatic transparent solvent-filled (water or hexane) bath. The micromodel was placed horizontally in the bath. No pressure gradient was applied, with all 4 corners of the micromodel being open for the solvent to penetrate into the micromodel.

The experiments were performed at various temperatures in the range of $20^oC - 30^oC$. The temperature in the water bath was controlled with a Grant digital thermostat (GD100, stability at 37^oC is 0.05^oC); the homogeneity of the solvent temperature was checked in several reference points with a Checktemp1 thermometer by Hanna Instruments (accuracy 0.3^oC).

Figure 4.3: Nikon AF Micro-Nikkor lens 60 mm f/2.8D mounted to the CCD camera.

The dissolution front was recorded with a system very similar to the one described in Section 3.2 including a CCD camera (LaVision Imager 3S) equipped with a Nikon AF Micro-Nikkor lens 60 mm f/2.8D, a diffuser (LaVision, VZ illumination high-efficiency diffuser) and a diode laser (Oxfordlaser Firefly system) used for illumination. All pieces of equipment used, except the Nikon lens were described in Section 3.2. The Nikon lens (Figure 4.3) was used in these experiments instead of the Questar lens in order to obtain a larger field of view so that the entire dissolution front could be tracked within the micromodel. To improve the image contrast the solute-liquids were coloured with methylene blue, Sudan IV, or eriochrome black T dyes purchased from Sigma Aldrich. For visualizing the shapes of the interfaces in the pores and throats of the micromodel, the Nikkor

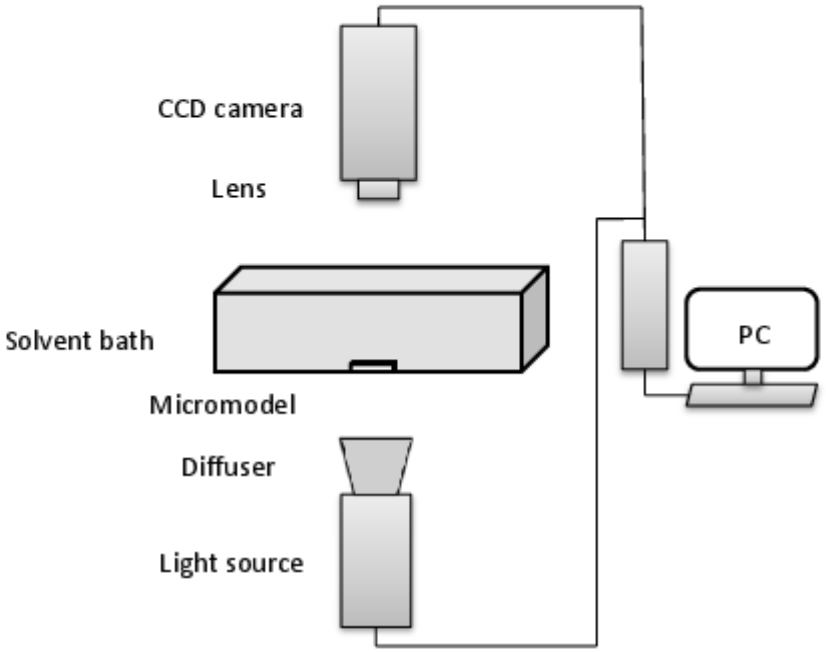

Figure 4.4: A schematic view of the experimental setup.

lens was replaced with the Questar lens (QM100 Model #30003). A schematic view of the experimental setup is depicted in Figure 4.4.

4.3 Experimental results

4.3.1 Glycerol/water mixture

Glycerol and water are completely miscible in all proportions in any conditions. The propagation of dissolution fronts was observed within a network model with a regular flow-path pattern. Some air bubbles remained trapped in the micromodel, which seemingly happened due to the filling procedure. The number of air bubbles was however rather small and could be disregarded as it did not affect any integral characteristics such as volume distribution in the entire micromodel. Still, their presence was important at pore-level leading to the non-symmetry of the dissolution front. Several snapshots showing the progression of the dissolution front are depicted in Figure 4.5 and Figure 4.6 for the experiments carried out at 20^oC and 30^oC. In these figures, frames 4.5(g-l) and 4.6(g-l), respectively show

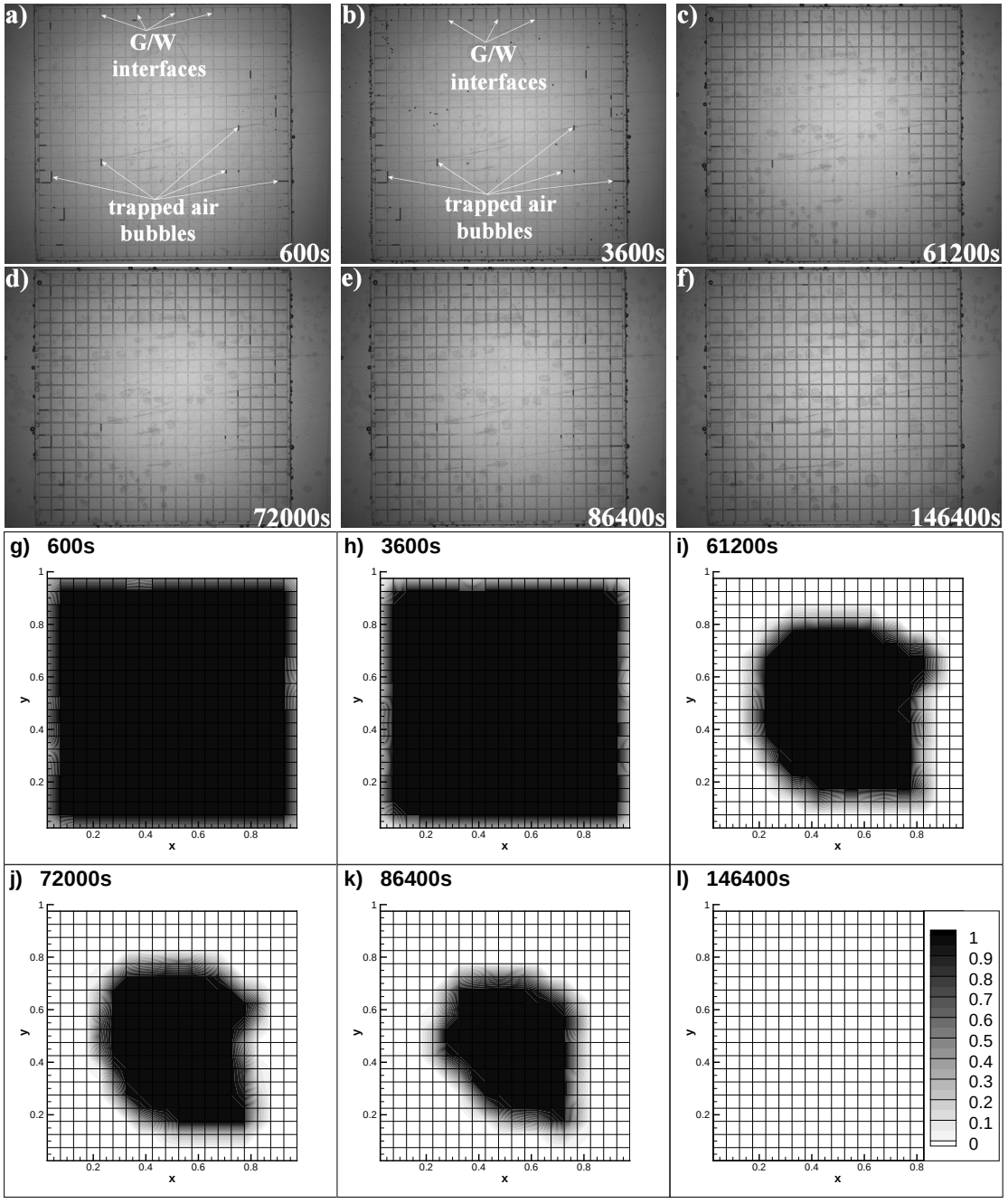

Figure 4.5: **(a-f)** Snapshots of the glycerol/water phase boundaries within micromodel; the channels filled with glycerol phase are shown with a lighter grey color and the ones filled with water have a darker grey color; air bubbles trapped within the channels are shown in black. **(g-l)** Interpretations of the experimental observations; each frame corresponds to one of the snapshots shown in frames **(a-f)**; the legend shows the volume fraction of glycerol in the micromodel; the data points were obtained by averaging the amount of glycerol remained in a unit cell of the micromodel at the time moment indicated on each frame; a unit cell is represented by a square with side channels of $2\,mm$ length; Temperature is T=20^oC. The corresponding time moments are indicated in the pictures.

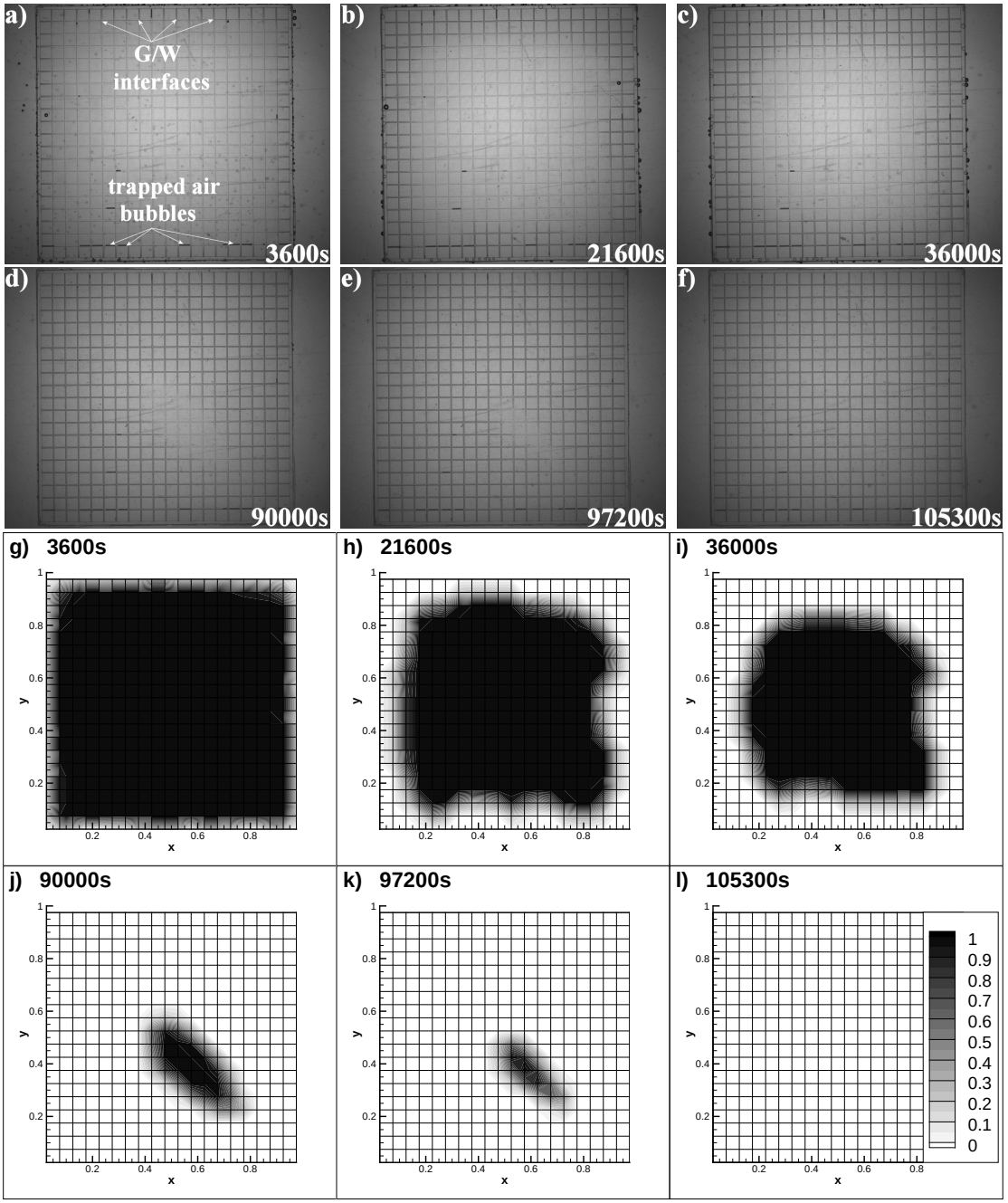

Figure 4.6: **(a-f)** Snapshots of the glycerol/water phase boundaries within micromodel; the channels filled with glycerol phase are shown with a lighter grey color and the ones filled with water have a darker grey color; air bubbles trapped within the channels are shown in black. **(g-l)** Interpretations of the experimental observations; each frame corresponds to one of the snapshots shown in frames **(a-f)**; the legend shows the volume fraction of glycerol in the micromodel; the data points were obtained by averaging the amount of glycerol remained in a unit cell of the micromodel at the time moment indicated on each frame; a unit cell is represented by a square with side channels of $2\,mm$ length; Temperature is T=30^oC. The corresponding time moments are indicated in the pictures.

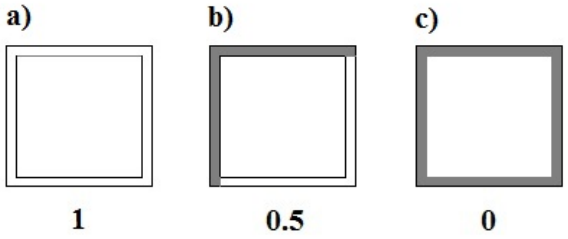

Figure 4.7: Schematic representation of a unit cell of the micromodel; **a)** Volume fraction of glycerol in the cell is 1; **b)** Volume fraction of glycerol remained in the cell is 0.5; **c)** Volume fraction of glycerol remained in the cell is 0.

the interpretations of the experimental observations. The contours shown in these frames are based on data points obtained by averaging the amount of glycerol remained in a unit cell of the micromodel at the time moment indicated on each frame. A unit cell of the micromodel is represented by a square with side channels of $2\,mm$ length. The amount of glycerol remained in each unit cell was calculated as $V_g = (V_1 + V_2 + V_3 + V_4)/4$ where V_i is the fraction of glycerol in every side channel ($i = [1, 4]$). V_i varies from 1 (i.e. fully filled with glycerol) to 0 (i.e. fully filled with water) and takes intermediate values in the range of 1 to 0 for the case of partially filled channels. For example, a schematic representation of a unit cell filled with glycerol, half glycerol/half water and water, respectively is shown in Figure 4.7.

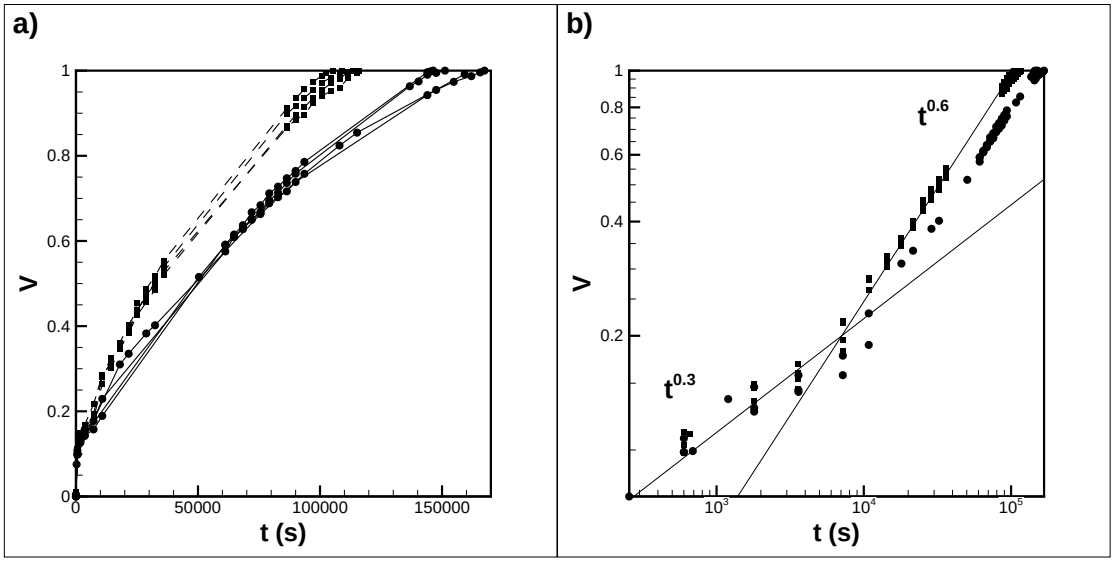

Figure 4.8: **a)** The volume fraction of water within the micromodel at different time moments; **b)** The same data set plotted in logarithmic coordinates; (•) T=20^oC and (■) T=30^oC.

The solvent penetrated uniformly into the micromodel indicating that the solute is dissolved rather than displaced. The mass transport is diffusion dominated. As noticed, even though the micromodel employed in the experiments is a homogeneous network the expected symmetry of the dissolution front was not observed owing to the trapped air bubbles. The dissolution front advanced past these bubbles signifying that water could bypass the bubbles but could not displace them.

Figure 4.8 shows the total volume of water-rich phase within the micromodel at different time moments. As expected the temperature increase shortens the dissolution time (Figure 4.8(a)). Complete dissolution of glycerol from the micromodel took on average $42\,h$ at 20^oC and around $30\,h$ at 30^oC with complete dissolution times varying slightly between different experiments due to the amount and position of air bubbles trapped in the micromodel. However, as it can be seen in Figure 4.8(a) the distribution of complete dissolution times is quite narrow and therefore considered acceptable. In Figure 4.8(b) it can be seen that two power laws, $t^{0.3}$ and $t^{0.6}$, can be identified to characterize the dissolution rate, but none of them corresponds to Fickian law time dependence. The coefficients of proportionality, A_r and B_r, introduced by the relations $V = A_r t^{0.3}$ and $V = B_r t^{0.6}$, are $0.13\,m^3 s^{-0.3}$ and $8 \cdot 10^{-4}\,m^3 s^{-0.6}$ at 20^oC and $0.14\,m^3 s^{-0.3}$ and $9.8 \cdot 10^{-4}\,m^3 s^{-0.6}$ at 30^oC.

In Chapter 3 was observed that the position of the glycerol/water front was moving into the capillary tube with the dependence $t^{2/3}$ in the beginning of the experiment, when water entered the capillary tube and the convective motion could be noticed, and with $t^{1/3}$ dependence characterizing the main diffusive run. When the speeds of the phase boundaries were considered these time dependencies became $t^{-1/3}$ and $t^{-2/3}$. The former expression characterized the initial evolution which was gravity-driven and the latter one characterized the evolution possibly driven by barodiffusion.

The data collected in the experiments described in this chapter also show that the time evolution can be divided into two stages, with an initial transient trend being $t^{0.3}$, and with a later main trend being $t^{0.6}$. If the speed of the dissolution front is considered these dependencies become $t^{-0.7}$ and $t^{-0.4}$. It can be noticed that the former expression obtained in this case has a very close value to the one obtained for the dissolution stage possibly driven by barodiffusion in single capillary tubes. The small difference in value is attributed to the slightly different topology. Thus, one can conclude that the dissolution within micromodel could possibly be driven by barodiffusion in the first stage. The latter expression, $t^{-0.4}$

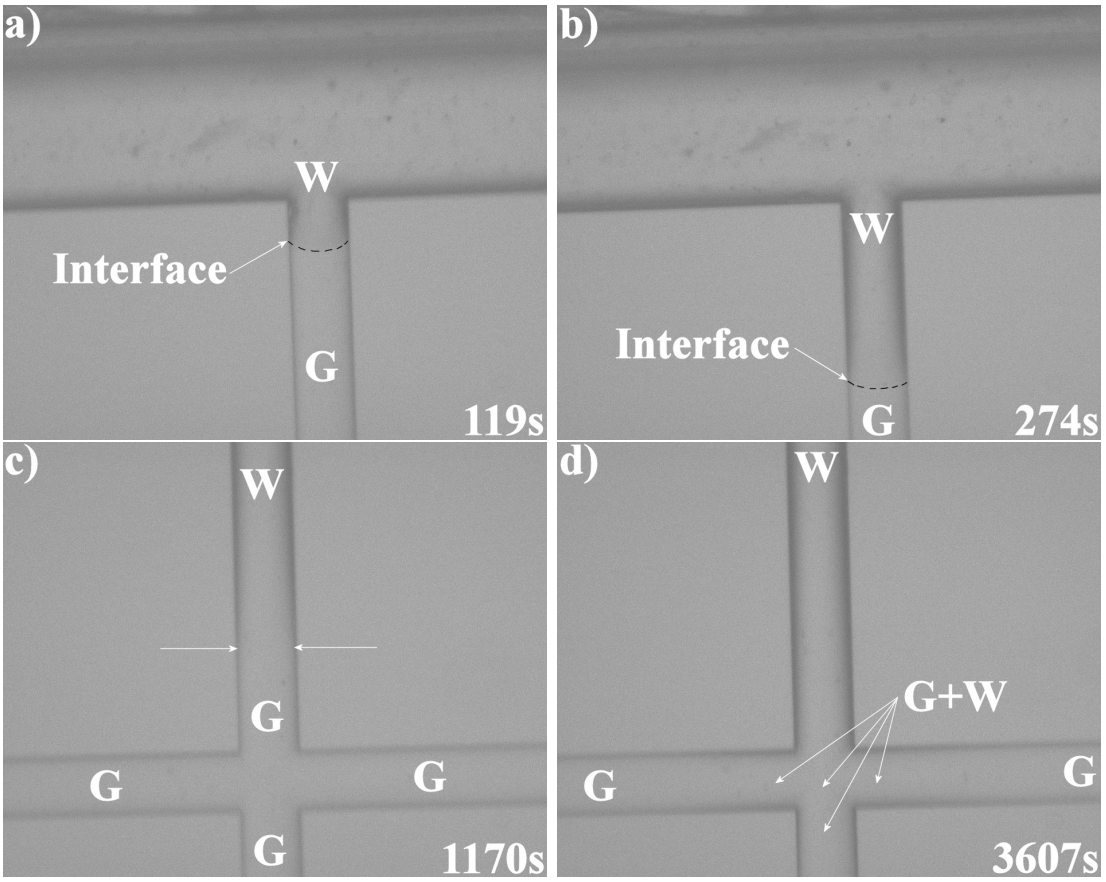

Figure 4.9: Magnified view within the micromodel during an experiment with glycerol/water at different time moments; **(a-b)** Top view of the interface at early time moments; **c)** The tip of the interface is already very diffused; the arrows indicate its approximate position which can be determined based on the color contrast; **d)** The two phases can be identified based on the color contrast; the channel filled only with water phase has a darker grey color, the ones filled only with glycerol phase have a lighter grey color and the channels where both phases are present are represented with lighter grey color in the middle and darker grey color on the channel edges. In all frames 'G' denotes glycerol phase and 'W' denotes water phase. Temperature is T=20.5^oC. The corresponding time moments are indicated in the pictures.

(also different from the classical diffusion $t^{1/2}$ dependence) characterizes the second stage of dissolution within micromodel which represents a subdiffusive regime. This second stage is much longer compared to the initial transient stage. Both regimes identified in these experiments are characterized by power laws that differ from the classical Fickian dependence which signifies that Fick's law is not capable of defining the observed behaviour, not even in a porous medium with a high degree of homogeneity.

In order to take a closer view at the shape of the interface the experimental setup was modified as described in Section 4.2.3. For glycerol/water mixture the shape

of the interface could be clearly distinguished for up to 10 min from the start of the experiment (Figure 4.9(a-b)), and after that the tip could not be clearly observed due to its diffusive smearing, but the dissolution front could still be followed (Figure 4.9(c-d)) up until the end of the experiment, as already shown in Figure 4.5 and Figure 4.6.

4.3.2 Soybean oil/hexane mixture

Soybean oil and hexane are completely miscible in all proportions in any conditions similar to glycerol and water. The same experiments as for glycerol/water mixture were performed at both 20^oC and 30^oC. Similar data were obtained with just a few particularities. More air bubbles remained trapped in the micromodel during the solute-filling phase. This happened most likely due to the different wetting properties of soybean oil relative to glass compared to the ones of glycerol. Moreover during the dissolution process these bubbles moved and formed larger aggregates that remained trapped in the network at the end of the experiment (Figure 4.10 and Figure 4.11). The dissolution times for soybean oil/hexane were shorter compared to the ones for glycerol/water (on average the dissolution took 19 h at 20^oC and 11 h at 30^oC, respectively) due to the higher diffusion coefficient of this mixture (Figure 4.12(a)). Similarly the asymmetry of the dissolution front was observed. It is also worth mentioning that even though the amount of air present in the micromodel was much higher (i.e. approximately double compared to the glycerol/water experiments) the dissolution front still continued its movement until the whole micromodel was filled with the solvent phase.

The dissolution process could be characterized with the same two power laws as in the case of glycerol/water (see Figure 4.8(b) and Figure 4.12(b)). The coefficients A_r and B_r, introduced by the relations $V = A_r t^{0.3}$ and $V = B_r t^{0.6}$ are $0.019 m^3 s^{-0.3}$ and $1.3 \cdot 10^{-3}\, m^3 s^{-0.6}$ at 20^oC and $0.02\, m^3 s^{-0.3}$ and $1.6 \cdot 10^{-3}\, m^3 s^{-0.6}$ at 30^oC. By comparing the B values for the glycerol/water and soybean oil/hexane experiments one finds that the diffusion front in the soybean oil/hexane experiments moves $1.6-1.7$ times faster which agrees with the similar data obtained in the experiments with single capillary tubes [213]. By taking into account the ratio of diffusion coefficients for these two binary mixtures, it can be concluded that the dissolution rate is proportional to $D^{1/3}$.

For soybean oil/hexane mixture the shape of the interface could not be clearly distinguished, not even in the early time moments of the experiments. As it can

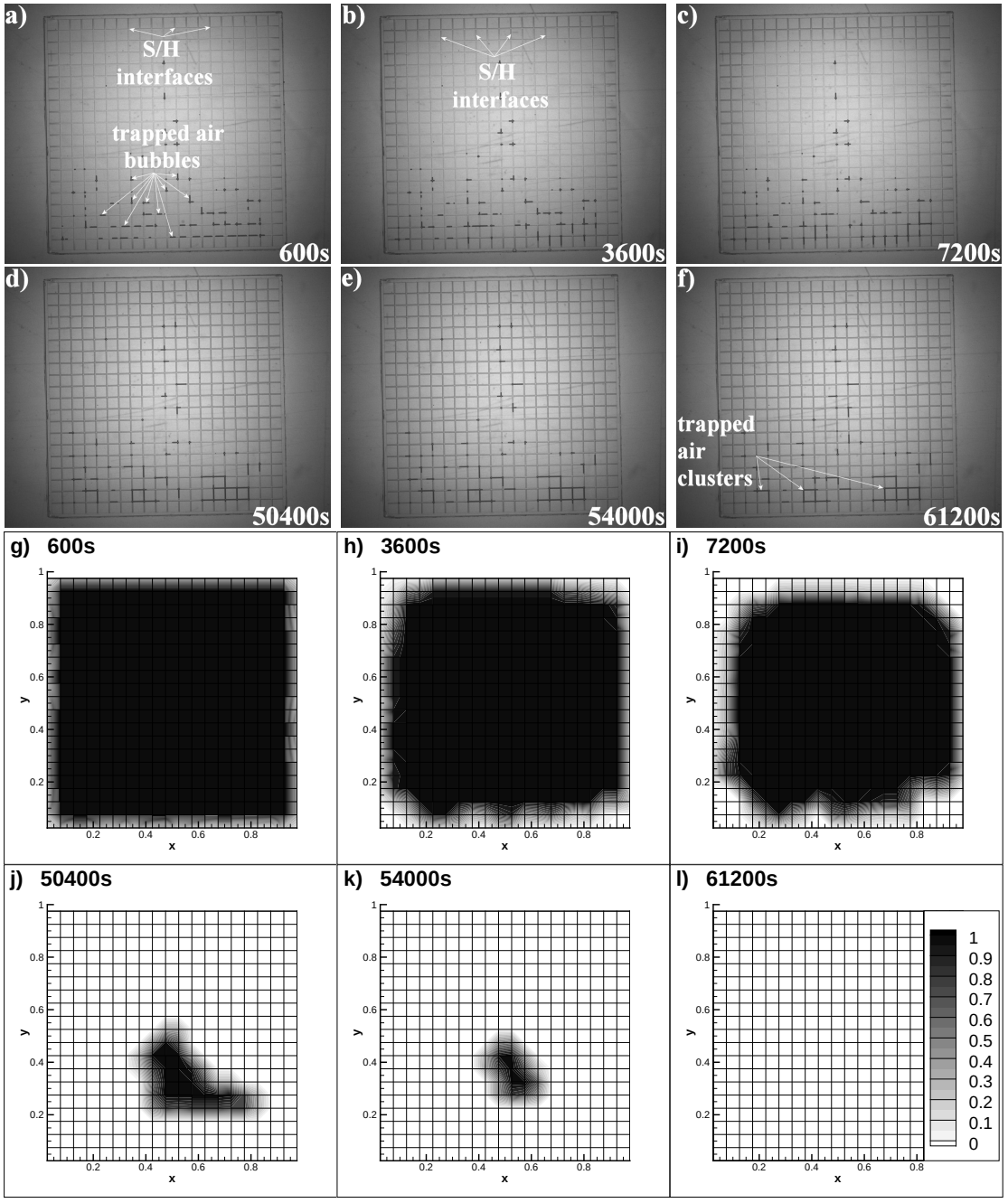

Figure 4.10: **(a-f)** Snapshots of the soybean oil/hexane phase boundaries within micromodel; the channels filled with soybean oil phase are shown with a lighter grey color and the ones filled with hexane have a darker grey color; air bubbles trapped in the channels are shown in black. **(g-l)** Interpretations of the experimental observations; each frame corresponds to one of the snapshots shown in frames **(a-f)**; the legend shows the volume fraction of soybean oil in the micromodel; the data points were obtained by averaging the amount of soybean oil remained in a unit cell of the micromodel at the time moment indicated on each frame; a unit cell is represented by a square with side channels of 2 mm length; Temperature is T=20^oC. The corresponding time moments are indicated in the pictures.

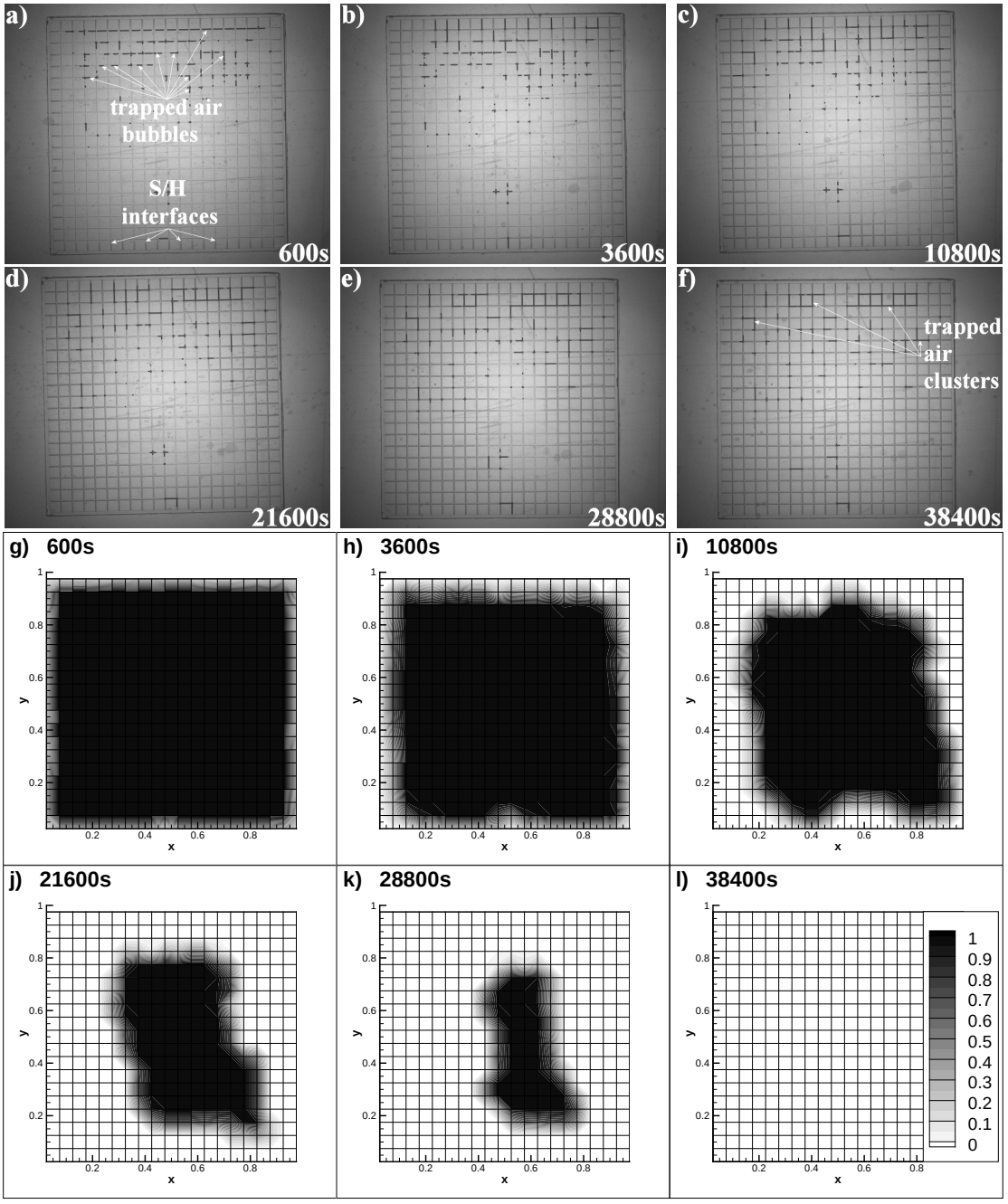

Figure 4.11: **(a-f)** Snapshots of the soybean oil/hexane phase boundaries within micromodel; the channels filled with soybean oil phase are shown with a lighter grey color and the ones filled with hexane have a darker grey color; air bubbles trapped in the channels are shown in black. **(g-l)** Interpretations of the experimental observations; each frame corresponds to one of the snapshots shown in frames **(a-f)**; the legend shows the volume fraction of soybean oil in the micromodel; the data points were obtained by averaging the amount of soybean oil remained in a unit cell of the micromodel at the time moment indicated on each frame; a unit cell is represented by a square with side channels of 2 mm length; Temperature is T=30^oC. The corresponding time moments are indicated in the pictures.

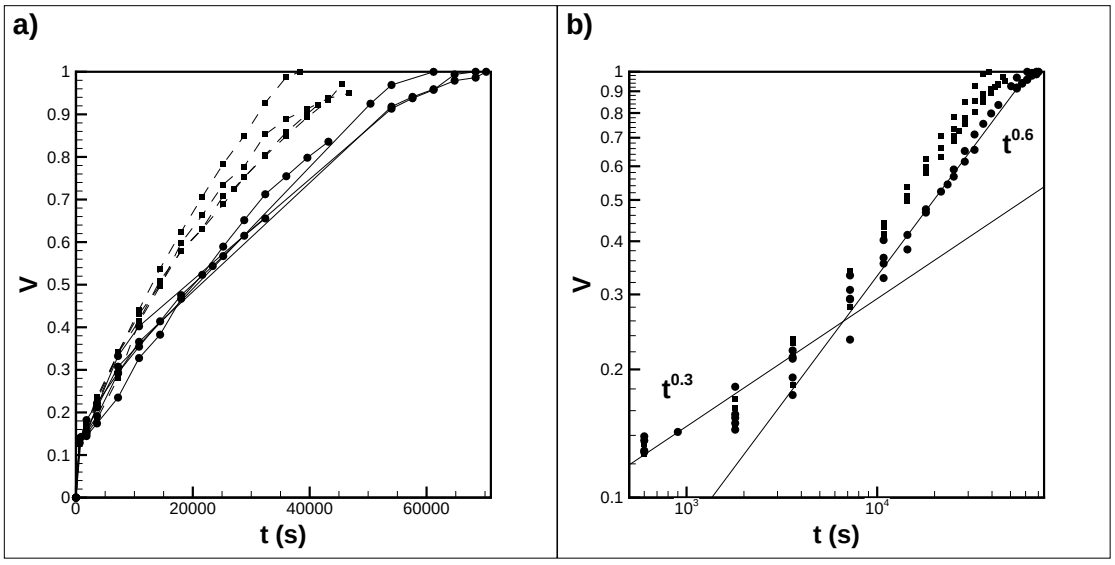

Figure 4.12: **a)** The volume fraction of hexane within the micromodel at different time moments; **b)** The same data set plotted in logarithmic coordinates; (•) T=20^oC and (■) T=30^oC.

be seen in Figure 4.13(a), at an early time moment the tip of the interface was already very diffused and could not be clearly identified. Still, similar to the case of glycerol/water the dissolution front could be easily followed (Figure 4.13(b-d) and Figure 4.14) up until the end of the experiment (i.e. when the whole micromodel was filled with hexane), as already shown in Figure 4.10 and Figure 4.11.

4.3.3 Isobutyric acid/water mixture

IBA/water is a partially miscible binary mixture with an upper critical solution temperature at $\sim 26.3^oC$. As already described in the previous chapter the behavior of this mixture below and above the critical point is completely different. Above the critical point the interfaces become very diffused in a very short period of time with the water phase underriding the IBA phase and thus the current method could not be used for investigation of the dissolution above the critical point. Below the critical point, in a single capillary tube the displacement of the IBA phase was governed by the capillary force (spontaneous imbibition). Within the micromodel several interfaces were observed for IBA/water mixture, but the contrast of the images obtained was not good enough to describe accurately the dissolution process. Therefore, in order to take a closer view the Nikkor lens was changed with the Questar one. The shapes of the IBA/water interfaces in pores and throats are depicted in Figure 4.15. As it can be seen in this figure, numerous interfaces were formed which moved in different parts of the micromodel, but

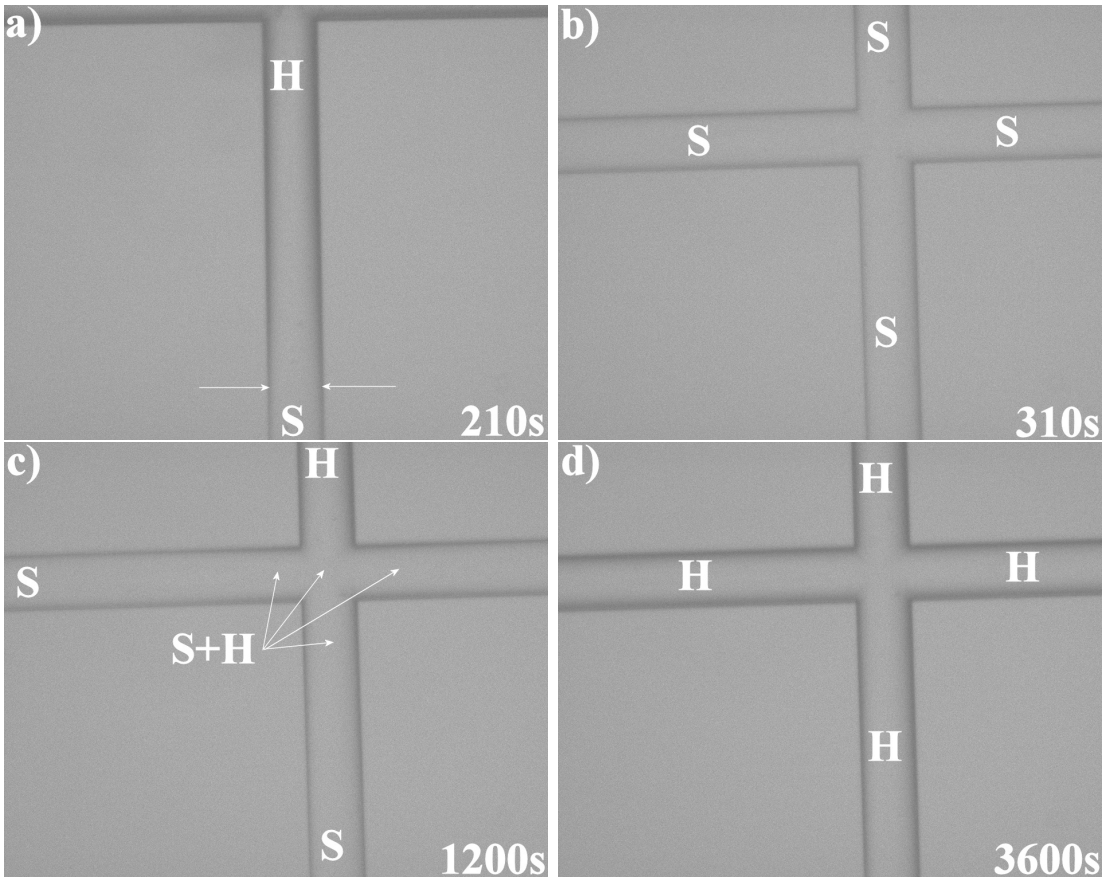

Figure 4.13: Magnified view within the micromodel during an experiment with soybean oil/hexane at different time moments; **a)** Even at early time moments the tip of the soybean oil/hexane interface is already very diffused; the arrows indicate its approximate position which can be determined based on the color contrast; **b)** All channels are filled only with soybean oil and are represented with a lighter grey color; **c)** The top channel is filled only with hexane and is represented with a darker grey color; the channels where both phases are present are represented with lighter grey color in the middle and darker grey color on the channel edges; **d)** All channels are filled only with hexane phase. Frames **(b-d)** show the same intersection of the channels. In all frames 'S' denotes soybean oil phase and 'H' denotes hexane phase. Temperature is T=22^oC. The corresponding time moments are indicated in the pictures.

no clear pattern could be deduced. The interfaces were still present within the micromodel even after long periods of time from the beginning of the experiment ($> 24\,h$, Figure 4.15(f-h)).

Surprisingly, in contrast to the previous observations made within single capillary tubes, the curvature of the interface shape indicates that in this case the IBA phase is more wetting which means that even though the capillary pressure is still the driving force, a drainage type displacement occurs in these experiments. This type of displacement also explains why the complete removal of IBA from the

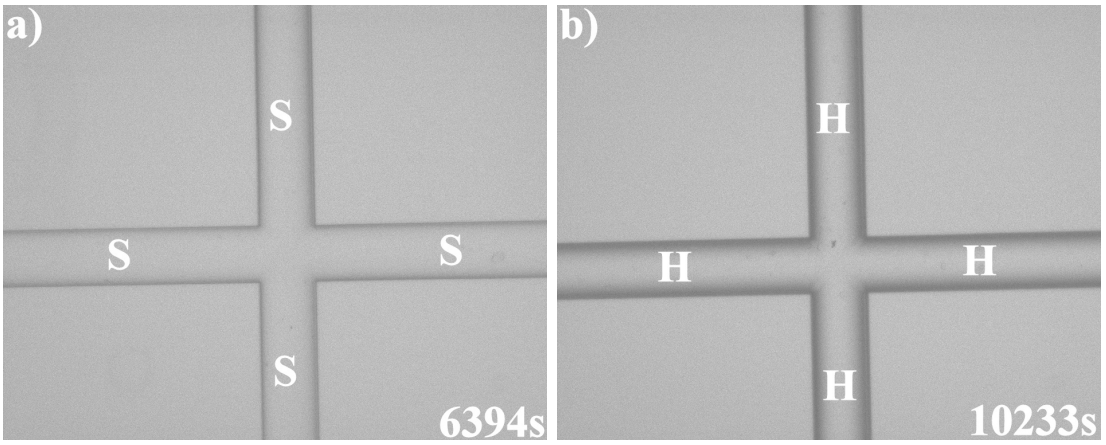

Figure 4.14: Magnified view within the micromodel during an experiment with soybean oil/hexane showing the same intersection of the channels at different time moments; **a)** All channels are filled only with soybean oil and are represented by a lighter grey color; 'S' denotes soybean oil phase; **b)** All channels are filled only with hexane and are represented by a darker grey color; 'H' denotes hexane phase. Temperature is T=30^oC. The corresponding time moments are indicated in the pictures.

micromodel was never observed. The trapping of the wetting phase in a drainage type displacement has also been previously mentioned in [113, 178, 182]. The interfaces shapes depicted in Figure 4.15 are very similar to the ones described by Lenormand et al. [113]. Note that the shape of the channels (in [113] the shape of the channels was rectangular and in this case the shape corresponds to a near-circular profile) does not affect the shapes of the interfaces neither in throats or pores. This different type of displacement for the same binary mixture could possibly be explained based on the fact that a different type of glass was used for the fabrication of the micromodel, even though, the $B270$ glass used is still a type of borosilicate glass.

4.4 Summary

Experimental observations were performed to study the dissolution behavior of miscible liquid/liquid interfaces in a homogeneous porous medium. The work described in this chapter represents a step further from the work reported in the previous chapter in which the dissolution behavior of liquid/liquid interfaces was investigated in single capillary tubes [213]. Basically, the study of dissolution of binary mixtures within capillary tubes was extended to a homogeneous glass-etched micromodel. This extension was necessary in order to make possible the

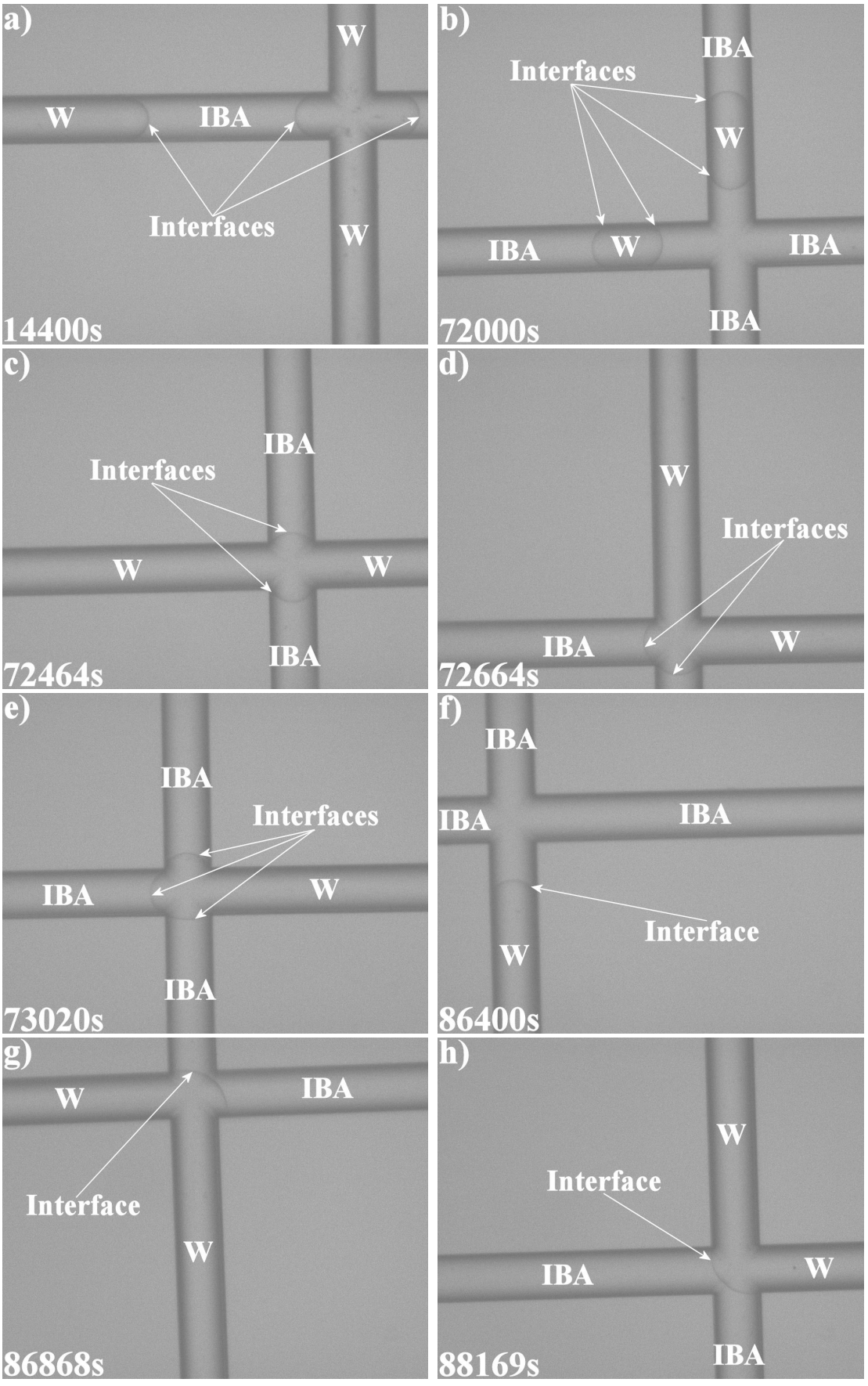

Figure 4.15: Isobutyric acid/water phase boundaries within the micromodel at different time moments. Arrows indicate the positions of the interfaces. T=22^oC.

incorporation of dissolution results in the development of pore-network models. In this manner, it is expected that the dissolution will no longer be omitted in the development of such theoretical models.

For glycerol/water and soybean oil/hexane (i.e. completely miscible) binary mixtures was found that the dissolution process was governed by diffusion. However, this is non-Fickian diffusion with the growth of the volume occupied by the solvent being proportional to $t^{0.3}$ in the initial stage and $t^{0.6}$ in the second stage which lasted for almost the entire duration of the experiments. There are several similarities between the results reported in this chapter and the ones reported in Chapter 3 which allow one to conclude that in at least one stage of the dissolution process the barodiffusion effect could possibly explain the discrepancy from the classical Fickian behaviour. The experiments performed with single capillary tubes were carried on until the interface boundaries could not be clearly distinguished. More specifically, when the tip of the interface was too diffused for its position to be accurately identified the measurements were terminated. In the experiments with the micromodel described in this chapter, the measurements were carried out for considerably longer time periods as the position of the whole boundary was tracked within the channels of the micromodel without considering the integrity of the tips of the interfaces. It may be possible that if the experiments within single capillary tubes would have been continued for longer time periods the final stage would have been characterized by another power law closer to the one characteristic to the subdiffusive regime ($t^{-0.4}$) identified in the experiments with the micromodel.

In the case of IBA/water binary mixture the experiments performed at undercritical temperatures revealed that diffusive mass transport was negligible, despite the fact that the mixture was out of its thermodynamic equilibrium. The motion of numerous interfaces within the micromodel could be noticed, but the complete removal of IBA from the micromodel was never observed.

Chapter 5

Conclusions

The principal aim of this experimental study was to achieve a deeper understanding of the dissolution dynamics of liquid/liquid binary mixtures within a porous medium. In this chapter, all the experimental work completed is summarized and the main conclusions are presented. It was found that even in simple configurations such as capillary tubes, the dynamics of liquid/liquid dissolution occurs unexpectedly. The dynamics becomes even more complicated when a more complex geometry is employed. The findings reported should be useful for the development of more accurate theoretical models for describing miscible multiphase flows in porous media.

5.1 Conclusions

All applications mentioned in the beginning of this thesis have as a central point the dissolution process in a porous medium and/or the fluid/fluid displacement from a porous medium. Even if the literature concerning with each of these applications in which dissolution and immiscible and miscible displacement processes play important roles is already very wide, the great complexity of the problems that need to be understood and solved at both microscopic and macroscopic scales for a viable implementation of newer technologies to be realized still attracts a lot of interest from both experienced and new researchers.

The focus of this project was on the experimental study of dissolution dynamics of binary mixtures within a single capillary tube and in network models which simulate the porous media. The dissolution is a very slow process affected by both diffusive and convective effects.

The shapes and dynamics of solute/solvent phase boundaries of three different binary mixtures were examined in open horizontal capillary tubes. No pressure difference was applied between the ends of the capillary tube. Tubes of different diameters, as small as $0.2\,mm$ were used. The task was to separate the interfacial diffusion from the hydrodynamic flows driven by either Marangoni and solutal convection or by capillary pressure. Traditionally, the dissolution process is reduced to a simple interphase diffusion. A classically expected scenario for the dissolution of a solute droplet from a capillary tube would be as follows: two solute/solvent interfaces are formed at the end of the capillary tube, and if no external pressure gradient is applied, no flows should be generated and hence the phase boundaries should not move. The boundaries should smear and finally disappear due to diffusion. In this study it was found that removal of solute phase occurs differently. Firstly, numerous physical phenomena are involved at different stages of these seemingly simple experiments. Secondly, even the diffusion dynamics of the solute/solvent interfaces differs from general expectations.

In the experiments with mixtures of glycerol/water and soybean oil/hexane the pure dissolution process could be isolated. The short initial evolution (for about $1\,min$, when diffusion is negligible) is gravity driven; the observed motion represents a gravity current also called a lock-exchange flow [105, 106, 107]. The contact lines are not closed within the capillary tube and the solvent phase displaces small portions of the solute at both ends. When the interfaces fully enter the capillary tube and the contact lines become closed within the tube, the solute phase becomes

locked. At this moment the gravity force is balanced by the capillary force, which ends the initial 'mechanical' displacement of the solute phase. From this moment, whole interfaces with almost steady shapes move towards the center of the capillary tube, which obviously cannot be interpreted as a gravity current. These phase boundaries smear in time seemingly due to mutual interphase diffusion, but the smearing rate is very small, considerably smaller compared to the speed of the boundary movement as a whole. The observed motion of the phase boundaries resembles the evaporation or solidification process: the interfacial mass transfer results in shrinking of the solute droplet, but the solute/solvent boundaries remain visible (if not sharp). The two interfaces move with equal speeds. The speeds of the interfaces slow down following the $t^{-2/3}$ power law in the capillary tubes of smaller diameters, i.e. do not follow the predictions of the diffusion theory, $t^{-1/2}$. The dissolution rate increases with growth of temperature, which was expectable, but it was also found that the rate of decrease of the length of the droplet is proportional to the area of the tube's cross-section, which is a surprising result. The final conclusion is that the phase boundaries could possibly be moving due to barodiffusion.

As the dissolution rates were assessed by considering the position of the tip of the interface, it is worth mentioning that for longer capillary tubes the measurements were stopped before the fusion of the two interfaces took place due to the strong smearing of the tips which might have led to inaccurate predictions of their position.

By comparing the interface speeds, it may also be concluded that the diffusion coefficient of the soybean oil/hexane mixture is obviously higher than the diffusion coefficient of the glycerol/water interface, which is in agreement with theoretical predictions [205]. Moreover, the values of the diffusion coefficients reported in the literature allowed us to conclude that the speed of the interface is proportional to $D^{1/3}$.

The behaviour of the IBA/water mixture was completely different. Below the critical point, IBA and water behaved like two immiscible liquids. Water penetrated into the capillary tube from one side; from another side IBA droplets were displaced. The droplets were detached when their size was sufficient to overcome the adhesion to the outer wall of the capillary tube. The speed of the interface propagation grew in the beginning up to a constant value, then the speed remained constant for the main part of the experiment and sharply decreased when the interface approached the second end of the capillary tube. The motion of the interface

was explained by spontaneous imbibition. In the experiments with microparticles dispersed in the IBA phase, it was observed that the interface was able to move the particles, but the IBA phase which was displaced by the water phase did not force the particles to move.

Above the critical point, IBA and water are miscible in all proportions. The observed meniscus shape was defined by the balance of the capillary and gravity forces, which seemed comparable. The capillary pressure was not sufficiently strong to initiate the spontaneous imbibition. The initial evolution of the interfaces could be explained by the gravity action. Two interfaces were observed within the capillary tube. One of them was initially moving but quickly became very diffusive and indistinguishable. The other interface was observed for considerably longer time periods but it remained stationary.

The diffusion and viscosity coefficients and density difference between mixture components for the IBA/water binary system are considerably lower in comparison to those of glycerol/water and soybean oil/hexane mixtures, both below and above the critical point. Below the critical point, the interfacial diffusion at the IBA/water boundaries was not observed at all. The interface speed is comparable to the initial speeds of glycerol/water and soybean oil/hexane interfaces, but the solute is removed faster as the speed of the undercritical IBA/water interface remains almost constant for the duration of the experiment. Above the critical point, two IBA/water interfaces penetrated into the capillary tube, and their motion should have been driven by mechanisms similar to those that governed the motion of glycerol/water and soybean oil/hexane interfaces. However, apparently owing to smaller diffusion and viscosity coefficients and smaller density difference the supercritical IBA/water phase boundaries moved differently.

Another interesting observation that needs to be mentioned is that the interface shapes and dissolution dynamics were qualitatively the same in capillary tubes with different cross-sections, in tubes made of different materials, and in new tubes and tubes previously used for the experiments and then washed with water and acetone and dried out. Bulk interfaces and contact lines always moved with the same speeds. No visible solute remained left on the walls of the capillary tube after the interface passage. Owing to gravity effect, in the horizontal capillary tubes the apparent contact angles were different at the lower and upper parts of the capillary tube. In the case of IBA/water mixture the contact angles obviously depend on the mixture temperature.

A set of experimental observations was also performed in order to study the dissolution behaviour of miscible liquid/liquid interfaces in homogeneous porous media. The same, slightly modified, experimental technique was employed to study the dissolution of glycerol/water and soybean oil/hexane binary mixtures within a micromodel in order for the results to be compared with the ones obtained for the dissolution in capillary tubes. Therefore, no external forces were imposed to drive the flow.

For glycerol/water and soybean oil/hexane binary mixtures was found that the dissolution process was governed by diffusion. However, this is non-Fickian diffusion with the growth of the volume occupied by the solvent being proportional to $t^{0.3}$ in the beginning and then to $t^{0.6}$ for almost the entire duration of the experiments. The similarities observed between the results obtained for capillary tubes and micromodel, including the dependencies on time and diffusivity also allow one to conclude that in the first stage of the experiments, when the speed of the solute/solvent phase boundary can be characterized by the dependence $t^{-0.7}$, the dissolution could possibly be driven by barodiffusion. In the second stage, the very diffusive solute/solvent boundary propagated with a speed characterized by the power law $t^{-0.4}$, which is closer to Fickian dependence, but still different (i.e. $t^{-0.4}$ describes a subdiffusive regime).

In the case of IBA/water binary mixture the experiments performed at undercritical temperatures revealed that diffusive mass transport was negligible, despite the fact that the mixture was out of its thermodynamic equilibrium. The motion of numerous interfaces within the micromodel could be seen, but the complete removal of IBA from the micromodel was never observed.

The experimental data collected in this study should be useful for developing the theoretical models for multiphase flows with undergoing phase transformations. For instance, in most current models (e.g. [2]), the dissolution of completely miscible binary mixtures is modelled with the use of the Fickian law, and the barodiffusion and capillary effects are disregarded. By utilizing the herein obtained results more accurate macroscale models for miscible multiphase flows within porous media can be developed. A regular flow-path pattern was chosen for the micromodel in order to make the results obtained easier employable by the researchers carrying out theoretical and computational modelling.

Chapter 6

Further research

The work presented in this thesis is deeply fundamental and thus there are many paths that further research could follow. The field of multiphase flows through porous media is enormous and future research can be aimed specifically at any of the major industrial applications of these types of flows. In this chapter two potential routes of continuing this project will be presented in more detail.

6.1 Introduction

The experimental work performed in this project was focused on the dissolution dynamics of miscible binary mixtures with emphasis on diffusive mass transfer. The results obtained herein should not be compared with results obtained in experiments of hydrodynamic dispersion in which convective mass transfer dominates. Because most of the experimental work available in the literature deals with hydrodynamic dispersion in various geometries due to high pressure gradients applied, one way of solving this issue would be to find the appropriate regime in which convective and diffusive effects equally influence the flow. Some preliminary displacement experiments within capillary tubes have already been performed for this purpose and therefore, the miscible displacement experiments represent the first route considered for continuing this project.

The second route considered includes experimental work more specific to EOR, as the promise of abundant energy from alternative sources does not change the fact that the mineral hydrocarbons are likely to remain the principal fuel in at least the foreseeable future. In addition, mineral hydrocarbons are to remain a valuable raw material for the chemical industry. World oil production is currently at its pick: oil fields are close to their depletion in terms that the techniques used for secondary recovery are inefficient for further oil production. Nevertheless, it is known that at least 40% of the oil is left in abandoned (depleted) fields.

6.2 Miscible displacement

6.2.1 Preliminary data on miscible displacement in capillary tubes

First, a preliminary set of miscible displacement experiments has been performed with glycerol/water binary mixture within capillary tubes. In this preliminary set of experiments the dissolution process of a liquid droplet within a capillary tube was examined with small pressure gradients applied at the ends of the tube as the idea was to obtain flows characterized by similar convective and diffusive time scales. A schematic view of the experimental setup is shown in Figure 6.1. All experiments were performed at room temperature ($\sim 20^oC$).

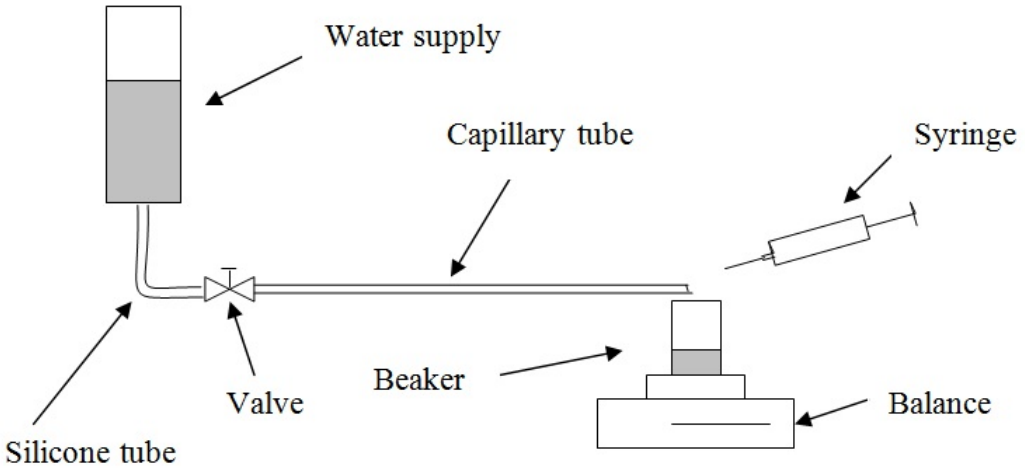

Figure 6.1: A schematic view of the experimental setup.

The ejected fluid was collected at different time intervals and weighted. Following, the flow rate, the density and the concentration of glycerol in the ejected fluid, the extraction rate, e_r and the amount of solvent spent for extraction, s_e were calculated.

In this set of experiments the shape of the interface having a parabolic profile was observed. The velocity of the interface increased after the water reached the middle of the capillary tube and the increase was even larger after the breakthrough moment (the moment when the water reached the other end of the capillary tube). The effect of gravity was noticed as water was overriding glycerol, but by the end of the experiment most of the glycerol was washed out from the capillary tube. Still, in none of the cases the whole glycerol injected was extracted.

The density of the ejected fluid was calculated by weighting a fixed volume ($200\mu l$) taken from the samples collected at different time moments. The experimental values obtained are shown in Figure 6.2a. At the initial moment, the ejected fluid was assumed to be pure glycerol. After knowing the density, the mass concentration was calculated with Equation 3.1 and the values are shown in Figure 6.2b. The values of density and concentration at the breakthrough time were calculated by interpolation and are marked in Figure 6.2 with letter 'B'.

In order to characterize the extraction efficiency two quantities were considered: 1) the extraction rate, e_r defined as the amount of glycerol extracted to the total amount of glycerol initially injected into the capillary tube, and 2) the amount of solvent spent for extraction, s_e defined as the ratio between the amount of solvent spent and the amount of glycerol extracted. The time dependencies for

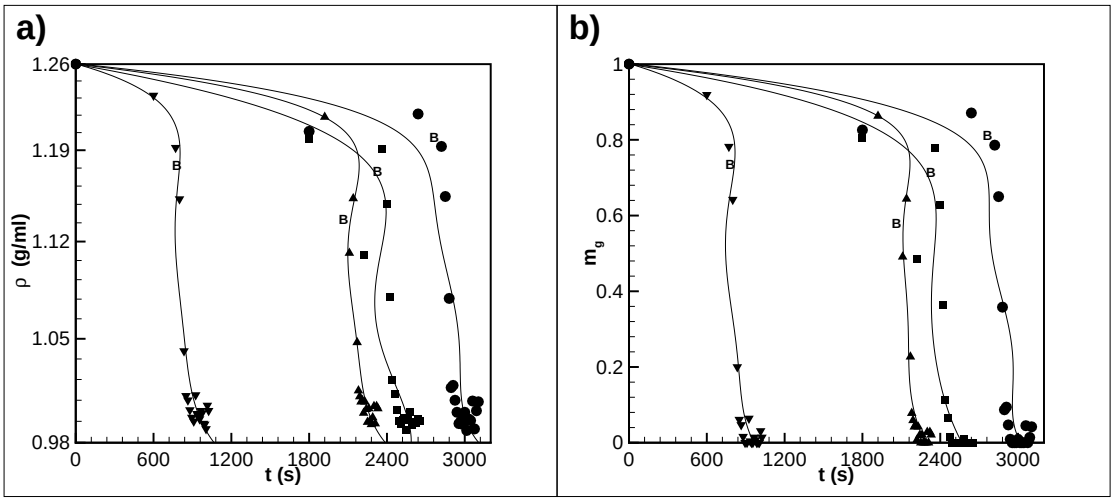

Figure 6.2: **a)** Density of the ejected fluid as a function of time; **b)** Mass fraction of glycerol in the ejected fluid as a function of time; (•) first experiment; (■) second experiment; (▲) third experiment; (▼) fourth experiment; B-breakthrough point; lines are used for guidance only.

these quantities are depicted in Figure 6.3. The mass of injected glycerol, m_i was calculated as follows: $m_i = \rho_g V_g$ and $V_g = V = (\pi d^2/4) \cdot L$. In these expressions ρ_g is the density of glycerol, V_g is the volume of glycerol injected which equals the volume of the capillary tube, V, d is the diameter of the tube and L its length.

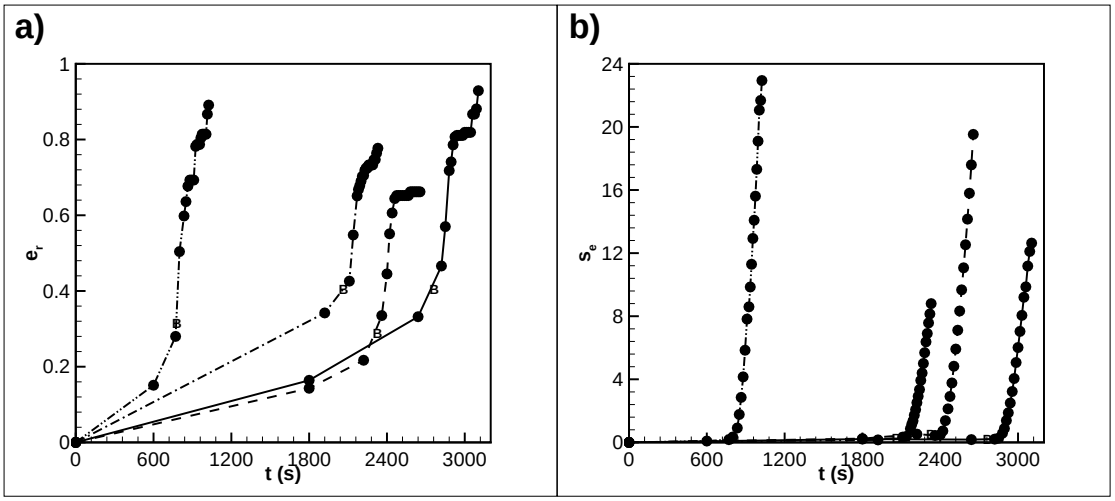

Figure 6.3: Experimental values for: **a)** the extraction rate and **b)** the amount of solvent spent for extracting the glycerol; different types of lines denote different experiments.

The capillary tube used in these experiments had quite a large diameter and length ($d = 1.6\,mm$, $L = 67.4\,cm$). Therefore, in these experiments the flow rates were too high and the time was too short for the diffusion process to take place. The sharp interface was clearly noticed until the breakthrough moment without any

type of optical equipment. The method is still under development as it requires optimization (i.e. a few adjustments are necessary for smaller capillary tubes to be utilized in order to minimize undesired effects).

6.2.2 Miscible displacement within micromodels

As soon as the experimental work on miscible displacement in capillary tubes will be completed, the data available will be used for setting up the displacement experiments within micromodels. Some additional pieces of equipment (e.g syringe pumps, microscope) are still necessary for this setup. The micromodels which will be used in these experiments have already been designed and manufactured (Figure A.2). In the end, correlation will be made between displacement and dissolution results in order to enable the development of better methodologies for solvent extraction.

6.3 Enhanced oil recovery

All conventional oil fields which are more or less closer to the UK shores (where CO_2 emitting power plants are located) are already depleted or close to depletion. Owing to their proximity (and hence less transportation costs) these fields are more promising for carbon sequestration however, these fields are not economically viable for secondary (i.e. displacement) oil recovery techniques. The idea is to assess the possibilities of the tertiary recovery of the oil still remained in these fields with the use of CO_2, which is to be injected into the oil reservoir and sealed there for a long time period to let CO_2 dissolve oil (or at least lighter fractions of the crude oil). Then, CO_2/oil mixture can be released from the reservoir, oil is separated, and CO_2 is injected back into the reservoir. CO_2 can dissolve oil from all dead-ends of the porous matrix, and ultimately, this technique is capable of complete recovering of oil reserves.

Hence, the second possible route of continuing the current project is to develop a new technique of tertiary oil recovery with the use of CO_2 as an extracting rather than pressurizing agent. Despite the fact that the CO_2 sequestration is one of the most studied themes in modern geosciences [17, 16, 20], this idea is novel and would favour enormously the energy sector if proved feasible. The currently discussed techniques of oil recovery with the use of CO_2 assume that CO_2 would

replace water as a displacing agent, which would bring some advantages (and disadvantages) but, still remain a modification of the secondary (displacement) recovery technique.

In order to assess the feasibility of the proposed technique the first objective would be to study the process with a laboratory model for the oil reservoir and with the use of modelling working liquids (hexane/soybean oil mixture). The oil field would be modelled by a sand-filled (glass or metallic microparticles-filled) container saturated with soybean oil. Several models will be prepared filled with particles of different sizes and of uniform and non-uniform compositions. Two tubes would be incorporated into the lid of the container to model the injection and production wells. At the first stage of the experiment, water would be injected into the container to model the secondary recovery. When water breaks-through the container, the secondary recovery would be stopped, and the resultant state would be used to represent a water-flooded reservoir. Next, a solvent (hexane) would be injected into the container. Hexane and soybean oil are completely miscible liquids, but liquid/liquid dissolution is a slow process, so the container would be sealed for some time to let hexane and soybean oil form a homogeneous solution. The following hexane portion could be injected through a different well to eject the hexane/soybean oil solution through the first well. The ejected mixture can be separated by evaporation (hexane) and gravity segregation (water). This would be a pump priming study possibly achievable with low costs. The idea of the experiment is summarized in Figure 6.4. A more sophisticated research work with the use of supercritical CO_2 and different fractions of crude oil would still be required to approach the practical settings for the proposed oil recovery technique, but this would be a much more costly research.

The idea for this project stems from the current technique for the chemical extraction used in food and pharmaceutical industries where supercritical CO_2 is employed as a low-temperature, benign and highly tuneable solvent. At supercritical conditions CO_2 has a good solvent strength, comparable to light hydrocarbons for most solutes, and in particular is capable of dissolving different essential oils. In addition, its solvent strength is tuneable (strongly varies with thermodynamic conditions). For instance, CO_2 is used for vegetable oil extraction: being injected into a crushed vegetable feedstock, CO_2 dissolves vegetable (essential) oil and carries it from the feedstock; the solvent (CO_2) and solute (oil) are easily separated by reducing the gas pressure, leading to precipitation of the dissolved oil.

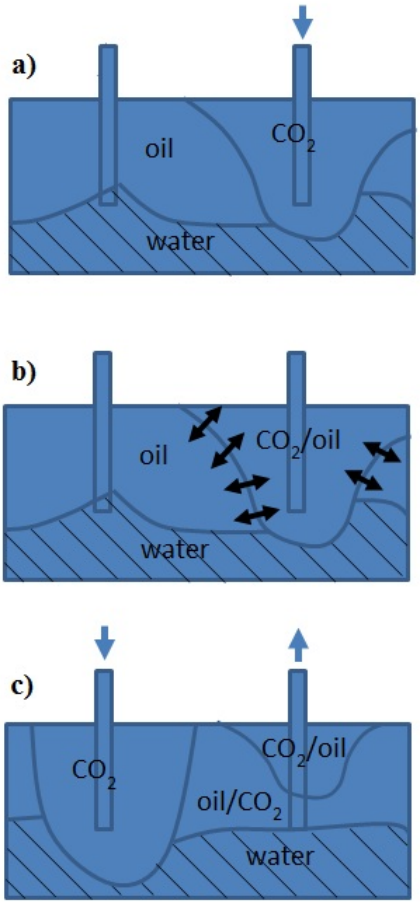

Figure 6.4: Enhanced oil recovery with CO_2 as an extracting rather than pressurizing agent: **a)** Solvent (hexane) injection into water-flooded reservoir; **b)** After some time, the solute/solvent mixture becomes homogeneous; **c)** The homogeneous solute/solvent mixture is pumped out by injection of a new portion of solvent through a different end. The oil is separated from the mixture by distillation.

This research idea would extend the current experimental work aimed at understanding the dissolution dynamics of binary mixtures saturating porous media. If the laboratory experiments with the modelling working liquids prove the feasibility of the proposed technique for the tertiary oil recovery, then the experiments with supercritical CO_2 could also be carried out. This study would allow the development of a technical protocol for an efficient tertiary recovery of oil inaccessible to secondary oil recovery.

6.4 Summary

Petroleum engineering, hydrogeology, biotechnology and medicine are just some of the fields in which the great importance of multiphase flows through porous media can be distinguished. Investigation of the role of various parameters and their interplay together with the way in which they affect these types of flows and various other specific aspects of particular applications can lead to numerous pathways of continuing the work done during this project. Two possible routes (miscible displacements and tertiary oil recovery with CO_2 used as an extracting rather than pressurizing agent) were briefly described in this chapter. They are focused mainly towards EOR, but some of the results obtained (i.e. miscible displacements) could also be applied to EAR, vegetable oil extraction and drug delivery.

Appendix A

Micromodels designs

Following the specifications and raw AutoCAD designs provided by the author, the Dolomite Centre Ltd. improved the designs to the format shown in Figure A.1 and Figure A.2. The Dolomite Centre also supplied custom connectors needed for micromodel *B* (Figure A.3).

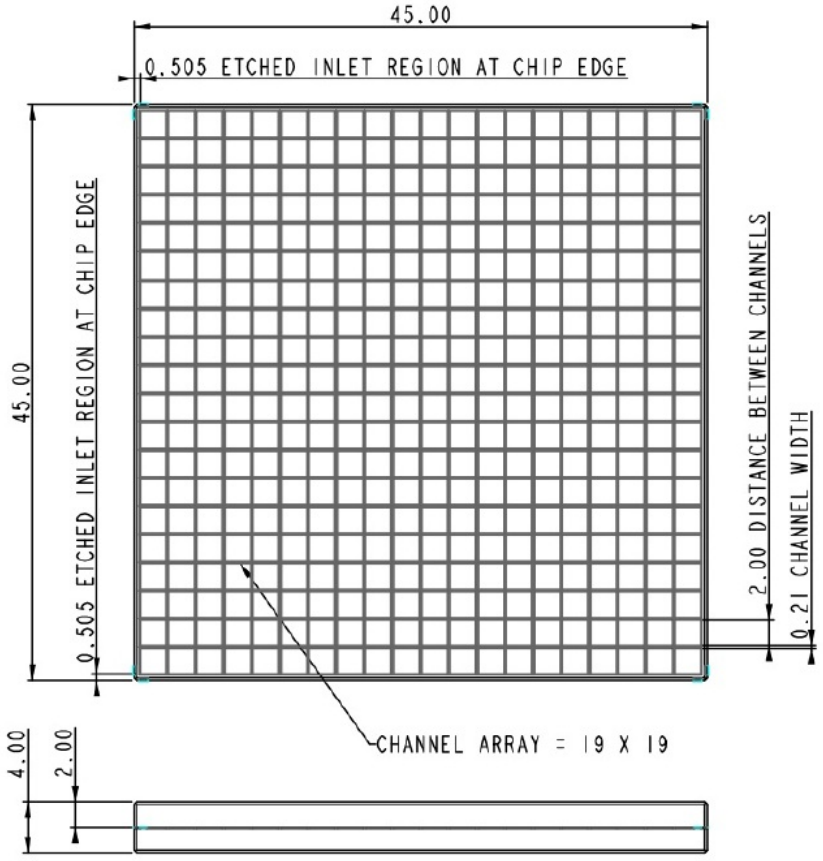

Figure A.1: Autocad design of micromodel *A* [214].

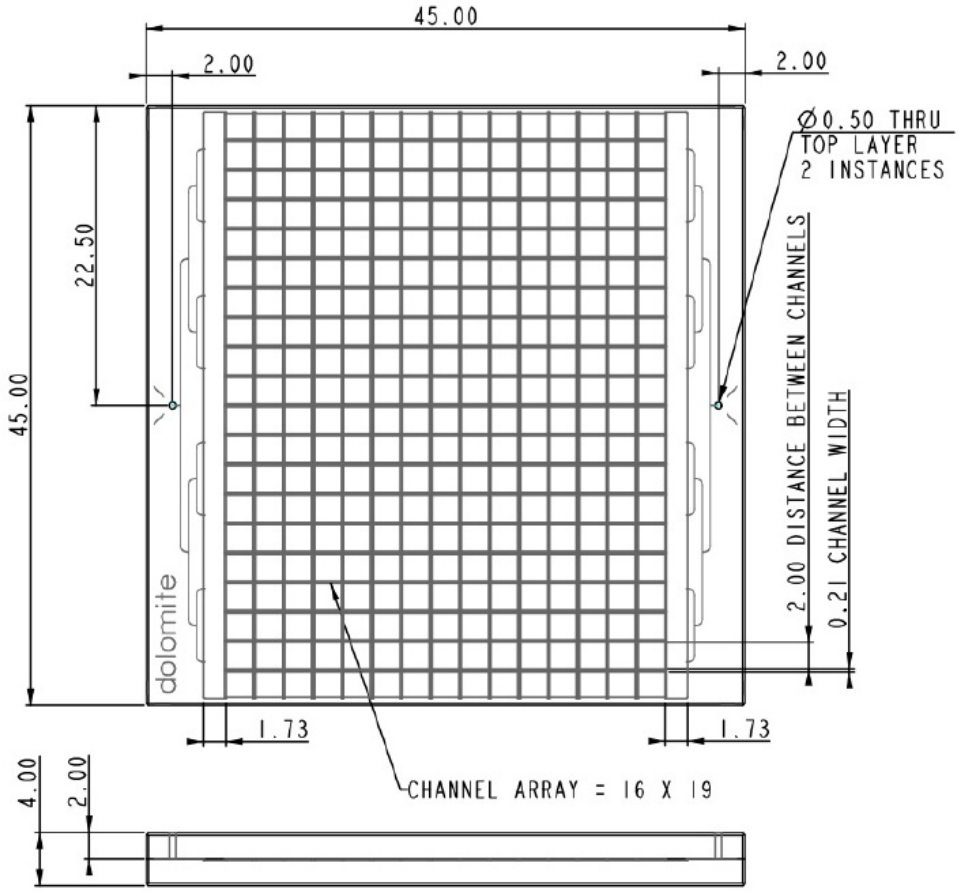

Figure A.2: Autocad design of micromodel *B* [214].

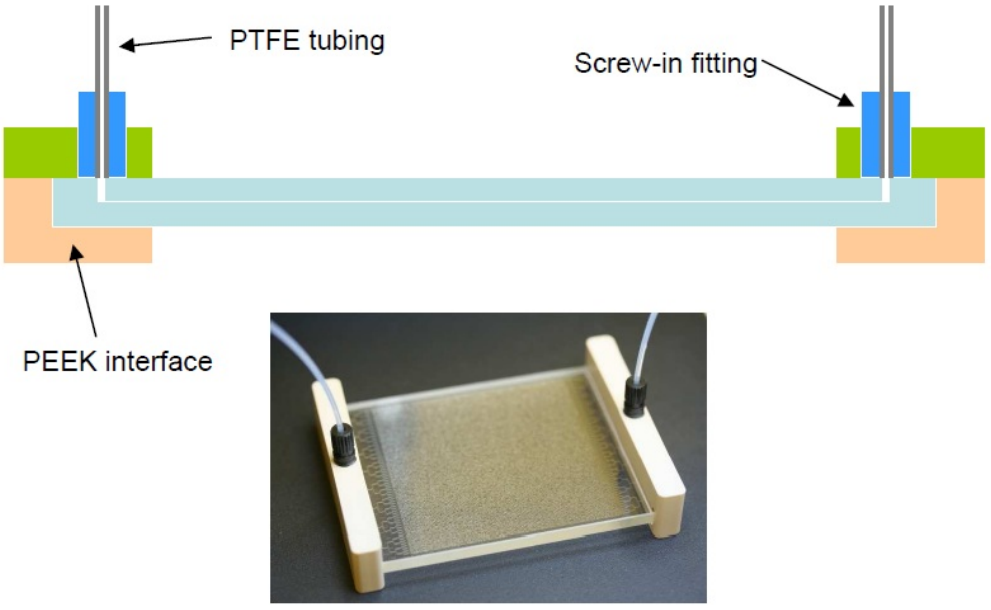

Figure A.3: Connectors design for micromodel *B* [214].

Appendix B

Additional experimental data

For reference, the following video type files are attached as part of this thesis:

- glycerol-water.wmw
- iba-water1.wmw
- iba-water2.wmw
- iba-water-particles.wmw

These videos are attached in order to help the reader to visualize easier the dissolution process. In the videos the dissolution process is shown at a speed 10 times faster than it occurred in reality.

Each video is related to one of the figures presented in Chapter 3, more specifically:

- Figure 3.7
- Figure 3.21
- Figure 3.21
- Figure 3.22

Thus, the reader should refer to these figures captions for the full description of the experimental details (capillary tube cross-section, diameter, length and temperature).

References

[1] D. D. Joseph and Y. Y. Renardy. *Fundamentals of two-fluid dynamics. Part II: Lubricated transport, drops and miscible liquids.* Springer-Verlag, Berlin, 1993.

[2] C.-Y. Chen and E. Meiburg. Miscible displacements in capillary tubes. Part 2. Numerical simulations. *Journal of Fluid Mechanics*, 326:57–90, 1996.

[3] M. Sahimi. Flow phenomena in rocks-from continuum models to fractals, percolation, cellular-automata and simulated annealing. *Reviews of Modern Physics*, 65:1393–1534, 1993.

[4] M. A. Tanksley and J. Koplik. Path-integral variational methods for flow through porous media. *Physical Review E*, 49:1353–1366, 1994.

[5] J. Chaoying and T. Maxworthy. An experimental study of miscible displacement with gravity-override and viscosity-contrast in a Hele Shaw cell. *Experiments in Fluids*, 44:781–794, 2008.

[6] V. V. Ugrozov, A. N. Filippov, C. A. Paraskeva, G. N. Constantinides, and V. M. Starov. Diffusive dissolution of a drop in a capillary. *Colloids and Surfaces A: Physicochemical and Engineering Aspects*, 239:129–133, 2004.

[7] S. H. Vanaparthy and E. Meiburg. Variable density and viscosity, miscible displacements in capillary tubes. *European Journal of Mechanics B-Fluids*, 27:268–289, 2008.

[8] `http://www.canopetro.com/technology.asp` -Accessed 30.10.2012 (12:15h).

[9] M. F. Nazar, S. S. Shah, and M. A. Khosa. Microemulsions in enhanced oil recovery: A review. *Petroleum Science and Technology*, 29:1353–1365, 2011.

[10] E. C. Donaldson, G. V. Chilingarian, and T. F. Yen. *Enhanced Oil Recovery.* Elsevier, New York, 1985.

[11] V. Alvarado and E. Manrique. Enhanced oil recovery: An update review. *Energies*, 3:1529–1575, 2010.

[12] `http://www.perisai.biz/eor/index.html` -Accessed 18.01.2010 (11:30h).

[13] T. Babadagli. Development of mature oil fields–A review. *Journal of Petroleum Science and Engineering*, 57:221–246, 2007.

[14] `www.shell.com.pk/home/content/pak/innovation/meeting_demand/` -Accessed 30.03.2011 (14:15h).

[15] M. M. Kulkarni and D. N. Rao. Experimental investigation of miscible and immiscible Water-Alternating-Gas (WAG) process performance. *Journal of Petroleum Science and Engineering*, 48:1–20, 2005.

[16] K. Jessen, A. R. Kovscek, and F. M. Orr Jr. Increasing CO_2 storage in oil recovery. *Energy Conversion and Management*, 46:293–311, 2005.

[17] K. Damen, A. Faaij, F. van Bergen, J. Gale, and E. Lysen. Identification of early opportunities for CO_2 sequestration-worldwide screening for $CO_2 - EOR$ and $CO_2 - ECBM$ projects. *Energy*, 30:1931–1952, 2005.

[18] A.T.F.S. Gaspar Ravagnani, E.L. Ligero, and S.B. Suslick. CO_2 sequestration through enhanced oil recovery in a mature oil field. *Journal of Petroleum Science and Engineering*, 65:129–138, 2009.

[19] S. T. McCoy, M. Pollak, and P. Jaramillo. Geologic sequestration through EOR: policy and regulatory considerations for greenhouse gas accounting. *Energy Procedia*, 4:5794–5801, 2011.

[20] A. Leach, C. F. Mason, and K. van't Veld. Co-optimization of enhanced oil recovery and carbon sequestration. *Resource and Energy Economics*, 33:893–912, 2011.

[21] `http://www.ec.gc.ca/eau-water/default.asp?lang=En&n=A6A38B97-1` -Accessed 30.10.2012 (11:45h).

[22] S. A. Bradford, K. M. Rathfelder, J. Lang, and L. M. Abriola. Entrapment and dissolution of DNAPLs in heterogeneous porous media. *Journal of Contaminant Hydrology*, 67:133–157, 2003.

[23] K. Soga, J.W.E. Page, and T.H. Illangasekare. A review of NAPL source zone remediation efficiency and the mass flux approach. *Journal of Hazardous Materials*, 110:13–27, 2004.

[24] S. W. Jeong, M. Y. Corapcioglu, and S. E. Roosevelt. Micromodel study of surfactant foam remediation of residual trichloroethylene. *Environmental Science and Technology*, 34:3456–3461, 2000.

[25] J. Bear and A. H.-D. Cheng. *Modeling groundwater flow and contaminant transport (Volume* 23 *of Theory and applications of transport in porous media)*. Springer, Dordrecht London, 2010.

[26] C. Jia, K. Shing, and Y. C. Yortsos. Visualization and simulation of non-aqueous phase liquids solubilization in pore networks. *Journal of Contaminant Hydrology*, 35:363–387, 1999.

[27] S. W. Jeong and M. Y. Corapcioglu. A micromodel analysis of factors influencing NAPL removal by surfactant foam flooding. *Journal of Contaminant Hydrology*, 60:77–96, 2003.

[28] C. Khachikian and T. C. Harmon. Nonaqueous phase liquid dissolution in porous media: Current state of knowledge and research needs. *Transport in Porous Media*, 38:3–28, 2000.

[29] L. M. Lanning and R. M. Ford. Glass micromodel study of bacterial dispersion in spatially periodic porous networks. *Biotechnology and Bioengineering*, 78:556–566, 2002.

[30] J. W. Jawitz, M. D. Annable, and P. S. C. Rao. Miscible fluid displacement stability in unconfined porous media: Two-dimensional flow experiments and simulations. *Journal of Contaminant Hydrology*, 31:211–230, 1998.

[31] V. Jain and A. H. Demond. Impact of surfactants for aquifer remediation on physical properties of the aqueous phase. *Journal of Contaminant Hydrology*, 40:25–35, 1999.

[32] S. W. Jeong, A. L. Wood, and T. R. Lee. Enhanced contact of cosolvent and DNAPL in porous media by concurrent injection of cosolvent and air. *Environmental Science and Technology*, 36:5238–5244, 2002.

[33] A. Martinho, H. A. Matos, R. Gani, B. Sarup, and W. Youngreen. Modelling and simulation of vegetable oil processes. *Food and Bioproducts Processing*, 86:87–95, 2008.

[34] M. L. Melgarejo Navarro Cerutti, A. A. Ulson de Souza, and S. M. de Arruda Guelli Ulson de Souza. Solvent extraction of vegetable oils: Numerical and experimental study. *Food and Bioproducts Processing*, 90:199–204, 2012.

[35] R. J. Hron Sr., S. P. Koltun, and A. V. Graci Jr. Biorenewable solvents for vegetable oil extraction. *Journal of the American Oil Chemists Society*, 59:674A–684A, 1982.

[36] H. Sovova, A. A. Galushko, R. P. Stateva, K. Rochova, M. Sajfrtova, and M. Bartlova. Supercritical fluid extraction of minor components of vegetable oils: β-Sitosterol. *Journal of Food Engineering*, 101:201–209, 2010.

[37] H. Sovova. Rate of the vegetable oil extraction with supercritical CO_2-I. Modelling of extraction curves. *Chemical Engineering Science*, 49:409–414, 1994.

[38] H. Sovova, J. Kuceraera, and J. Jez. Rate of the vegetable oil extraction with supercritical CO_2-II. Extraction of grape oil. *Chemical Engineering Science*, 49:415–420, 1994.

[39] J. Stastova, J. Jez, M. Bartlova, and H. Sovova. Rate of the vegetable oil extraction with supercritical CO_2-III. Extraction from sea buckthorn. *Chemical Engineering Science*, 51:4347–4352, 1996.

[40] E. Reverchon and C. Marrone. Modeling and simulation of the supercritical CO_2 extraction of vegetable oils. *The Journal of Supercritical Fluids*, 19:161–175, 2001.

[41] F. J. Eller, S. Taylor, and M. Curren. Use of liquid carbon dioxide to remove hexane from soybean oil. *Journal of the American Oil Chemists' Society*, 81:989–992, 2004.

[42] E. R. Baumler, A. A. Carelli, G. H. Crapiste, and M. E. Carrin. Solvent extraction modeling of vegetable oil and its minor compounds. *Journal of Food Engineering*, 107:186–194, 2011.

[43] G.O. Veloso, V.G. Krioukov, and H.A. Vielmo. Mathematical modeling of vegetable oil extraction in a counter-current crossed flow horizontal extractor. *Journal of Food Engineering*, 66:477–486, 2005.

[44] G.C. Thomas, V.G. Krioukov, and H.A. Vielmo. Simulation of vegetable oil extraction in counter-current crossed flows using the artificial neural network. *Chemical Engineering and Processing: Process Intensification*, 44:579–590, 2005.

[45] G.C. Thomas, G.O. Veloso, and V.G. Krioukov. Mass transfer modelling in counter-current crossed flows in an industrial extractor. *Food and Bioproducts Processing*, 85:77–84, 2007.

[46] M.E. Carrin and G.H. Crapiste. Mathematical modeling of vegetable oil-solvent extraction in a multistage horizontal extractor. *Journal of Food Engineering*, 85:418–425, 2008.

[47] S. M. Wong, I. W. Kellaway, and S. Murdan. Enhancement of the dissolution rate and oral absorption of a poorly water soluble drug by formation of surfactant-containing microparticles. *International Journal of Pharmaceutics*, 317:61–68, 2006.

[48] A. Dokoumetzidis and P. Macheras. A century of dissolution research: From Noyes and Whitney to the Biopharmaceutics Classification System. *International Journal of Pharmaceutics*, 321:1–11, 2006.

[49] A. A. Noyes and W.R. Whitney. The rate of solution of solid substances in their own solutions. *Journal of the American Chemical Society*, 19:930–934, 1897.

[50] V. Pillay and R. Fassihi. Unconventional dissolution methodologies. *Journal of Pharmaceutical Sciences*, 88:843–851, 1999.

[51] J. Wong, A. Brugger, A. Khare, M. Chaubal, P. Papadopoulos, B. Rabinow, J. Kipp, and J. Ning. Suspensions for intraveneous (IV) injection: A review of development, preclinical and clinical aspects. *Advanced Drug Delivery Reviews*, 60:939–954, 2008.

[52] A. A. Thorat and S. V. Dalvi. Liquid antisolvent precipitation and stabilization of nanoparticles of poorly water soluble drugs in aqueous suspensions: Recent developments and future perspective. *Chemical Engineering Journal*, 181-182:1–34, 2012.

[53] J.B. Lloyd. Soluble polymers as targetable drug carriers. In P. Johnson and J. G. Lloyd-Jones, editors, *Drug delivery systems: fundamentals and techniques*. Ellis Horwood, Chichester, 1987.

[54] A. Xiang and A. J. McHugh. A generalized diffusion-dissolution model for drug release from rigid polymer membrane matrices. *Journal of Membrane Science*, 366:104–115, 2011.

[55] www.sigmaaldrich.com/materials-science/biomaterials/tutorial.html -Accessed 06.11.2012 (16:00h).

[56] G. Frenning and M. Stromme. Drug release modeled by dissolution, diffusion and immobilization. *International Journal of Pharmaceutics*, 250:137–145, 2003.

[57] H. J. Smith and H. Williams. *Introduction to the principles of drug design.* J. Wright, Bristol, 1983.

[58] M. E. Aguilera, R. L. Cerro, and A. L. Lopez de Ramos. Enhanced CO_2 diffusion in wedges. *Chemical Engineering Journal*, 87:31–40, 2002.

[59] A. E. Scheidegger. *The physics of flow through porous media.* University of Toronto Press, Toronto, 1960.

[60] F. A. L. Dullien. *Porous media: Fluid transport and pore structure.* Academic Press Inc., New York, 2nd edition, 1992.

[61] L. D. Landau and E. M. Lifshitz. *Course of theoretical physics. Vol. 5. Statistical Physics.* Elsevier. Butterworth Heinemann, 1980.

[62] T. S. Venkataraman and L. M. Narducci. Critical properties of the binary fluid system isobutyric acid-water. *Journal of Physics C: Solid State Physics*, 10:2849–2861, 1977.

[63] J. A. Pojman, C. Whitmore, M. L. Turco Liveri, R. Lombardo, J. Marszalek, R. Parker, and B. Zoltowski. Evidence for the existence of an effective interfacial tension between miscible fluids: Isobutyric acid-water and 1-butanol-water in a spinning-drop tensiometer. *Langmuir*, 22:2569–2577, 2006.

[64] A. A. Nepomnyashchy, M. G. Velarde, and P. Colinet. *Interfacial phenomena and convection (Volume* 124 *of Monographs and Surveys in Pure and Applied Mathematics).* Chapman and Hall/CRC, London, 2001.

[65] P.-G. de Gennes, F. Brochard-Wyart, and D. Quere. *Capillarity and wetting phenomena: Drops, Bubbles, Pearls, Waves.* Springer, New York, 2004.

[66] D. J. Korteweg. Sur la forme que prennent les equations du mouvements des fluides si l'on tient compte des forces capillaires causes par des variations de densite considerables mais coninues et sur la theorie de la capillarite dans l'hypothese d'une variation continue de la densite. *Archives Neerlandaises des Sciences Exactes et Naturelles*, 6:1–24, 1901.

[67] Y. B. Zeldovich. About surface tension of a boundary between two mutually soluble liquids. *Zhur. Fiz. Khim.*, XXIII:931–935, 1949.

[68] S. E. May and J. V. Maher. Capillary-wave relaxation for a meniscus between miscible liquids. *Physical Review Letters*, 67:2013–2016, 1991.

[69] B. Zoltowski, Y. Chekanov, J. Masere, J. A. Pojman, and V. Volpert. Evidence for the existence of an effective interfacial tension between miscible fluids. 2. Dodecyl acrylate-poly(dodecyl acrylate) in a spinning drop tensiometer. *Langmuir*, 23:5522–5531, 2007.

[70] L. Lacaze, P. Guenoum, D. Beysens, M. Delsanti, P. Petitjeans, and P. Kurowski. Transient surface tension in miscible liquids. *Physical Review E*, 82:041606, 2010.

[71] P. Petitjeans and T. Maxworthy. Miscible displacements in capillary tubes. *I*. Experiments. *Journal of Fluid Mechanics*, 326:37–56, 1996.

[72] J. A. Pojman, N. Bessonov, and V. Volpert. Miscible fluids in microgravity (MFMG): A zero-upmass investigation on the International Space Station. *Microgravity Science and Technology*, XIX:33–41, 2007.

[73] M. Santiago-Rosanne, M. Vignes-Adler, and M. G. Velarde. Dissolution of a drop on a liquid surface leading to surface waves and interfacial turbulence. *Journal of Colloid and Interface Science*, 191:65–80, 1997.

[74] V. D. Sobolev, N. V. Churaev, M. G. Velarde, and Z. M. Zorin. Surface tension and dynamic contact angle of water in thin quartz capillaries. *Journal of Colloid and Interface Science*, 222:51–54, 2000.

[75] M. J. Blunt and H. Scher. Pore-level modeling of wetting. *Physical Review E*, 52:6387–6403, 1995.

[76] H. B. Ma, G. P. Peterson, and D. M. Pratt. Disjoining pressure effect on the wetting characteristics in a capillary tube. *Microscale Thermophysical Engineering*, 2:283–297, 1998.

[77] K. Spildo and J. S. Buckley. Uniform and mixed wetting in square capillaries. *Journal of Petroleum Science and Engineering*, 24:145–154, 1999.

[78] A. T. Corey. *Mechanics of heterogeneous fluids in porous media*. Michigan: Water Resources Publications, Fort Collins, Colorado, 1977.

[79] E. Aker, K. J. Maloy, A. Hansen, and G. G. Batrouni. A two-dimensional network simulator for two-phase flow in porous media. *Transport in Porous Media*, 32:163–186, 1998.

[80] G. Mason and N. R. Morrow. Meniscus curvatures in capillaries of uniform cross-section. *Journal of the Chemical Society, Faraday Transactions 1: Physical Chemistry in Condensed Phases*, 80:2375–2393, 1984.

[81] S. M. Hassanizadeh and W. G. Gray. Thermodynamic basis of capillary pressure in porous media. *Water Resources Research*, 29:3389–3405, 1993.

[82] J. Crank. *The mathematics of diffusion*. Clarendon Press, Oxford, 1976.

[83] L. D. Landau and E. M. Lifshitz. *Course of theoretical physics. Vol. 6. Fluid Mechanics*. Elsevier. Butterworth Heinemann, 2009.

[84] J. A. Currie. Gaseous diffusion in porous media Part 1.-A non-steady state method. *British Journal of Applied Physics*, 11(8):314, 1960.

[85] J. A. Currie. Gaseous diffusion in porous media. Part 2.-Dry granular materials. *British Journal of Applied Physics*, 11(8):318, 1960.

[86] J. A. Currie. Gaseous diffusion in porous media. Part 3.-Wet granular materials. *British Journal of Applied Physics*, 12(6):275, 1961.

[87] Q. Zheng, B. Yu, S. Wang, and L. Luo. A diffusivity model for gas diffusion through fractal porous media. *Chemical Engineering Science*, 68:650–655, 2012.

[88] J. M. P. Q. Delgado. Longitudinal and transverse dispersion in porous media. *Chemical Engineering Research and Design*, 85:1245–1252, 2007.

[89] M. R. Merrill and Z. Jin. Velocity measurements in natural porous rocks. *Magnetic Resonance Imaging*, 12:345–348, 1994.

[90] V. Rajanayagam, S. Yao, and J. M. Pope. Quantitative magnetic resonance flow and diffusion imaging in porous media. *Magnetic Resonance Imaging*, 13:729–738, 1995.

[91] C.-Y. Chen and E. Meiburg. Miscible displacements in capillary tubes: Influence of Korteweg stresses and divergence effects. *Physics of Fluids*, 14:2052–2058, 2002.

[92] A. Vorobev. Boussinesq approximation of the Cahn-Hilliard-Navier-Stokes equations. *Physical Review E*, 82:056312, 2010.

[93] Y. Marcus. Some thermodynamic and structural aspects of mixtures of glycerol with water. *Physical Chemistry Chemical Physics*, 2:4891–4896, 2000.

[94] D. V. Batov, A. M. Zaichikov, V. P. Slyusar, and V. P. Korolev. Enthalpies of mixing and state of components in aqueous-organic mixtures with nets of Hydrogen bonds. *Russian Journal of General Chemistry*, 71:1208–1214, 2001.

[95] E. du Plessis, S. Woudberg, and J. Prieur du Plessis. Pore-scale modelling of diffusion in unconsolidated porous structures. *Chemical Engineering Science*, 65:2541–2551, 2010.

[96] P. N. Sen. Non-gaussian statistics and anomalous diffusion in porous media. In Govindan Rangarajan and Mingzhou Ding, editors, *Processes with Long-Range Correlations*, volume 621 of *Lecture Notes in Physics*, pages 181–192. Springer Berlin Heidelberg, 2003.

[97] D. Jou, J. Casas-Vazquez, and M. Criado-Sancho. Taylor dispersion and anomalous diffusion. In *Thermodynamics of Fluids Under Flow*, pages 187–209. Springer Netherlands, 2011.

[98] S. Fomin, V. Chuganov, and T. Hashida. Mathematical modeling of anomalous diffusion in porous media. *Fractional Differential Calculus*, 1:1–28, 2011.

[99] J. Glimm and D. H. Sharp. A random field model for anomalous diffusion in heterogeneous porous media. *Journal of Statistical Physics*, 62:415–424, 1991.

[100] J-W. Kim, E. Perfect, and H. Choi. Anomalous diffusion in two-dimensional euclidean and prefractal geometrical models of heterogeneous porous media. *Water Resources Research*, 43:W01405, 2007.

[101] S. Fomin, V. Chuganov, and T. Hashida. Application of fractional differential equations for modeling the anomalous diffusion of contaminant from fracture into porous rock matrix with bordering alteration zone. *Transport in Porous Media*, 81:187–205, 2010.

[102] S. Bekki, M. Vignes-Adler, E. Nakache, and P. M. Adler. Solutal marangoni effect: I. pure interfacial transfer. *Journal of Colloid and Interface Science*, 140:492–506, 1990.

[103] S. Bekki, M. Vignes-Adler, and E. Nakache. Solutal marangoni effect: Ii. dissolution. *Journal of Colloid and Interface Science*, 152:314–324, 1992.

[104] M. Vignes-Adler M. Santiago-Rosanne and M. G. Velarde. On the spreading of partially miscible liquids. *Journal of Colloid and Interface Science*, 234:375–383, 2001.

[105] E. E. Zukoski. Influence of viscosity, surface tension, and inclination angle on motion of long bubbles in closed tubes. *Journal of Fluid Mechanics*, 25:821–837, 1966.

[106] T. B. Benjamin. Gravity currents and related phenomena. *Journal of Fluid Mechanics*, 31:209–248, 1968.

[107] R. J. Lowe, J. W. Rottman, and P. F. Linden. The non-Boussinesq lock-exchange problem. Part 1. Theory and experiments. *Journal of Fluid Mechanics*, 537:101–124, 2005.

[108] E. W. Washburn. The dynamics of capillary flow. *Physical Review*, 17:273–283, 1921.

[109] W. Rose. Modeling forced versus sponataneous capillary imbibition processes commonly occurring in porous sediments. *Journal of Petroleum Science and Engineering*, 30:155–166, 2001.

[110] H. Ovdat and B. Berkowitz. Pore-scale imbibition experiments in dry and prewetted porous media. *Advances in Water Resources*, 30:2373–2386, 2007.

[111] U. Hatiboglu and T. Babadagli. Experimental and visual analysis of co- and counter-current spontaneous imbibition for different viscosity ratios, interfacial tensions and wettabilities. *Journal of Petroleum Science and Engineering*, 70:214–228, 2010.

[112] B. Markicevic, K. Hoff, H. Li, A. R. Zand, and H. K. Navaz. Capillary force driven primary and secondary unidirectional flow of wetting liquid into porous medium. *International Journal of Multiphase Flow*, 39:193–204, 2012.

[113] R. Lenormand, C. Zarcone, and A. Sarr. Mechanisms of the displacement of one fluid by another in a network of capillary ducts. *Journal of Fluid Mechanics*, 135:337–353, 1983.

[114] V. Joekar-Niasar and S. M. Hassanizadeh. Analysis of fundamentals of two-phase flow in porous media using dynamic pore-network models: A review. *Critical Reviews in Environmental Science and Technology*, 42:1895–1976, 2012.

[115] M. S. Al-Gharbi and M. J. Blunt. Dynamic network modeling of two-phase drainage in porous media. *Physical Review E*, 71:016308, 2005.

[116] G. F. Pinder. *Flow through porous media: Recent developments*. Computational Mechanics Publications, Ashurst, Hants, 1983.

[117] M. J. Blunt, M. D. Jackson, M. Piri, and P. H. Valvatne. Detailed physics, predictive capabilities and macroscopic consequences for pore-network models of multiphase flow. *Advances in Water Resources*, 25:1069–1089, 2002.

[118] G. Lovoll, Y. Meheust, K. J. Maloy, E. Aker, and J. Schmittbuhl. Competition of gravity, capillary and viscous forces during drainage in a two-dimensional porous medium, a pore scale study. *Energy*, 30:861–872, 2005.

[119] V. Joekar-Niasar, M. I. J. van Dijke, and S. M. Hassanizadeh. Pore-scale modeling of multiphase flow and transport: Achievements and perspectives. *Transport in Porous Media*, 94:461–464, 2012.

[120] M. J. Blunt. Flow in porous media - pore-network models and multiphase flow. *Current Opinion in Colloid and Interface Science*, 6:197–207, 2001.

[121] D. Zhou, L. A. Dillard, and M. J. Blunt. A physically based model of dissolution of nonaqueous phase liquids in the saturated zone. *Transport in Porous Media*, 39:227–255, 2000.

[122] L. A. Dillard and M. J. Blunt. Development of a pore network simulation model to study nonaqueous phase liquid dissolution. *Water Resources Research*, 36:439–454, 2000.

[123] R. J. Held and A. Celia. Pore-scale modeling and upscaling of nonaqueous phase liquid mass transfer. *Water Resources Research*, 37:539–549, 2001.

[124] C. Pan, E. Dalla, D. Franzosi, and C. T. Miller. Pore-scale simulation of entrapped non-aqueous phase liquid dissolution. *Advances in Water Resources*, 30:623–640, 2007.

[125] V. Joekar-Niasar, S. M. Hassanizadeh, L. J. Pyrak-Nolte, and C. Berentsen. Simulating drainage and imbibition experiments in a high-porosity micromodel using an unstructured pore network model. *Water Resources Research*, 45:W02430, 2009.

[126] C. Laroche, O. Vizika, and F. Kalaydjan. Network modeling as a tool to predict three-phase gas injection in heterogeneous wettability porous media. *Journal of Petroleum Science and Engineering*, 24:155–168, 1999.

[127] M. D. Jackson, P. H. Valvatne, and M. J. Blunt. Prediction of wettability variation and its impact on flow using pore- to reservoir-scale simulations. *Journal of Petroleum Science and Engineering*, 39:231–246, 2003.

[128] M. I. J. van Dijke, K. S. Sorbie, M. Sohrabi, and A. Danesh. Simulation of WAG floods in an oil-wet micromodel using a 2-D pore-scale network model. *Journal of Petroleum Science and Engineering*, 52:71–86, 2006.

[129] R. Chertcoff, A. Calvo, I. Paterson, M. Rosen, and J.P. Hulin. Transient effects in liquid-liquid interface motions through glass capillaries. *Journal of Interface and Colloid Science*, 154:194–201, 1992.

[130] G. I. Taylor. Deposition of a viscous fluid on the wall of a tube. *Journal of Fluid Mechanics*, 10:161–165, 1961.

[131] B. G. Cox. On driving a viscous fluid out of a tube. *Journal of Fluid Mechanics*, 14:81–96, 1962.

[132] B. G. Cox. An experimental investigation of the streamlines in viscous fluid expelled from a tube. *Journal of Fluid Mechanics*, 20:193–200, 1964.

[133] E. J. Soares, M. S. Carvalho, and P. R. Souza Mendes. Gas-displacement of non-Newtonian liquids in capillary tubes. *International Journal of Heat and Fluid Flow*, 27:95–104, 2006.

[134] E. J. Soares, M. S. Carvalho, and P. R. Souza Mendes. Immiscible liquid-liquid displacement in capillary tubes. *Journal of Fluids Engineering*, 127:24–31, 2005.

[135] E. Unsal, G. Mason, N. R. Morrow, and D. W. Ruth. Co-current and counter-current imbibition in independent tubes of non-axissymmetric geometry. *Journal of Colloid and Interface Science*, 306:105–117, 2007.

[136] E. Unsal, G. Mason, D. W. Ruth, and N. R. Morrow. Co- and counter-current spontaneous imbibition into groups of capillary tubes with lateral connections permitting cross-flow. *Journal of Colloid and Interface Science*, 315:200–209, 2007.

[137] Z. M. Zorin and N. V. Churaev. Immiscible liquid-liquid displacement in thin quartz capillaries. *Advances in Colloid and Interface Science*, 40:85–108, 1992.

[138] F. P. Bretherton. The motion of long bubbles in tubes. *Journal of Fluid Mechanics*, 10:166–188, 1961.

[139] V. G. Levich. *Physicochemical hydrodynamics*. Prentice-Hall, Inc., Englewood Cliffs, N.J., 1962.

[140] V. M. Starov, V. V. Kalinin, and V. I. Ivanov. Influence of surface forces on hydrodynamics of wetting. *Colloids and Surfaces A: Physicochemical and Engineering Aspects*, 91:149–154, 1994.

[141] N. V. Churaev. Derjaguin's disjoining pressure in the colloid science and surface phenomena. *Advances in Colloid and Interface Science*, 104:XV–XX, 2003.

[142] N. V. Churaev. Surface forces in wetting films. *Advances in Colloid and Interface Science*, 103:197–218, 2003.

[143] N. V. Churaev, V. M. Starov, and B. V. Derjaguin. The shape of the transition zone between a thin film and bulk liquid and the line tension. *Journal of Colloid and Interface Science*, 89:16–24, 1982.

[144] J. Kuang, T. Maxworthy, and P. Petitjeans. Miscible displacements between silicone oils in capillary tubes. *European Journal of Mechanics-B/Fluids*, 22:271–277, 2003.

[145] J. Kuang, T. Maxworthy, and P. Petitjeans. Velocity fields and streamline patterns of miscible displacements in cylindrical tubes. *Experiments in Fluids*, 37:301–308, 2004.

[146] R. Balasubramaniam, N. Rashidnia, T. Maxworthy, and J. Kuang. Instability of miscible interfaces in a cylindrical tube. *Physics of Fluids*, 17:052103, 2005.

[147] J. Bico and D. Quere. Rise of liquids and bubbles in angular capillary tubes. *Journal of Colloid and Interface Science*, 247:162–166, 2002.

[148] M. Hilpert. Effects of dynamic contact angle on liquid infiltration into horizontal capillary tubes: (Semi)-analytical solutions. *Journal of Colloid and Interface Science*, 337:131–137, 2009.

[149] M. Hilpert. Liquid withdrawal from capillary tubes: Explicit and implicit analytical solution for constant and dynamic contact angle. *Journal of Colloid and Interface Science*, 351:267–276, 2010.

[150] M. Bouzid, L. Mercury, and A. Lassin amd J.-M. Matray. Salt precipitation and trapped liquid cavitation in micrometric capillary tubes. *Journal of Colloid and Interface Science*, 360:768–776, 2011.

[151] H. Foroughi, A. Abbasi, K. S. Das, and M. Kawaji. Immiscible displacement of oil by water in a microchannel: Asymmetric flow behavior and nonlinear stability analysis of core-annular flow. *Physical Review E*, 85:026309, 2012.

[152] C. A. Oyarzun and L. A. Segura. Design and construction of glass micromodels for the study of moisture transport in softwoods. *Drying Technology*, 27:14–29, 2009.

[153] J. S. Buckley. Multiphase displacement in micromodels. In N. R. Morrow, editor, *Interfacial phenomena in petroleum recovery*, pages 157–189. Marcel Dekker, New York, 1991.

[154] J. Wan, K. Tokunaga, C-F. Tsang, and G. Bodvarsson. Improved glass micromodel methods for studies of flow and transport in fractured porous media. *Water Resources Research*, 32:1955–1964, 1996.

[155] A. Bazylak, V. Berejnov, B. Markicevic, D. Sinton, and N. Djilali. A microfluidic pore network approach to investigate water transport in fuel cell porous transport layers. In *Proceedings of the Sixth International ASME Conference on Nanochannels, Microchannels and Minichannels ICNMM-62349, Darmstadt, Germany*, June 2008.

[156] C. V. Chrysikopoulos, C. C. Plega, and V. E. Katzourakis. Non-invasive in situ concentration determination of fluorescent or color tracers and pollutants in a glass pore network model. *Journal of Hazardous Materials*, 198:299–306, 2011.

[157] M. Buchgraber, M. Al-Dossary, C. M. Ross, and A. R. Kovscek. Creation of a dual-porosity micromodel for pore-level visualization of multiphase flow. *Journal of Petroleum Science and Engineering*, 86-87:27–38, 2012.

[158] H. H. Al-Sharji, C. A. Grattoni, R.A. Dawe, and R. W. Zimmerman. Flow of oil and water through elastic polymer gels. *Oil and Gas Science and Technology*, 56:145–152, 2001.

[159] C. L. Perrin, P. M. J. Tardy, K. S. Sorbie, and J. C. Crawshaw. Experimental and modeling study of Newtonian and non-Newtonian fluid flow in pore network micromodels. *Journal of Colloid and Interface Science*, 295:542–550, 2006.

[160] B. Y. Jamaloei, R. Kharrat, and K. Asghari. Pore-scale events in drainage process through porous media under high- and low-interfacial tension flow conditions. *Journal of Petroleum Science and Engineering*, 75:223–233, 2010.

[161] B. Y. Jamaloei and R. Kharrat. Analysis of microscopic displacement mechanisms of dilute surfactant flooding in oil-wet and water-wet porous media. *Transport in Porous media*, 81:1–19, 2010.

[162] B. Y. Jamaloei, R. Kharrat, K. Asghar, and F. Torabi. The influence of pore wettability on the microstructure of residual oil in surfactant-enhanced water flooding in heavy oil reservoirs: Implications for pore-scale flow characterization. *Journal of Petroleum Science and Engineering*, 77:121–134, 2011.

[163] B. Y. Jamaloei, K. Asghari, and R. Kharrat. Pore-scale flow characterization of low-interfacial tension flow through mixed-wet porous media with different pore geometries. *Experimental Thermal and Fluid Science*, 35:253–264, 2011.

[164] B. Y. Jamaloei and R. Kharrat. Pore-scale description of surfactant-enhanced waterflooding for heavy oil recovery. *Journal of Petroleum Science and Engineering*, 92-93:89–101, 2012.

[165] M. Sohrabi, A. Danesh, D. H. Tehrani, and M. Jamiolahmady. Microscopic mechanisms of oil recovery by near-miscible gas injection. *Transport in Porous Media*, 72:351–367, 2008.

[166] M. Sohrabi, A. Danesh, and M. Jamiolahmady. Visualization of residual oil recovery by near-miscible gas and SWAG injection using high-pressure micromodels. *Transport in Porous Media*, 74:239–257, 2008.

[167] M. Riazi, M. Sohrabi, and M. Jamiolahmady. Experimental study of pore-scale mechanisms of carbonated water injection. *Transport in Porous Media*, 86:73–86, 2011.

[168] R. T. Armstrong and D. Wildenschild. Investigating the pore-scale mechanisms of microbial enhanced oil recovery. *Journal of Petroleum Science and Engineering*, 94-95:155–164, 2012.

[169] J. K. Williams and R. A. Dawe. Modelling pore-scale displacement processes at near-critical conditions. *Journal of Petroleum Science and Engineering*, 2:225–233, 1989.

[170] R. A. Dawe and Y. Zhang. Kinetics of calcium carbonate scaling using observations from glass micromodels. *Journal of Petroleum Science and Engineering*, 18:179–187, 1997.

[171] A. A. Keller, M. J. Blunt, and P. V. Roberts. Micromodel observation of the role of oil layers in three-phase flow. *Transport in Porous Media*, 26:277–297, 1997.

[172] S. W. Jeong, A. L.Wood, and T. R. Lee. Enhanced removal of DNAPL trapped in porous media using simultaneous injection of cosolvent with air: influencing factors and removal mechanisms. *Journal of Hazardous Materials*, B101:109–122, 2003.

[173] L. Zhong, A. Mayer, and R. J. Glass. Visualization of surfactant-enhanced nonaqueous phase liquid mobilization and solubilization in a two-dimensional micromodel. *Water Resources Research*, 37:523–537, 2001.

[174] N. A. Sahloul, M. A. Ioannidis, and I. Chatzis. Dissolution of residual nonaqueous phase liquids in porous media: pore-scale mechanisms and mass transfer rates. *Advances in Water Resources*, 25:33–49, 2002.

[175] S. Sirivithayapakorn and A. Keller. Transport of colloids in saturated porous media: A pore-scale observation of the size exclusion effect and colloid acceleration. *Water Resources Research*, 39:1109, 2003.

[176] M. Auset and A. A. Keller. Pore-scale processes that control dispersion of colloids in saturated porous media. *Water Resources Research*, 40:W03503, 2004.

[177] T. Baumann, L. Toops, and R. Niessner. Colloid dispersion on the pore scale. *Water Research*, 44:1246–1254, 2010.

[178] I. Chatzis and F. A. L. Dullien. Dynamic immiscible displacement mechanisms in pore doublets: Theory versus experiment. *Journal of Colloid and Interface Science*, 91:199–222, 1983.

[179] R. Lenormand, E. Touboul, and C. Zarcone. Numerical models and experiments on immiscible displacements in porous media. *Journal of Fluid Mechanics*, 189:165–187, 1988.

[180] C. D. Tsakiroglou, M. Theodoropoulou, V. Karoutsos, D. Papanicolaou, and V. Sygouni. Experimental study of the immiscible displacement of shear-thinning fluids in pore networks. *Journal of Colloid and Interface Science*, 267:217–232, 2003.

[181] E. R. Rangel-German and A. R. Kovscek. A micromodel investigation of two-phase matrix fracture transfer mechanisms. *Water Resources Research*, 42:W03401, 2006.

[182] B. Y. Jamaloei, K. Asghari, R. Kharrat, and F. Ahmadloo. Pore-scale two-phase filtration in imbibition process through porous media at high- and low-interfacial tension flow conditions. *Journal of Petroleum Science and Engineering*, 72:251–269, 2010.

[183] M. Jamiolahmady, A. Danesh, D. H. Tehrani, and D. B. Duncan. A mechanistic model of gas-condensate flow in pores. *Transport in Porous Media*, 41:17–46, 2000.

[184] M. A. Theodoropoulou, V. Karoutsos, C. Kaspiris, and C. D. Tsakiroglou. A new visualization technique for the study of solute dispersion in model porous media. *Journal of Hydrology*, 274:176–197, 2003.

[185] G. M. Badillo, L. A. Segura, and J. B. Laurindo. Theoretical and experimental aspects of vacuum impregnation of porous media using transparent etched networks. *International Journal of Multiphase Flow*, 37:1219–1226, 2011.

[186] B. Tohidi, R. Anderson, M.B. Clennell, R. W. Burgass, and A. B. Biderkab. Visual observation of gas-hydrate formation and dissociation in synthetic porous media by means of glass micromodels. *Geology*, 29:867–870, 2001.

[187] C. Chalbaud, M. Robin, J-M. Lombard, F. Martin, P. Egermann, and H. Bertin. Interfacial tension measurments and wettability evaluation for geological CO_2 storage. *Advances in water resources*, 32:98–109, 2009.

[188] The Dolomite Centre Ltd. *Dolomite Microfluidics Guide full product catalog*, 2012.

[189] M. Mukhopadhyay. *Natural extracts using supercritical carbon dioxide*. CRC Press LLC, 2000.

[190] A. Silva, C. Delerue-Matos, and A. Fiuza. Use of solvent extraction to remediate soils contaminated with hydrocarbons. *Journal of Hazardous Materials*, 124:224–229, 2005.

[191] G. Viner and J. A. Pojman. Studying diffusion of partially miscible and systems near their consolute point by laser line deflection. *Optics and Lasers in Engineering*, 46:893–899, 2008.

[192] J. Dambrine, B. Geraud, and J.-B. Salmon. Interdiffusion of liquids of different viscosities in a microchannel. *New Journal of Physics*, 11:075015, 2009.

[193] B. Chu, F. J. Schoenes, and W. P. Kao. Spatial and time-dependent concentration fluctuations of the isobutyric acid-water system in the neighborhood of its critical mixing point. *Journal of the American Chemical Society*, 90:3042, 1968.

[194] J. B. Segur and H. E. Oberstar. Viscosity of glycerol and its aqueous solutions. *Industrial and Engineering Chemistry*, 43:2117–2120, 1951.

[195] N. Ouerfelli, T. Kouissi, N. Zrelli, and M. Bouanz. Competition of viscosity correlation equations in isobutyric acid+water binary mixtures near and far away from the critical temperature. *Journal of Solution Chemistry*, 38:983–1004, 2009.

[196] J. Kim and Y. S. Ju. On-chip characterization of the transport properties of liquids using microfluidic channel-based Brownian microscopy. In *Micro Electro Mechanical Systems 2008, MEMS2008, Proceedings of IEEE 21st International conference, Tucson AZ, USA*, pages 587–590, Jan 2008.

[197] N. Rashidnia and R. Balasubramaniam. Measurement of the mass diffusivity of miscible liquids as a function of concentration using a common path shearing interferometer. *Experiments in Fluids*, 36:619–626, 2004.

[198] G. D'Errico, O. Ortona, F. Capuano, and V. Vitagliano. Diffusion coefficients for the binary system glycerol+water at 25^oC. A velocity correlation study. *Journal of Chemical Engineering Data*, 49:1665–1670, 2004.

[199] B. Chu and F.J. Schoenes. Diffusion coefficient of the isobutyric acid-water system in the critical region. *Physical Review Letters*, 21:6, 1968.

[200] R. L. Rowley and F. H. Horne. Critical exponent of the heat of transport of water-isobutyric acid mixtures. *The Journal of Chemical Physics*, 71:3841, 1979.

[201] N-C. Wong and C. M. Knobler. Light-scattering studies of phase separation in isobutyric acid+water mixtures: Hydrodynamic effects. *Physical Review A*, 24:3205–3211, 1981.

[202] U. Kaatze and S. Z. Mirzaev. Slowing down in chemical reactions.the isobutyric acid/water system in the critical region. *The Journal of Physical Chemistry A*, 104:5430–5436, 2000.

[203] V.-M. Melzer, W. Baldauf, and H. Knapp. Measurement of diffusivity, viscosity, density and refractivity of eight binary liquid mixtures. *Chemical Engineering amd Processing: Process Intensification*, 26:71–79, 1989.

[204] R. G. Howland, N-C. Wong, and C. M. Knobler. Experimental studies of nucleation in near-critical liquid mixtures. *Journal of Chemical Physics*, 73:522–531, 1980.

[205] J. C.-S. Wu and E.-H. Lee. Ultrafiltration of soybean oil/hexane extract by porous ceramic membranes. *Journal of Membrane Science*, 154:251–259, 1999.

[206] LaVision. *Imager 3 Camera System operation manual*, May 2002.

[207] A. Kourmatzis. *Pulsed charge injection atomization and turbulent electrohydrodynamics*. PhD thesis, University of Southampton, 2011.

[208] D. Ju. *Experimental and numerical research on pharmaceutical aerosols*. PhD thesis, University of Southampton, 2012.

[209] Questar Corporation. *Questar QM-100 long-distance microscope*, November 2001.

[210] LaVision. *High efficiency diffuser product manual*, January 2010.

[211] Oxford Lasers. *Firefly High Speed Imaging Laser user manual*, January 2009.

[212] D. S. Cohen and A. B. White. Sharp fronts due to diffusion and viscoelastic relaxation in polymers. *SIAM J. Appl. Math.*, 51:472–483, 1991.

[213] M. S. P. Stevar and A. Vorobev. Shapes and dynamics of miscible liquid/liquid interfaces in horizontal capillary tubes. *Journal of Colloid and Interface Science*, 383:184–197, 2012.

[214] T. Atkins. *Quotation and Design note.* The Dolomite Centre Ltd., 2011.